Signal Sampling and Reconstruction from Noisy Data

by

Vu-Luu Nguyen

A thesis submitted in partial fulfillment of the requirements

for the degree of Doctor of Philosophy

Department of Electrical and Computer Engineering

The University of Manitoba

Winnipeg, Canada

June 2, 2004

THE UNIVERSITY OF MANITOBA

FACULTY OF GRADUATE STUDIES

*****

COPYRIGHT PERMISSION

Signal Sampling and Reconstruction from Noisy Data

BY

Vu-Luu Nguyen

A Thesis/Practicum submitted to the Faculty of Graduate Studies of The University of Manitoba in partial fulfillment of the requirement of the degree

Of

DOCTOR OF PHILOSOPHY

To my parents and sister

Abstract

The Whittaker-Shannon sampling theorem has been widely used to reconstruct a bandlimited signal from the set of its sampled values. In many practical applications, noise is often contained in the observed samples. Given this situation, the Whittaker-Shannon interpolation formula is no longer suitable since it interpolates noise. Although oversampling and filtering has been widely used as a tool for improving the reconstruction accuracy of the Whittaker-Shannon reconstruction scheme, this method has several limitations. Firstly, it uses large amount of bits for representation of the original analog signal. Secondly, since a high sampling rate is used, its realization requires costly high-speed electronic circuits. Finally, there is the potential problem of increasing the correlation between successive samples as the sampling rate increases, which leads to an unstable reconstruction.

The aim of this work is to develop new reconstruction schemes for recovering signals from noisy data, which are more accurate and robust than the classical Whittaker-Shannon interpolation scheme and the oversampling/filtering reconstruction schemes proposed in the literature. In particular, we propose a class of nonlinear reconstruction algorithms known as thresholding that does not depend on oversampling for noise reduction. We also propose a new sampling scheme that relies on thresholding to transform a sequence of uniformly-spaced samples to a sequence of nonuniformly-spaced samples prior to transmission or storage. We show that the proposed sampling scheme is more resistant to noise than the classical uniform sampling scheme considered in the Whittaker-Shannon sampling theorem. Moreover, in certain cases, the proposed sampling scheme requires a smaller number of bits for representation and reconstruction of the original signal. As a result, it provides a reduction in data storage. The proposed sampling and reconstruction schemes have a potential application in designing signal acquisition and reconstruction systems operating in highly noisy environments. They also have a potential application in speech acquisition and reconstruction.

As an alternative to oversampling, we propose a new technique that collects multiple sets of sampled values acquired at the Nyquist sampling rate and uses thresholding-based algorithms for recovering the signal. This technique gives better reconstruction accuracy than the oversampling/filtering method, provided that the same amount of bits is used to represent the signal. We also propose a thresholding-based multi-channel sampling scheme, which not only offers better reconstruction accuracy but requires smaller amount of bits for representation of the original signal than the oversampling/filtering method. Since the proposed techniques do not use oversampling, its realizations do not require costly high-speed electronic circuits and can be used for acquisition of ultra wideband signals. It also avoids the problem of high correlation between successive samples encountered in the oversampling/filtering method. The proposed techniques have potential applications in multi-channel communication and multi-sensor information systems.

Acknowledgements

I would like to express my sincerest thanks to my advisor Professor Miroslaw Pawlak, for his mentoring, professional support and the kindness he gave me. Without him, I would not fulfill this dissertation. I also like to thank him for introducing the subject to me and for his patient in the early days of my doctoral study. My thesis is a continuation of his work on signal sampling and recovering from noisy observations. I have benefited so much from his expertise in this area.

I am very grateful to Professor Edward Shwedyk, who's enthusiasm in teaching and research has inspired me. From him, I learned the value of hardwork, dedication, organization and respect.

I would like to thank Dr. Andrzej Tarczynski, the external examiner, for reading the thesis and for his insights, valuable comments and suggestions that improve the thesis.

I also would like to thank Dr. Pradeepa Yahampath and Dr. Jose Rueda for serving in the advisory committee and for their valuable suggestions that help me improving the results of this research.

I specially thank Telecommunication Research Laboratory (TRLabs) for its financial support and for providing me with comfortable working environments, which I would not have enjoyed elsewhere. I also thank University of Manitoba for awarding the graduate fellowships. I would like to thank Marcia and Kate at the Department of Electrical and Computer Engineering for their administrative support and for answering my many questions.

I am indebted to Ha for his assistant that made my graduate study in Canada possible. Thank you for your helps during my early days in Canada.

I want to thank Trang for sharing with me so much, for your emotional support and encouragement. Without you, my time in Canada would not be fulfilled.

Last, but most importantly, I thank my parents and sister, who always stand by me through my many ups and downs during the course of this work. Their love and understanding have encouraged me so much that I can follow my voyage to the destination. This dissertation is dedicated to them.

Contents

List of Figures

List of Tables

Acronyms

ADC	Analog-to-Digital Converter
SNR	Signal-to-Noise Ratio
MISE	Mean Integrated Squared Error
EMISE	Empirical Mean Integrated Squared Error
IVAR	Integrated Variance
IBIAS	Integrated Bias
W-S	Whittaker-Shannon
MA	Moving Average
BL	Band-Limited
OSF	Oversampling Factor
PDF	Probability Density Function
DSRR	Data Storage Reduction Ratio

A Guide to The Symbols

E_0	Energy of signal
σ^2	Variance of noise
σ_1^2	$\sigma_1^2 = \sigma^2/L$
Ω	Bandwidth of signal
T	Threshold level
T_{opt}	The optimal threshold level
τ_q	Nyquist sampling period (Nyquist interval)
τ	Sampling period ($\tau \leq \tau_q$)
n_q	$2n_q + 1$ is the number of acquired samples when the sampling period is τ_q
n	$2n + 1$ is the number of acquired samples when the sampling period is τ
$x(t)$	Original signal
$\widetilde{x}(t)$	The signal reconstructed by the W-S interpolation scheme
$\breve{x}(t)$	The signal reconstructed by data smoothing and interpolation
$\breve{\breve{x}}(t)$	The signal reconstructed by oversampling and post-filtering
$\dot{x}(t),\ \ddot{x}(t)$	The signals reconstructed via orthogonal expansion
$\bar{x}(t)$	The signal reconstructed via multiple observations
$\widehat{x}(t)$	The signal reconstructed by the proposed sampling and

	reconstruction scheme
$x_1(t), x_2(t), x_3(t)$	Test signals used in simulations
Q	In Chapter 4, Q is the size of each constitute data set
L	In Chapter 4, L is the number of constitute date sets.
	In Chapter 6 and Chapter 7, L is the number of the sets of
	sampled values acquired at the Nyquist rate
I_p	The index set defined as $I_p = \{k : \ \|x_k\| > T\}$
I_d	The index set defined as $I_p = \{k : \ \|x_k\| \leq T\}$
η	The length of sequence $\{x'_k\}$ defined as $\{x'_k\} = \{x_k : \ \|x_k\| > T\}$
m	The resolution of a quantizer
D_R	Data storage reduction ratio

Chapter 1

Introduction

Most real-world signals, such as voices, sounds, video and scientific signals are "analog" in nature. That is, they vary continuously over time or space. In many practical applications such as digital storage, digital audio/video, digital communications and digital signal processing, we want to store, transmit or process these signals digitally. This can be implemented through a process of sampling, discrete-time processing and subsequent reconstruction of continuous-time signals. Here, sampling is the process of recording sampled values $x(t_k)$ of a signal $x(t)$ at time instants t_k. Reconstruction is the process of reproducing the signal $x(t)$ from a set of its sampled values $\{x(t_k)\}$. Sampling and reconstruction are integral parts of every digital system nowadays.

The simplest and most widely-used sampling strategy is uniform sampling, where sampled values $x(t_k)$ are acquired at equally-spaced instants $t_k = k\tau$, where τ is the sampling period. The sampling process is generally not invertible, i.e., given a set of sampled values $\{x(t_k)\}$, it is not possible in general to reconstruct the signal $x(t)$. This is due to the fact that many continuous-time signals can have the same set of sampled values. However, by restricting the class of input signals to the sampler, the ambiguity

can be removed. For the class of bandlimited signals, the Whittaker-Shannon (W-S) sampling theorem says that a signal $x(t)$ can be reconstructed exactly from the sequence of its uniformly-spaced samples $\{x(k\tau)\}$, provided that τ is sufficiently small [1, 2].

The W-S sampling theorem considers the case when the sampled values of a signal $x(t)$ are available for signal reconstruction without any distortions. However, in practical applications, due to imperfect data acquisition devices, physical damages in storage medium and/or transmission errors, the data available for signal reconstruction is not the sampled values of the original signal but its noisy version. Given this situation, the classical W-S reconstruction scheme is no longer optimal. In fact, it has been pointed out in [3] that the W-S reconstruction scheme does not have a noise-diminishing property, yielding a diverged reconstruction.

Several reconstruction methods incorporating some smoothing schemes were proposed in order to overcome this problem [3, 4, 5, 6, 7, 8]. For instance, moving average filtering and exponential weighting algorithms were proposed for smoothing the noisy data prior to reconstruction [4, 7]. On other hand, in [5, 6, 8], noise reduction was obtained by using oversampling and post-filtering. Since these methods rely on the use of a high sampling rate for noise removal, its realizations require costly high-speed electronic circuits. There also exists the potential problem of increasing the correlation between successive samples as the sampling rate increases, which leads to an unstable reconstruction.

In this thesis, a class of nonlinear algorithms for sampling and recovering signals from noisy data without oversampling is proposed. It is shown that the proposed techniques are more accurate and robust than the standard W-S interpolation scheme

as well as the other oversampling/filtering reconstruction schemes. The detailed theoretical performance analysis and simulation of the proposed sampling and reconstruction schemes are presented in the thesis.

1.1 Background

Consider continuous-time signals which can be modelled by the mathematical set $BL(\Omega)$ which represents the space of all finite energy functions bandlimited to $\Omega < \infty$. Mathematically, $BL(\Omega)$ is the space of all functions $x(t)$ which can be expressed as follows:

$$x(t) = \frac{1}{2\pi} \int_{-\Omega}^{\Omega} X(\omega) e^{j\omega t} d\omega \tag{1.1}$$

where $X(\omega)$, the Fourier transform of $x(t)$, is square integrable over $[-\Omega, \Omega]$, and is zero outside the finite interval $[-\Omega, \Omega]$, i.e., $X(\omega) = 0$ for $|\omega| > \Omega$. The finite number Ω is called the bandwidth of the signal.

The set of all bandlimited functions is quite large and is rich enough to model many signals of practical engineering interest. This is because most real-world signals have some effective bandwidth, i.e., above some frequency they contain very little energy. For example, speech signals can be well modelled as bandlimited functions whose bandwidth is 4 KHz and audio signals can be well modelled as bandlimited functions whose bandwidth is 20 KHz [9]. This bandlimited assumption is often used when dealing with analog signals, though in recent years some work has been done in the area of sampling and reconstruction of non-bandlimited functions which lie in shift-invariant subspaces or wavelet subspaces [10, 11, 12, 13, 14]. However, in this thesis, only bandlimited signals are considered.

The W-S sampling theorem says that every $x(t) \in BL(\Omega)$ can be reconstructed

exactly from the set of its sampled values $\{x(k\tau)\}$, $k = 0, \pm 1, \pm 2, ... \pm \infty$, by:

$$x(t) = \sum_{k=-\infty}^{\infty} x(k\tau) \cdot \text{sinc}\left(\frac{t}{\tau} - k\right), \tag{1.2}$$

provided that $\tau \leq \pi/\Omega$, where $\text{sinc}(t) = \sin(\pi t)/\pi t$.

A number of properties and extensions of (1.2) have been given in the signal processing and Fourier analysis literature. In particular, truncation, aliasing, location (jitter), amplitude errors of the W-S interpolation series have been examined. Furthermore, generalizations to multiple dimensions, random signals, not necessarily bandlimited signals, missing data, wavelet subspaces and irregular sampling have been proposed. The reader is referred to [5, 11, 15, 16, 17, 18] for an extensive overview of the theory and applications of (1.2) and its extensions.

In this thesis, the statistical aspects of the W-S sampling theorem are considered, i.e., the statistical analysis of (1.2) when only a finite record of noisy data is available for signal reconstruction. Specifically, the following observation model is assumed:

$$y_k = x(k\tau) + \varepsilon_k = x_k + \varepsilon_k, \qquad |k| \leq n, \tag{1.3}$$

where $\{\varepsilon_k\}$ is an additive noise process. It is assumed further that ε_k are independent random variables with zero mean and variance σ^2.

The classical W-S interpolation scheme would replace $\{x(k\tau)\}$ in (1.2) by $\{y_k\}$ yielding the following estimate:

$$\widetilde{x}(t) = \sum_{|k| \leq n} y_k \cdot \text{sinc}\left(\frac{t}{\tau} - k\right) \tag{1.4}$$

The mean integrated squared error (MISE) is used as a measure of performance of $\widetilde{x}(t)$ and other estimates examined in the thesis.

$$MISE(\widetilde{x}) \triangleq E \int_{-\infty}^{\infty} (\widetilde{x}(t) - x(t))^2 dt \tag{1.5}$$

MISE can be decomposed into the integrated variance (IVAR) and integrated bias (IBIAS) components as follows.

$$MISE(\widetilde{x}) = IVAR(\widetilde{x}) + IBIAS(\widetilde{x}) \tag{1.6}$$

where,

$$IVAR(\widetilde{x}) \triangleq E \int_{-\infty}^{\infty} (\widetilde{x}(t) - E\widetilde{x}(t))^2 dt \tag{1.7}$$

and,

$$IBIAS(\widetilde{x}) \triangleq \int_{-\infty}^{\infty} (E\widetilde{x}(t) - x(t))^2 dt \tag{1.8}$$

The terms $IBIAS(\widetilde{x})$ describes the truncation error, whereas $IVAR(\widetilde{x})$ reflects the existence of random error in the observed samples.

It was shown in [3] that:

$$MISE(\widetilde{x}) = \tau\sigma^2(2n+1) + \tau \sum_{|k|>n} x_k^2 \tag{1.9}$$

$$IVAR(\widetilde{x}) = \tau\sigma^2(2n+1) \tag{1.10}$$

$$IBIAS(\widetilde{x}) = \tau \sum_{|k|>n} x_k^2 \tag{1.11}$$

Thus, for any τ, $IBIAS(\widetilde{x})$ approaches zero, but $IVAR(\widetilde{x})$ approaches infinity as $n \rightarrow \infty$. This drawback of $\widetilde{x}(t)$ is due to the fact that $\widetilde{x}(t)$ is an interpolation scheme, i.e., $\widetilde{x}(k\tau) = y_k$. Therefore, it retains random errors presented in the data.

Several reconstruction methods incorporating some smoothing schemes were proposed in order to overcome this problem [3, 4, 5, 6, 7, 8]. For instance, local smoothing schemes based on moving average filtering and exponential weighting algorithms have been proposed for smoothing the noisy data prior to reconstruction [4, 7]. A global smoothing scheme based on oversampling and post-filtering has been also proposed [6, 8]. Note that these reconstruction schemes are linear and they rely on oversampling for noise removal.

In this thesis, new techniques are developed for reconstruction of signals from noisy data that do not require oversampling, i.e., the signal is sampled at the Nyquist sampling rate. Specifically, it is shown that the nonlinear signal processing algorithm known as thresholding is an effective tool to deal with the problem of recovering signals from noisy data. The proposed sampling and reconstruction schemes are distinguished from those presented in [4, 5, 6, 7, 8] in the sense that they are nonlinear and they do not rely on oversampling for noise removal.

A class of sampling and reconstruction schemes are also proposed that utilize multiple observations and thresholding-based algorithms for recovering the signals. These techniques reduce the reconstruction error of the thresholding-based sampling and reconstruction schemes mentioned above. They also give better reconstruction accuracy than the oversampling/filtering methods, and in certain cases, reduce the amount of bits for representing and reconstructing the original signal.

In summary, the contributions of the thesis are listed below:

- Development of a new signal reconstruction scheme based on thresholding
- Development of a new signal reconstruction scheme based on adaptive thresholding
- Development of a thresholding-based sampling scheme that takes into account the effect of noise
- Development of a new sampling and reconstruction scheme based on multiple observations and thresholding
- Development of a thresholding-based multi-channel sampling scheme
- Error analysis of the above mentioned sampling and reconstruction schemes

1.2 Thesis Outline

The thesis is organized as follows. In Chapter 2, the problem of signal sampling and reconstruction, emphasizing signal reconstruction from noisy data is discussed. Chapter 3 and 4 introduce two new reconstruction schemes for recovering signals from noisy data without oversampling. The accuracy of the proposed reconstruction schemes is evaluated analytically and experimentally. Extending the results of Chapter 3, in Chapter 5, a new sampling scheme that takes into account the effect of noise is developed. Performance of this sampling scheme is studied analytically and experimentally. In Chapter 6, a new sampling and reconstruction scheme is presented which is based on multiple observations and thresholding. The theoretical performance analysis of the proposed scheme is also presented. Chapter 7 extends the results of Chapter 5 and introduces a thresholding-based multi-channel sampling scheme. The error analysis of this sampling scheme is also presented. Chapter 8 is conclusions and suggests further research.

Chapter 2

Signal Sampling and Reconstruction

2.1 The Whittaker-Shannon Sampling Theorem and Its Extensions

The sampling theorem first introduced to the engineering community in [2] is one of the most useful tools in the analysis of signals and their processing. It is a fundamental result that allows continuous-time signals to be processed digitally. It also provides the mean by which continuous-time signals can be reconstructed from their sampled values. The reconstruction formula that complements the sampling theorem is the formula (1.2) presented in the previous chapter. The theorem has been frequently referred to as the W-S sampling theorem in the signal processing literature because it was originated by J. M. Whittaker [1]. In the mathematical literature, (1.2) is known as the cardinal series expansion. Since its introduction, the W-S sampling theorem has been extended in many directions. A review of important developments is given

in this section.

Non-Uniform Sampling

The first important extension of the W-S sampling theorem is irregular (or non-uniform) sampling, where the samples $x(t_k)$ of a continuous-time signal $x(t)$ are acquired at non-equal intervals, i.e., $t_k \neq k\tau$. Non-uniform sampling appears in a number of practical applications. Some of examples are [18]:

- Non-uniform sampling is done intentionally for better representation of signals
- Missing data due to channel erasures (packets loss) or damages on physical storage mediums
- Uniform sampling with jitter
- Data read from and recorded on a tape or disk with speed fluctuations
- Data measured in a moving vehicle with fluctuations in speech
- Data tracked in digital flight control

For non-uniform sampling, the critical question to ask is how to select the set of sampling instants $\{t_k\}$ and the interpolating function so that the continuous-time signal $x(t)$ can be reconstructed uniquely from $\{x(t_k)\}$. In [19], Yen considered the case when the sampling points are divided into N groups. Each group has a recurrent period of $N/2W$, where W is the maximum frequency of the bandlimited function $x(t)$. He gave a formula for exactly recovering function $x(t)$ from its sampled values at $t = t_k + m\frac{N}{2W}$; $m = 0, \pm 1, \pm 2, ...$; $k = 1, 2, \cdots, N$. In [20], Beutler proved that a bandlimited signal $x(t)$ can be represented by any linear combination of irregularly spaced samples $x(t_k)$, provided that the average sampling rate exceeds the Nyquist

rate, i.e., the number of samples per a unit of time exceed (on average) twice the highest frequency of the signal. In [16], Jerri quoted Brown's condition on the non-uniform sampling set $\{t_k\}$ which allows a bandlimited function $x(t)$ to be uniquely determined from its samples $x(t_k)$ by:

$$x(t) = \sum_{k=-\infty}^{\infty} x(t_k)\varphi_k(t) \tag{2.1}$$

where, $\varphi_k(t)$ is a Lagrange interpolating function defined below [21]:

$$\varphi_k(t) = \frac{G(t)}{G'(t_k)(t - t_k)} \tag{2.2}$$

and,

$$G(z) = z\prod_{1}^{\infty}\left(1 - \frac{z^2}{t_k^2}\right) \tag{2.3}$$

The condition on the sampling set $\{t_k\}$ is that $\{e^{j\omega t_k}\}$ is a complete basis for the bandlimited signal in the frequency domain, i.e., any signals bandlimited to Ω can be represented in the frequency domain as:

$$X(\omega) = \sum_{k=-\infty}^{\infty} c_k e^{j\omega t_k}, \quad |\omega| < \Omega$$

An example of the sampling set $\{t_k\}$ that satisfies the above condition is [22]:

$$|t_k - k\tau_q| \leq d < \frac{1}{4} \tag{2.4}$$

where, $\tau_q = \pi/\Omega$ is the Nyquist sampling period. This result was known as the Kadec theorem. Note that the uniform sampling set considered in the W-S sampling theorem is a special case of (2.4) when $d = 0$.

References [13, 18] have a complete review and discussion on non-uniform sampling and its applications.

Papoulis's Generalization of the Sampling Theorem

Another important extension of the W-S sampling theorem is Papoulis's generalization of the sampling theorem. In [23], Papoulis proved that a band-limited signal can be reconstructed exactly from the output samples of N filters sampled at $1/N^{th}$ the Nyquist rate. He also gave examples showing that Yen's bunched sampling expansion [19] and signal-derivative sampling expansion [2, 24] are special cases of his generalized sampling theorem.

Sampling in Shift-Invariance Signal Spaces

The W-S sampling theorem is only applicable for reconstruction of the signals in bandlimited signal space. Recently, thanks in part to the recent developments in wavelet theory, the sampling theorem has been revisited and some important connections between the sampling theorem and wavelet theory has been established. Researchers have developed more general formulations of the sampling theorem that turn out to be quite practical from point of view of implementation. For instance, the W-S sampling theorem has been generalized to the shift-invariant signal spaces. The shift-invariant signal spaces are defined as follows [25].

$$V(\varphi) = \left\{ x : x(t) = \sum_{k \in \mathbb{Z}} c(k)\varphi(t-k) \right\} \tag{2.5}$$

where $c(k) \in l_2$ and $\varphi(t)$ is a known function.

The name "shift-invariant spaces" comes from the fact that if $x(t) \in V(\varphi)$, then $x(t-l) \in V(\varphi)$ for an arbitrary integer l. Signals that belong to shift-invariant signal spaces are not necessary bandlimited, but retain a certain structure that can be explored to design signal acquisition and reconstruction units [11]. These signal spaces may be more suitable for modeling the real-world signals than the bandlimited signal model since we have the freedom of choosing a suitable generating function $\varphi(t)$ for a practical problem [13].

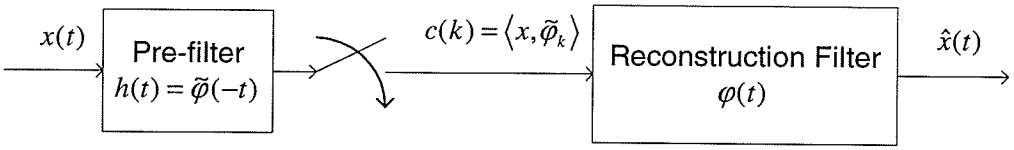

Figure 2.1: Signal sampling and reconstruction in shift-invariance signal space

For $x(t) \in L_2$, the least squared approximation of $x(t)$ in $V(\varphi)$ is given by [11],[26]:

$$\widehat{x}(t) = P_V x = \sum_{k \in \mathbb{Z}} \langle x, \widetilde{\varphi}_k \rangle \varphi(t-k) \tag{2.6}$$

where $\{\widetilde{\varphi}_k\}_{k \in \mathbb{Z}}$ is the dual basis of $\{\varphi_k\}_{k \in \mathbb{Z}}$ and is determined by the biorthogonality condition:

$$\langle \widetilde{\varphi}_k, \varphi_l \rangle = \delta_{k-l}$$

The dual basis $\widetilde{\varphi}_k$ belongs to $V(\varphi)$ and is unique. It also inherits the translation-invariant structure of the basic functions i.e. $\widetilde{\varphi}_k = \widetilde{\varphi}(t-k)$.

If $x(t) \in V(\varphi)$, then (2.6) is the exact representation of $x(t)$, i.e.

$$x(t) = \sum_{k \in \mathbb{Z}} \langle x, \widetilde{\varphi}_k \rangle \varphi(t-k), \quad \forall\, x \in V(\varphi) \tag{2.7}$$

Interestingly, due to the shift-invariant nature of the basis function and its dual, (2.6) can be simply implemented using a pre-filter, a sampler and a post-filter (reconstruction filter) as in Figure 2.1. The similarity between the model of Figure 2.1 with the traditional W-S sampling paradigm has been pointed out in [11]. Indeed, the traditional W-S sampling paradigm with an ideal anti-aliasing filter (ideal low-pass filter) following by a sampler and an ideal reconstruction filter (ideal low-pass filter) yields the approximation $\widehat{x}_{BL}(t) = P_V x$, where V is the space of band-limited functions. In other words, $\widehat{x}_{BL}(t)$ is the approximation of $x(t) \in L_2$ in the space of bandlimited functions with minimum mean squared error.

In summary, the advantages of representing L_2 signals (non-bandlimited signals) in shift-variant signal spaces are:

- Easy to implement. The procedure can be implemented in the similar manner with the traditional W-S sampling paradigm with an anti-aliasing filter, following by a sampler and a reconstruction filter.
- Flexibility to choose the pre-filter and reconstruction filter to fit with a particular application.

2.2 Error Analysis in Sampling Theory

When the W-S sampling theorem is utilized in practice, various sources of error may arise. This includes *truncation error* due to a finite number of samples available for signal reconstruction, *aliasing error* due to violation of bandlimited condition required by the W-S sampling theorem, *jitter error* due to jitter in the recording times $k\tau$, and *round-off* or *amplitude error* due to the uncertainty in measuring the magnitude of the signal's samples.

Truncation Error

Recall from (1.2) that the exact reconstruction of the original bandlimited signal requires the availability of an infinite number of samples. In practice, however, only a finite number of samples is available since the signal is often measured in a finite interval. The truncated version of the W-S sampling expansion in (1.2) is shown below:

$$x_n(t) = \sum_{k=-n}^{n} x(k\tau) \cdot \text{sinc}\left(\frac{t}{\tau} - k\right),$$

The truncation error is defined as [16, 27]:

$$e_n(t) = x(t) - x_n(t) = \sum_{|k|>n} x(k\tau) \cdot \text{sinc}\left(\frac{t}{\tau} - k\right), \tag{2.8}$$

Many authors have established the upper bounds on the truncation error of the W-S sampling expansion, see [16, 27, 28, 29] and the references cited herein. However, it is still unclear which bound is the best one in term of its tightness. For reference, the bound established in [27] is given:

$$|e_n(t)| \leq \frac{|\sin \omega_s t|}{\sqrt{\pi \omega_s}} \left\{ \left[\frac{1}{n\tau + t} \sum_{k=-\infty}^{-(n+1)} x^2(k\tau) \right]^{1/2} + \left[\frac{1}{n\tau - t} \sum_{k=n+1}^{\infty} x^2(k\tau) \right]^{1/2} \right\} \tag{2.9}$$

where $\omega_s = \pi/\tau$.

Aliasing Error

Another source of error is the aliasing error. It appears in practice when the signal's bandwidth is not known a priori or when the sampling frequency must be set smaller than the Nyquist sampling frequency due to limitation of electronic circuits or data storage capacity. Suppose that the sampled signal $x(t)$ is bandlimited to Ω with sampling frequency $\omega_s = \pi/\tau < \Omega$ and the W-S sampling theorem is applied to form the following signal:

$$x_A(t) = \sum_{k=-\infty}^{\infty} x(k\tau) \cdot \text{sinc}\left(\frac{t}{\tau} - k\right), \tag{2.10}$$

The aliasing error is defined as follows [27]:

$$e_A(t) = x_A(t) - x(t) \tag{2.11}$$

It was shown in [27] that $e_A(t)$ is upper bounded by:

$$|e_A(t)| \leq \frac{B}{2\pi} |\sin \omega_s t|, \tag{2.12}$$

where, $B = \int_{-\infty}^{\infty} |E_A(\omega)| d\omega$, and $E_A(\omega)$ is the Fourier transform of $e_A(t)$. Clearly, $e_A(t)$ is small if B is small, or equivalently, the portion of the spectrum of $x(t)$ above

ω_s is small. In [30], Brown showed that the aliasing error can be reduced by using a pre-filter, which is the ideal low-pass filter with cut-off frequency equal to the highest frequency of the signal, prior to the sampler. It is interesting to note that the aliasing error can be avoided under certain conditions and when non-uniform sampling is used [31, 32].

Jitter Error

The jitter error occurs when signal's samples are taken near but not exactly at the desired sample locations. In [27], Papoulis considered the problem of reconstruction of a band-limited signal $x(t)$ from the set of sampled values $\{x(k\tau - \mu_k)\}$, where μ_k are known jitter offsets of $k\tau$. He proposed a method that transforms $x(t)$ into another function $g(t')$ such that the nonuniform samples at $t_k = k\tau - \mu_k$ of $x(t)$ are mapped into uniform samples at $t'_k = k\tau$ of $g(t')$, i.e, $x(k\tau - \mu_k) = g(k\tau)$. His method involves the transformation of time variables as $t' = f(t)$. Consequently, $g(t')$ can be reconstructed from $g(k\tau)$ if $g(t')$ is bandlimited and $x(t)$ can be found from $g(t')$ if the transformation of time variables is one-to-one. Since $g(t')$ is not bandlimited in general, the reconstruction is not exact. However, the reconstruction error can be neglected if the jitter offsets μ_k are small. The reconstruction formula is:

$$x(t) = g(f(t)) \approx \sum_{k=-\infty}^{\infty} x(k\tau - \mu_k) \cdot \text{sinc}\left(\frac{f(t)}{\tau} - k\right) \tag{2.13}$$

Amplitude Error

The amplitude error appears when the measured samples are different from the samples of the original signal. Let $y(k\tau)$ be the measuring sampled values and $\varepsilon_k = y(k\tau) - x(k\tau)$ be the measuring errors. Consider the following reconstructed signal:

$$x_r(t) = \sum_{k=-\infty}^{\infty} y(k\tau) \cdot \text{sinc}\left(\frac{t}{\tau} - k\right), \tag{2.14}$$

The amplitude error is defined as [27]:

$$e_r(t) = x(t) - x_r(t) = \sum_{k=-\infty}^{\infty} \varepsilon_k \cdot \text{sinc}\left(\frac{t}{\tau} - k\right), \tag{2.15}$$

Papoulis showed in [27] that when ε_k are uncorrelated random variables with the same mean μ and variance σ^2, $e_r(t)$ is a wide-sense stationary process with mean and auto-covariance given by:

$$E[e_r(t)] = \mu \tag{2.16}$$

$$R(\Delta t) = \sigma^2 \cdot \text{sinc}(\frac{\Delta t}{\tau}) \tag{2.17}$$

Since the estimate $x_r(t)$ in (2.14) interpolates noise, it does not have noise-diminishing property, yielding a reconstruction that diverges [3]. In order to overcome this problem, a certain degree of data smoothing must be incorporated. This problem is studied in detail in section 2.4.

Stability or Well-Posedness

Since the amplitude error always occurs in practice, an important issue that must be addressed is the stability (or well-posedness) of sampling and reconstruction schemes. Here, a sampling and reconstruction scheme is considered stable if a small error in reading the sampled values produces only a small error in the recovered signal [33]. A class of bandlimited functions possesses a stable sampling expansion with respect to the sampling sequence $\{t_k\}$, if there exists a positive finite absolute constant C such that [33]:

$$\int_{-\infty}^{\infty} |x(t)|^2 dt \leq C \sum_k |x(t_k)|^2 \tag{2.18}$$

For example, a sampling sequence $\{t_k\}$ that satisfies (2.4) guarantees the stability of the sampling expansion given in (2.1). Since the uniform sampling sequence $\{t_k = k\tau\}$ is a special case of (2.4), the W-S sampling expansion is stable with respect to the

sampling sequence $\{t_k = k\tau\}$, provided that $\tau \leq \pi/\Omega$. It was shown in [34] that stable sampling can not be performed at a rate lower than the Nyquist rate, regardless of the location of sampling instants and method of reconstruction.

A sampling and reconstruction scheme, which is not stable, is called ill-posed [5]. Such a sampling and reconstruction scheme should be avoided in the practice. In [35], Cheung and Marks showed that a sufficient condition for a sampling expansion to be ill-posed is that there exists an interpolating function with infinite energy. An example of ill-posed sampling and reconstruction scheme is the signal-derivative sampling expansion [36]. In [37], Brown considered the well-posedness of the Papoulis's generalized sampling expansion. He proved that the condition for well-posedness of this sampling expansion is that all interpolating functions are square-integrable. As an example, he showed that the non-uniform sampling expansion proposed by Yen in [19] is well-posed.

Many studies have used the concept of stable sampling to measure the sensitivity of sampling and reconstruction schemes with respect to measurement errors [5, 38, 39, 40]. The measurement errors considered in those studies are deterministic in nature. In this thesis, however, random errors are considered.

2.3 Signal Reconstruction from Noisy Data

In many practical applications, noise is often contained in the observed samples. For instance, measurement, quantization and/or communication channel noises are potential noise sources. Given this situation, the degradation in reconstruction accuracy of the signal recovering algorithms primarily developed for the noiseless case have been reported. Some authors have studied the behavior of the reconstruction error when

random noise is taken into account.

In [41], the authors considered the class of bandlimited signals bounded by M, which can be represented as:

$$x(t) = \int_{-\Omega}^{\Omega} e^{j\omega t} dG(\omega) \tag{2.19}$$

where $G(\omega)$ is of bounded variation.

For this signal class, there exists a function $\theta(t)$ so that a signal $x(t)$ can be reconstructed perfectly from its regularly spaced samples by:

$$x(t) = \sum_{k=-\infty}^{\infty} x(k\tau)\theta(t - k\tau)$$

provided that $\tau \leq \pi/\Omega$.

In this study, an observation model similar to (1.3) was assumed:

$$y_k = x(k\tau) + \varepsilon_k, \qquad |k| \leq n$$

where ε_k are uncorrelated zero-mean additive noise samples having variance σ^2.

The authors studied the reconstruction error of the following signal recovery scheme, which is used to estimate $x(t)$ in the interval $|t| \leq \tau/2$.

$$\widehat{x}(t) = \sum_{k=-n}^{n} y_k \theta(t - k\tau) \tag{2.20}$$

The reconstruction error was defined as follows:

$$e(t) = x(t) - \widehat{x}(t) = e_c(t) + e_T(t) \tag{2.21}$$

where, $e_c(t) = \sum_{k=-n}^{n} \varepsilon_k \theta(t - k\tau)$ was called channel error and $e_T(t) = = \sum_{|k|>n} x(k\tau)\theta(t - k\tau)$ was called the truncation error.

The reconstruction mean-square error is:

$$E|e(t)|^2 = \sigma^2 \sum_{k=-n}^{n} \theta^2(t - k\tau) + [e_T(t)]^2$$

When using the self-truncating filter class given below for signal reconstruction

$$\theta(t) = \frac{\sin\Omega t(1-\delta)}{\Omega t(1-\delta)} \cdot \left[\frac{\sin[\delta\Omega t/(1-\delta)m]}{\delta\Omega t/(1-\delta)m}\right]^m \tag{2.22}$$

where m in any nonnegative integer (The $m = 0$ case is the W-S sampling threorem), the following upper bound of $E|e(t)|^2$ was found:

$$E|e(t)|^2 \leq M^2\left(\sin\frac{\pi t}{\tau}\right)^2 \frac{4}{\pi^2 m^2}\left[\frac{m}{\pi n\delta}\right]^{2m} + \sigma^2\left(\left[1-\frac{1}{3}\delta m^{-0.515}\right]\left[1-\cos\frac{2\pi t}{T}\right]+\cos\frac{2\pi t}{T}\right) \tag{2.23}$$

The first term in the RHS of (2.23) is the upper bound of $|e_T(t)|^2$, whereas the second term is the upper bound of $E|e_c(t)|^2$. For a given n and δ, there exists the optimal m that minimizes $E|e(t)|^2$.

In [42], the problem of reconstructing a finite-duration finite-energy (FDFE) signal that has been band limited and sampled was considered. An interpolation formula was derived that permits perfect signal reconstruction in the noiseless case, provided only that the sampling frequency exceeds the cut-off frequency of the band-limiting filter (i.e. one-half the Nyquist sampling rate). The degradation introduced by measurement noise on the samples was evaluated. The same observation model as assumed in (1.3) was considered.

Specifically, the author considered the class of signals defined below:

$$x(t) = x(t)\text{rect}(t/T) \tag{2.24}$$

with $E_0 = \int_{-T/2}^{T/2} x^2(t)dt < \infty$.

The signal $x(t)$ is passed through an ideal low-pass filter having cut-off frequency f_c. The output of the filter is:

$$z(t) = \int_{-T/2}^{T/2} x(\lambda)2f_c \cdot \text{sinc}[2f_c(t-\lambda)]d\lambda$$

The observed quantity was assumed to be the noisy samples $y_k = z(k\tau) + \varepsilon_k$ of $z(t)$, where ε_k denotes additive noise samples and $f_s = 1/\tau$ is the sampling rate.

Only requiring $f_c < f_s < 2f_c$ (i.e. the sampling frequency is smaller than the Nyquist rate required by the W-S sampling theorem), the author introduced the following interpolation formula for recovering $x(t)$ from y_k:

$$\widehat{x}_N(t) = \tau \sum_{i=0}^{N} \sum_{k=-\infty}^{\infty} y_k \phi_i(k\tau)\phi_i(t), \qquad |t| < T/2 \tag{2.25}$$

where $\{\phi_i\}$ is a complete orthogonal set over the interval $(-T/2, T/2)$, which is chosen to be the solutions to the integral equation:

$$\int_{-T/2}^{T/2} \phi_i(\nu) 2f_1 \cdot \mathrm{sinc}[2f_1(t-\nu)]d\nu = \lambda_i \phi_i(t)$$

where,

$$f_1 = \begin{cases} f_s - f_c & \text{if} \quad f_c < f_s < 2f_c \\ \\ f_c & \text{if} \quad f_s \geq 2f_c. \end{cases}$$

The solution to the above equation are given by:

$$\phi_i(c,t) = \left[S_{oi}\left(c, \frac{t}{0.5\ T}\right)\right] \Big/ u_i(c)$$

$$\lambda_i(c) = (2c/\pi)[R^1_{oi}(c,1)]^2$$

where

$$[u_i(c)]^2 = \int_{-T/2}^{T/2} \left[S_{oi}\left(c, \frac{t}{0.5\ T}\right)\right]^2 dt$$

The function $S_{oi}(c, t/\alpha)$ is the angular prolate spheroidal wave function; $R^1_{oi}(c,1)$ is the radial prolate spheroidal wave function; and $c = \pi f_1 T$.

The reconstruction error was found to be:

$$\frac{1}{T}\int_{-T/2}^{T/2} E[e_N^2(t)]dt = \frac{\tau\sigma^2}{T} \sum_{i=0}^{N} \frac{1}{\lambda_i(c)} \tag{2.26}$$

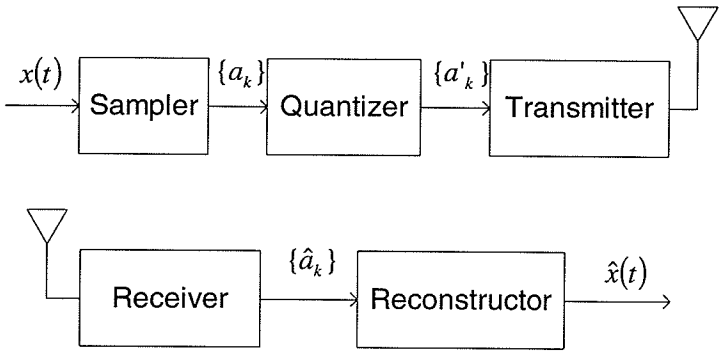

Figure 2.2: A system for digital transmission of analog waveforms

where,

$$e_N(t) = \tau \sum_{i=0}^{N} \sum_{k=-\infty}^{\infty} \varepsilon_k \phi_i(k\tau)\phi_i(t), \qquad |t| < T/2$$

In [43], the reconstruction error in digital transmission of analog signals was investigated. The system illustrated in Figure 2.2 was considered. The signal was assumed to be a sample function of a random process, which is represented as follows.

$$x(t) = \sum_{k=1}^{\infty} a_k \phi_k(t) \tag{2.27}$$

where a_k are the generalized Fourier coefficients and $\{\phi_k(t)\}$ is an arbitrary set of orthogonal (over time interval I) basic functions.

The mean-integral-square error between the original signal $x(t)$ and the reconstructed signal $x_r(t)$ was defined as:

$$\epsilon^2 = E \int_I [x(t) - \widehat{x}(t)]^2 dt \tag{2.28}$$

In this study, three sources of error were taken into account: approximation error ϵ_a^2 incurred by representing the waveform by a finite number of samples; quantization error ϵ_q^2 incurred by quantizing samples and channel error ϵ_c^2 due to an incorrect decision made at the receiver. It was shown that when the quantization is optimally performed, the reconstruction error can be expressed as the summation of the above

mentioned errors, each of them is independent from the others, i.e.

$$\epsilon^2 = \epsilon_a^2 + \epsilon_q^2 + \epsilon_c^2 \tag{2.29}$$

where,

$$\epsilon_a^2 = E\int_I \left[x(t) - \sum_{k=1}^{n} a_k\phi_k(t)\right]^2 dt$$

$$\epsilon_q^2 = E\int_I \left[\sum_{k=1}^{n} a_k\phi_k(t) - \sum_{k=1}^{n} a'_k\phi_k(t)\right]^2 dt = E\sum_{k=1}^{n}(a_k - a'_k)^2$$

$$\epsilon_c^2 = E\int_I \left[\sum_{k=1}^{n} a'_k\phi_k(t) - \sum_{k=1}^{n} \widehat{a}_k\phi_k(t)\right]^2 dt = E\sum_{k=1}^{n}(a'_k - \widehat{a}_k)^2$$

In [5], a detailed noise sensitivity analysis of the W-S interpolation formula and other sampling schemes was presented. The author pointed out that oversampling can reduce the interpolation noise variance by allowing suppression of high frequency noise components. Interestingly, he also suggested that there may exist an optimal sampling rate that minimizes the overall mean square error, which is the summation of truncation error and the error due to noisy data. More recent studies that address the noise sensitivity of various sampling schemes are [38, 39, 44, 45].

Finally, let us conclude this section by saying that even though the importance of the problem of signal sampling and recovering in the presence of noise is obvious, this problem has not been received much attention in the signal processing literature. Very few studies have considered this problem as the main subject. Rather, it was considered as a minor subject to the sampling results derived under the noise-free assumption. The studies that are reviewed in the next section are, in the author's opinion, the only ones that consider this problem seriously. Very often, a signal representation which is exact for the noise-free case will not work for the noisy case, and over-modelling of signals results in lack of robustness.

2.4 Signal Reconstruction from Noisy Data with Smoothing Corrections

The preceding section has reviewed studies that address the problem of signal reconstruction from noisy data. It was clear that degradation in reconstruction accuracy is noticed when noise is taken into account. Nevertheless, no specific methods have been proposed to improve the reconstruction accuracy. Recent studies have shown that the reconstruction accuracy of the classical W-S interpolation scheme can be improved by incorporating some smoothing schemes [3, 4, 5, 6, 7, 8]. In these studies, the observation model of (1.3) was assumed:

$$y_k = x(k\tau) + \varepsilon_k = x_k + \varepsilon_k, \qquad |k| \leq n,$$

where $x(k\tau)$ are sampled values of the signal and ε_k are noise's samples.

In this section, the results reported in these studies are reviewed.

2.4.1 Signal Reconstruction by Data Smoothing and Interpolation

In [4], the following reconstruction scheme was proposed for improving the accuracy of the standard W-S interpolation scheme in (1.4) when noise is taken into account:

$$\breve{x}(t) = \sum_{|k|\leq N} \breve{y}_k \cdot \mathrm{sinc}\left(\frac{t}{\tau} - k\right) \tag{2.30}$$

where,

$$\breve{y}_k = \sum_{|i|\leq M} w_i y_{k-i}, \qquad k = 0, \pm 1, \pm 2, ..., \pm N \tag{2.31}$$

Here, $\{w_i\}$ is a set of weights satisfying $\sum_{|i|\leq M} w_i = 1$. Note that parameters M and N are related to each other by $M + N = n$. The block diagram of this reconstruction

scheme is illustrated in Figure 2.3.

Consider the simplest case where uniform weights $w_i = 1/(2M+1)$ are chosen. With this choice of weights, $\{\breve{y}_k\}$ is the moving average (MA) of $\{y_k\}$. It has been shown that:

$$IVAR(\breve{x}) = \tau\sigma^2 \frac{2N+1}{2M+1} \tag{2.32}$$

Since $\frac{2N+1}{2M+1} \leq (2n+1)$, $IVAR(\breve{x}) \leq IVAR(\widetilde{x})$. Here, $IVAR(\widetilde{x})$ is the IVAR of the standard W-S interpolation scheme defined in (1.4). The equality holds for $M = 0$. In this case, $\breve{x}(t)$ and $\widetilde{x}(t)$ are identical. $IVAR(\breve{x})$ can be reduced by increasing M. However, this results in increasing $IBIAS(\breve{x})$. Therefore, there exists the optimum M for which $MISE(\breve{x})$ is minimum. This optimum M was not found in [4]. Nevertheless, the provided simulation results confirmed the existence of the optimum M.

For general weights, one can show that:

$$IVAR(\breve{x}) = \tau\sigma^2(2N+1)\sum_{|i|\leq M} w_i^2 \tag{2.33}$$

There is still an open problem on finding the optimum weights w_i so that $\sum_{|i|\leq M} w_i^2$ is minimum under certain constraints. More detailed discussion on that issue can be found in [4].

The convergent property of this reconstruction scheme was also studied in [4]. It was shown in this paper that $\breve{x}(t)$ converges to $x(t)$ if τ depends on n in such a way that $n\tau_n \to \infty$ and $\tau_n \to 0$ as $n \to \infty$. Interestingly, there exists the optimal τ_n that

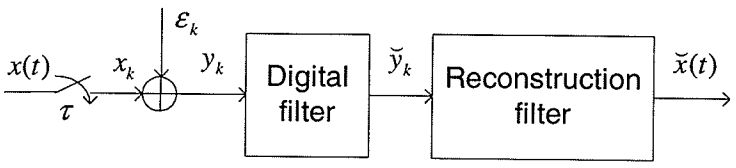

Figure 2.3: Signal reconstruction by data smoothing and interpolation

minimizes $MISE(\breve{x})$.

2.4.2 Signal Reconstruction by Oversampling and Post-Filtering

In [8], the reconstruction scheme of the following type was proposed:

$$\breve{\breve{x}}(t) = \sum_{|k|\leq n} y_k \cdot \mathrm{sinc}\left(\frac{t}{\tau} - k\right) * h(t) \tag{2.34}$$

where, $\tau \leq \tau_q = \pi/\Omega$ and $h(t)$ is the impulse response of the post-filter. The block diagram of this reconstruction scheme is illustrated in Figure 2.4.

Since $x(t)$ is bandlimited to Ω, the post-filter should be selected to be an ideal low-pass filter with cutoff frequency Ω, i.e., its impulse response is given by $h(t) = \tau_q^{-1}\mathrm{sinc}(t/\tau_q)$. With this choice of $h(t)$, one has the following estimate:

$$\breve{\breve{x}}(t) = \frac{\tau}{\tau_q} \sum_{|k|\leq n} y_k \cdot \mathrm{sinc}\left(\frac{t}{\tau_q} - k\frac{\tau}{\tau_q}\right) \tag{2.35}$$

It can be shown that:

$$IVAR(\breve{\breve{x}}) = \tau\sigma^2(2n+1)\frac{\tau}{\tau_q} \tag{2.36}$$

When $\tau = \tau_q$, $IVAR(\breve{\breve{x}}) = IVAR(\widetilde{x})$ and noise reduction can not be achieved. Therefore, the reconstruction scheme in (2.35) relies on oversampling for noise removal.

From (2.36) and (1.10), one has:

$$\frac{IVAR(\widetilde{x})}{IVAR(\breve{\breve{x}})} = \frac{\tau_q}{\tau} \geq 1 \tag{2.37}$$

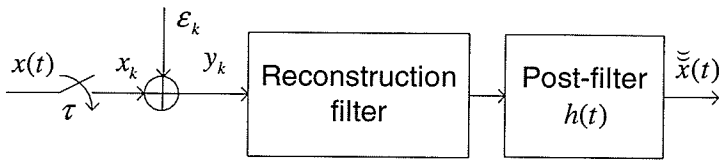

Figure 2.4: Signal reconstruction by oversampling and post-filtering

Thus, the reconstruction scheme in (2.35) reduces the IVAR of the W-S interpolation scheme in (1.4) by a factor equal to oversampling factor (OSF) τ_q/τ.

The convergent property of this reconstruction scheme was also studied in [8]. It was shown in this paper that $\breve{\breve{x}}(t)$ converges to $x(t)$ if τ depends on n in such a way that $n\tau_n \to \infty$ and $\tau_n \to 0$ as $n \to \infty$. Interestingly, there exists an optimal τ_n that minimizes $MISE(\breve{\breve{x}})$.

The estimate $\breve{\breve{x}}(t)$ in (2.35) and $\breve{x}(t)$ in (2.30) are similar in the sense that they rely on oversampling and smoothing for noise reduction. The difference between these two estimates is that the estimate $\breve{\breve{x}}(t)$ is a global smoothing scheme, whereas the estimate $\breve{x}(t)$ is a local smoothing scheme. The performance and the convergent properties of these estimates were compared in [46]. It was concluded that for the class of band-limited signals the estimate $\breve{\breve{x}}(t)$ gives better reconstruction accuracy than the estimate $\breve{x}(t)$.

2.4.3 Signal Reconstruction via Orthogonal Expansion

It is well-known that (1.2) can be re-written as following:

$$x(t) = \sum_{k=-\infty}^{\infty} c_k s_k(t) \tag{2.38}$$

where,

$$c_k = \frac{1}{h} \int_{-\infty}^{\infty} x(t) s_k(t) dt \tag{2.39}$$

and $s_k(t) = \text{sinc}(t/h - k), \quad k = 0, \pm 1, \pm 2, ...$ defines the orthogonal and complete system in $\text{BL}(\Omega)$ if $h \leq \pi/\Omega$. Note that h^{-1} is called the reconstruction rate and is different from sampling rate τ^{-1}.

Using the above interpretation of the classical W-S interpolation formula, the

following reconstruction scheme was proposed in [3].

$$\dot{x}(t) = \sum_{|k|\leq N} \bar{c}_k s_k(t) \tag{2.40}$$

where

$$\bar{c}_k = \frac{1}{h} \sum_{|j|\leq n} y_j \int_{A_j} s_k(z)dz \tag{2.41}$$

and $A_j = ((2j-1)/2)\tau, (2j-1)/2)\tau)$.

Hence, the estimate $\dot{x}(t)$ relies on (2.38) with c_k replaced by the piecewise constant approximation of integral $\int_{-\infty}^{\infty} x(t)s_k(t)dt$ and with the truncation of the series in (2.38). The integral $\int_{A_j} s_k(z)dz$ in (2.41) can be evaluated numerically. The simplest strategy is to use a middle point approximation, i.e. to replace $\int_{A_j} s_k(z)dz$ by $\tau s_k(j\tau)$. This yields the following estimate of $x(t)$:

$$\ddot{x}(t) = \sum_{|k|\leq N} \bar{\bar{c}}_k s_k(t) \tag{2.42}$$

where,

$$\bar{\bar{c}}_k = \frac{\tau}{h} \sum_{|j|\leq n} y_j s_k(j\tau) \tag{2.43}$$

In order to transform the estimates $\dot{x}(t)$ in (2.40) and $\ddot{x}(t)$ in (2.42) into implementable forms, re-write (2.41) and (2.43) as follows:

$$\bar{c}_k = \sum_{|j|\leq n} w_j y_j \tag{2.44}$$

where, weights w_j in (2.44) are computed as follows:

$$w_j = \frac{1}{h} \int_{A_j} s_k(z)dz \tag{2.45}$$

and,

$$\bar{\bar{c}}_k = \sum_{|j|\leq n} w_j y_j \tag{2.46}$$

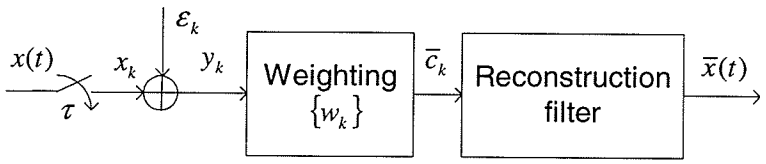

Figure 2.5: Signal reconstruction via orthogonal expansion

where, weights w_j in (2.46) are computed as follows:

$$w_j = \frac{\tau}{h} s_k(j\tau) \tag{2.47}$$

Now, the estimates $\dot{x}(t)$ in (2.40) and $\ddot{x}(t)$ in (2.42) can be implemented in a similar manner as the estimate $\breve{x}(t)$ in (2.30), see Figure 2.5.

It was shown in [3] that:

$$IVAR(\dot{x}) = h \sum_{|k|\leq N} \text{var}(\bar{c}_k) \tag{2.48}$$

where,

$$\text{var}(\bar{c}_k) = \sigma^2 h^{-2} \sum_{|j|\leq n} \left(\int_{A_j} s_k(z) dz \right)^2 \tag{2.49}$$

And,

$$IVAR(\ddot{x}) = h \sum_{|k|\leq N} \text{var}(\bar{\bar{c}}_k) \tag{2.50}$$

where,

$$\text{var}(\bar{\bar{c}}_k) = \sigma^2 \frac{\tau^2}{h^2} \sum_{|j|\leq n} s_k^2(j\tau) \tag{2.51}$$

The convergence of the estimates $\dot{x}(t)$ and $\ddot{x}(t)$ requires that τ depend on n in such a way that $n\tau_n \to \infty$ and $\tau_n \to 0$ as $n \to \infty$. It was also pointed out that both estimates attain the same asymptotic rate of convergence even though the tighter upper bound on MISE of $\dot{x}(t)$ has been derived. Interestingly, there exists optimum values of τ_n and N that minimize the upper bound of $MISE(\dot{x})$ and $MISE(\ddot{x})$. More detailed discussion on these estimates and their properties can be found in [3].

Chapter 3

Signal Reconstruction by Thresholding

3.1 Introduction

In this chapter, we introduce a modification of the W-S interpolation formula to deal with noisy data, i.e., we assume the observation model of equation (1.3). Recall that the signal reconstruction methods discussed in Section 2.4 of the previous chapter require oversampling for noise reduction. Therefore, these methods are not suitable for some practical applications where the use of a high sampling frequency is not allowed. In this chapter, the objective is to develop a new signal reconstruction scheme for recovering signals from noisy data without oversampling, which reduces the MISE of the classical W-S interpolation scheme given by equation (1.4).

To achieve the above objective, the observed data set is transformed nonlinearly into another data set prior to signal reconstruction. Specifically, when the magnitudes of the observed samples are large (signal component dominates the noise component), those samples are unchanged. On other hand, when the magnitudes of the observed

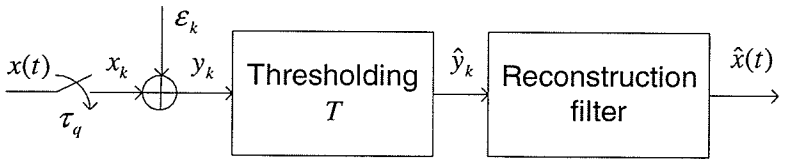

Figure 3.1: Signal reconstruction by thresholding

samples are small (the noise component dominates the signal component), they are set to zero. This is justified by looking at the signal-to-noise ratio (SNR). Hence, this implements a thresholding scheme on the noisy data. The proposed reconstruction scheme consists of two steps as follows:

Step 1: Threshold the noisy sampled values to obtain:

$$\widehat{y}_k = \begin{cases} y_k & \text{if} \quad |y_k| > T \\ \\ 0 & \text{if} \quad |y_k| \leq T. \end{cases} \tag{3.1}$$

where, T is a threshold level. Its value is to be determined later.

Step 2: Use the $\{\widehat{y}_k\}$ found above to form the following estimate:

$$\widehat{x}(t) = \sum_{|k| \leq n_q} \widehat{y}_k \cdot \text{sinc}\left(\frac{t}{\tau_q} - k\right) \tag{3.2}$$

The block diagram of the proposed scheme is shown in Figure 3.1

The idea of using thresholding for removal of noise is well-known in wavelet literature [47, 48, 49]. Unlike wavelet thresholding procedures where wavelet coefficients are thresholded, in the proposed reconstruction scheme, thresholding is applied directly to the plain data, which is a sequence of noisy signal's samples.

The subsequent section presents the error analysis of the proposed reconstruction scheme. The influence of threshold level on the performance of the proposed reconstruction scheme is also investigated. Some simulation results are provided to verify the theoretical results.

3.2 Error Analysis

The following theorem gives an exact formula for computing the MISE of the proposed reconstruction scheme. The proof of the theorem is given in the Appendix A.

Theorem 3.1. *Consider the observation model of (1.3), where ε_k are independent Gaussian random variables with zero mean and variance σ^2. The MISE of estimate $\widehat{x}(t)$ of (3.2) is given by:*

$$MISE(\widehat{x}) = \tau_q \sigma^2 (2n_q + 1) + \tau_q \sum_{|k|>n_q} x_k^2 - \tau_q \sigma^2 D, \tag{3.3}$$

with,

$$\begin{aligned} D &= f(x_k, \sigma^2, T) \\ &= \sum_{\substack{|k|\le n_q \\ x_k < -T}} \frac{1}{\sqrt{\pi}} \left[\gamma\left(\frac{3}{2}, \frac{(x_k - T)^2}{2\sigma^2}\right) - \gamma\left(\frac{3}{2}, \frac{(x_k + T)^2}{2\sigma^2}\right) \right] \\ &\quad + \sum_{\substack{|k|\le n_q \\ |x_k| \le T}} \frac{1}{\sqrt{\pi}} \left[\gamma\left(\frac{3}{2}, \frac{(x_k - T)^2}{2\sigma^2}\right) + \gamma\left(\frac{3}{2}, \frac{(x_k + T)^2}{2\sigma^2}\right) \right] \\ &\quad + \sum_{\substack{|k|\le n_q \\ x_k > T}} \frac{1}{\sqrt{\pi}} \left[\gamma\left(\frac{3}{2}, \frac{(x_k + T)^2}{2\sigma^2}\right) - \gamma\left(\frac{3}{2}, \frac{(x_k - T)^2}{2\sigma^2}\right) \right] \\ &\quad - \sum_{|k|\le n_q} \frac{x_k^2}{\sigma^2} \left[\frac{1}{2}\mathrm{erf}\left(\frac{x_k + T}{\sigma\sqrt{2}}\right) - \frac{1}{2}\mathrm{erf}\left(\frac{x_k - T}{\sigma\sqrt{2}}\right) \right], \end{aligned} \tag{3.4}$$

where, $\gamma(\alpha, x)$ and $\mathrm{erf}(x)$ are the incomplete gamma function and error function, respectively [50].

Remark 3.1. The MISE of the classical W-S interpolation scheme of (1.4) can be expressed as follows [3]:

$$MISE(\widetilde{x}) = \tau_q \sigma^2 (2n_q + 1) + \tau_q \sum_{|k|>n_q} x_k^2$$

Thus, (3.3) can be re-written as:

$$MISE(\widehat{x}) = MISE(\widetilde{x}) - \tau_q \sigma^2 D, \tag{3.5}$$

If the second term in the RHS of (3.5) is positive, it represents the degree of noise reduction of the proposed estimate. By setting threshold level properly, we can make $D > 0$.

The following theorem confirms the existence of the optimal threshold level that minimizes the MISE of the proposed reconstruction scheme. The proof of the theorem is given in Appendix A. Since in the proof, it is not assumed that ε_k have a Gaussian distribution, the theorem is valid for arbitrary distributions.

Theorem 3.2. *Consider the observation model of (1.3), where ε_k are independent random variables with zero mean and variance σ^2. For a given signal $x(t)$ and noise variance σ^2, there always exists the optimal threshold level T_{opt} so that the MISE of estimate $\widehat{x}(t)$ of (3.2) is minimum.*

The following theorem gives exact formulas for computing the IBIAS and IVAR of the proposed reconstruction scheme. The proof of the theorem is given in the Appendix A.

Theorem 3.3. *Consider the observation model of (1.3), where ε_k are independent Gaussian random variables with zero mean and variance σ^2. The IBIAS and the IVAR of estimate $\widehat{x}(t)$ of (3.2) are given by:*

$$IBIAS(\widehat{x}) = \tau_q \sum_{|k|\le n_q} d_k^2 + \tau_q \sum_{|k|>n_q} x_k^2, \tag{3.6}$$

$$IVAR(\widehat{x}) = \tau_q \sigma^2 (2n_q + 1) - \tau_q \sum_{|k|<n_q} d_k^2 - \tau_q \sigma^2 D, \tag{3.7}$$

where D is given in (3.4) and

$$\begin{aligned} d_k &= \frac{\sigma}{\sqrt{2\pi}} \left[e^{-(x_k+T)^2/2\sigma^2} - e^{-(x_k-T)^2/2\sigma^2} \right] \\ &\quad + \frac{x_k}{2} \left[\operatorname{erf}\left(\frac{x_k+T}{\sigma\sqrt{2}} \right) - \operatorname{erf}\left(\frac{x_k-T}{\sigma\sqrt{2}} \right) \right]. \end{aligned} \tag{3.8}$$

3.3 Choice of Threshold Level

In this section, the influence of the choice of threshold level on the reconstruction accuracy of the proposed reconstruction scheme is investigated. In particular, it is shown how the threshold level can be optimally pre-determined during the data acquisition process. A sub-optimal criteria for setting threshold level is suggested.

3.3.1 Pre-Determination of the Optimal Threshold Level

Theorem 3.2 shows that there exists the optimal threshold level that minimizes the MISE of the proposed reconstruction scheme. Moreover, Theorem 3.1 gives an exact formula for computing the MISE of the proposed reconstruction scheme. Since the first two terms in the RHS of (3.3) do not depend on threshold level T, one concludes that the optimal threshold level is the value of T, at which the term D defined in (3.4) is maximum.

The Figure 3.3, Figure 3.4, and Figure 3.5 plot D as a function of T for various values of E_0/σ^2. The following test signal was used:

$$x_1(t) = \frac{1}{\sqrt{\pi\Omega}} \cdot \frac{\sin \Omega t}{t} \tag{3.9}$$

where $\Omega = 2\pi f_{max}$ is the radian frequency and $f_{max} = 3900$ Hz. Here, $x_1(t)$ is a unit energy $BL(\Omega)$ signal. The existence of the optimal threshold level is clearly seen.

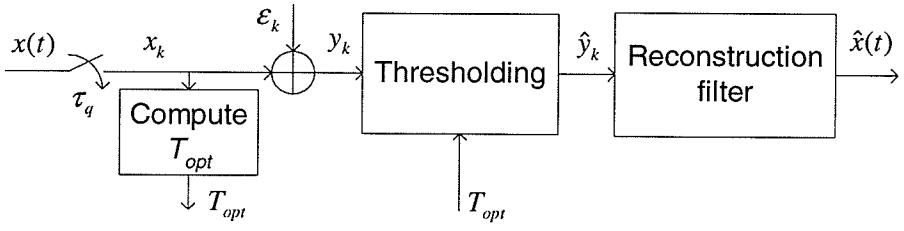

Figure 3.2: Signal reconstruction using the optimally pre-determined threshold level

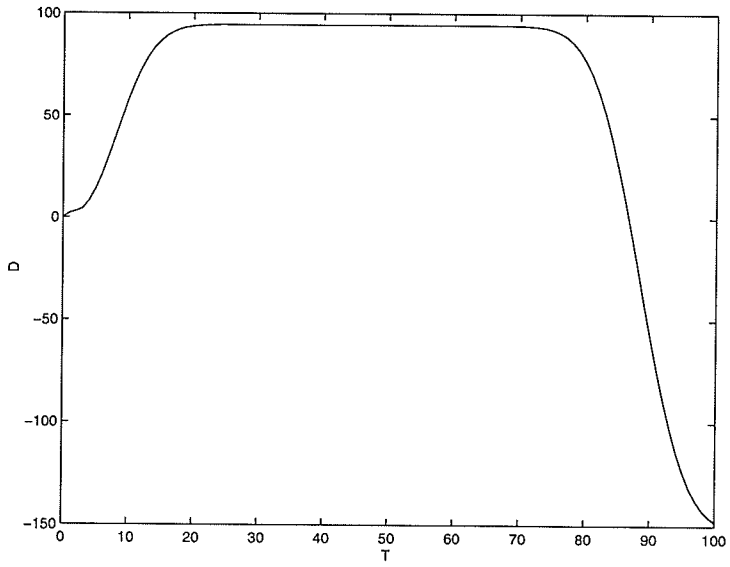

Figure 3.3: D versus T $(E_0/\sigma^2 = -15dB)$

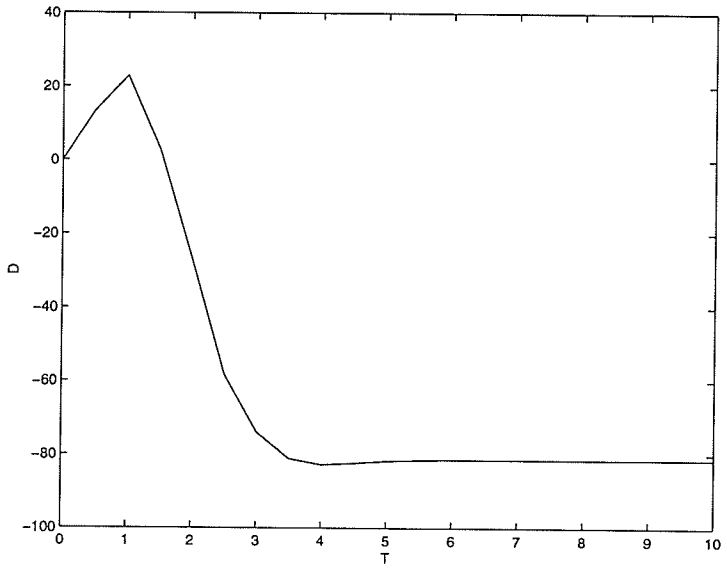

Figure 3.4: D versus T $(E_0/\sigma^2 = 0dB)$

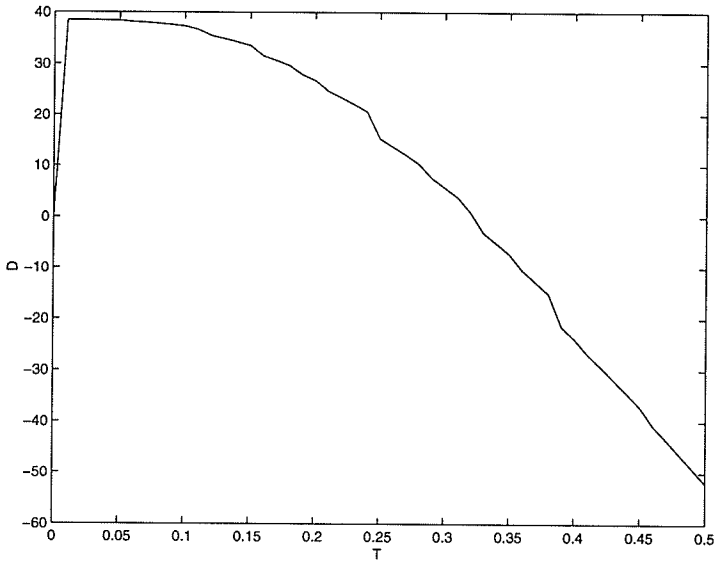

Figure 3.5: D versus T ($E_0/\sigma^2 = 15dB$)

The plots also indicate that when SNR is low, the reconstruction accuracy of the proposed signal recovering scheme is not sensitive to the mismatch in identifying the optimal threshold level. In fact, the threshold level can be set within a relatively wide range, without effecting the reconstruction accuracy. In contrast, when SNR is high, the reconstruction accuracy becomes sensitive to the error in identifying the optimal threshold level. Nevertheless, when SNR is high, the classical W-S interpolation scheme already gives a reasonable reconstruction precision and one may want to simply set $T = 0$. If more accurate reconstruction is desired, then care has to be taken in order to correctly identify the optimal threshold level. Even though the above observations are made based on a specific example, it is conjectured that these

Table 3.1: The optimal threshold levels for various E_0/σ^2

E_0/σ^2 (dB)	-25	-20	-15	-10	-5	0	5	10	15
T_{opt}	60.40	49.00	46.10	30.00	17.68	1.00	0.10	0.05	0.01

observations are applied to other signals as well.

The term D can be pre-computed during the data acquisition process and the optimal threshold level T_{opt} can be pre-determined accordingly. T_{opt} is considered as the side information and can be made available for signal reconstruction by various methods. Table 3.1 shows the optimal threshold levels T_{opt} for various values of E_0/σ^2. The test signal $x_1(t)$ defined in (3.9) was considered. It is observed from the table that the optimal threshold level increases as noise variance increases, and decreases as noise variance decreases. If $\sigma^2 \to 0$, then $T_{opt} \to 0$.

The corresponding block diagram of the proposed scheme is shown in Figure 3.2.

3.3.2 A Sub-Optimal Criteria for Setting Threshold Level

Reconstruction of the signal using the optimal threshold level requires pre-determination of T_{opt} and a mechanism for delivering T_{opt} to the receiver. Therefore, a sub-optimal method is suggested where the threshold level T is set adaptively to the noise variance. For instance, one may set $T = \sigma\sqrt{a}$, where a is the parameter used to control the reconstruction accuracy. In order to investigate the dependence of $MISE(\widehat{x})$ on parameter a, the following theorem is established. The proof of the theorem is given in Appendix A.

Theorem 3.4. *Consider the observation model in (1.3), where ε_k are independent Gaussian random variables with zero mean and variance σ^2. The MISE of estimate $\widehat{x}(t)$ in (3.2) is upper bounded by:*

$$\begin{aligned} MISE(\widehat{x}) \;\leq\; & \tau_q\sigma^2\left[1-\frac{2}{\sqrt{\pi}}\gamma\left(\frac{3}{2},\frac{T^2}{2\sigma^2}\right)\right](2n_q+1) \\ & + \operatorname{erf}\left(\frac{T}{\sigma\sqrt{2}}\right)E_0 + \left(\tau_q\sum_{|k|>n_q}x_k^2\right)\operatorname{erfc}\left(\frac{T}{\sigma\sqrt{2}}\right) \end{aligned} \tag{3.10}$$

where, $E_0 = \tau_q\sum_{|k|\leq\infty}x_k^2 = \int_{-\infty}^{\infty}x^2(t)dt$ is the signal's energy.

Re-write (3.10) as the following:

$$\begin{aligned} MISE(\widehat{x}) \;\leq\; & \tau_q\sigma^2(2n_q+1) + \tau_q \sum_{|k|>n_q} x_k^2 \\ & - \tau_q\sigma^2(2n_q+1)\left[\frac{2}{\sqrt{\pi}}\gamma\left(\frac{3}{2},\frac{T^2}{2\sigma^2}\right) - \frac{\sum_{|k|\leq n_q} x_k^2}{\sigma^2(2n_q+1)}\text{erf}\left(\frac{T}{\sigma\sqrt{2}}\right)\right] \end{aligned}$$

Let

$$f(G_n,T) = \frac{2}{\sqrt{\pi}}\gamma\left(\frac{3}{2},\frac{T^2}{2\sigma^2}\right) - G_n\text{erf}\left(\frac{T}{\sigma\sqrt{2}}\right) \tag{3.11}$$

where,

$$G_n \triangleq \frac{\frac{1}{2n_q+1}\sum_{|k|\leq n_q} x_k^2}{\sigma^2}, \tag{3.12}$$

The preceding inequality can be re-written as follows:

$$MISE(\widehat{x}) \leq \tau_q\sigma^2(2n_q+1) + \tau_q \sum_{|k|>n_q} x_k^2 - \tau_q\sigma^2(2n_q+1)f(G_n,T)$$

or,

$$\Delta \triangleq MISE(\widetilde{x}) - MISE(\widehat{x}) \geq \tau_q\sigma^2(2n_q+1)f(G_n,T) \tag{3.13}$$

where, $MISE(\widetilde{x})$ is the MISE of the classical W-S interpolation scheme in (1.4).

Consequently, to maximize Δ, one has to choose T such that $f(G_n,T)$ is maximum. Figure 3.6 plots $f(G_n,a)$ as a function of a for various values of G_n, where a relates to T by $T=\sigma\sqrt{a}$. Here, parameter a is used to control the reconstruction accuracy.

The following conclusions can be drawn from the plot:

- For $G_n \geq 1$, one should select $T=0$. In this case, the W-S interpolation scheme in (1.4) yields better reconstruction accuracy than the proposed reconstruction scheme with a sub-optimal threshold level.

- For $G_n < 1$, $T=0$ is no longer the best choice. In fact, one should select $3\sigma \leq T \leq 5\sigma$. In this case, the proposed reconstruction scheme with a

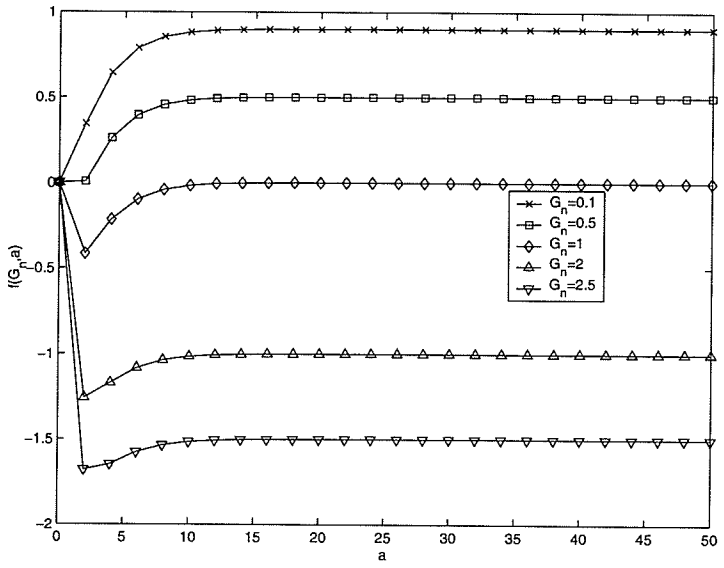

Figure 3.6: $f(G_n, a)$ versus a

sub-optimal threshold level yields better reconstruction accuracy than the W-S interpolation scheme.

Taking the above observation into account, the following joint detection/estimation scheme for reconstruction of bandlimited signals from noisy data is proposed:

Step 1: Estimate $P \triangleq \sum_{|k|\leq n_q} x_k^2$ from the data. Compute G_n using the estimated P

Step 2: If $G_n \geq 1$, set $T = 0$. Otherwise, set $T \in [3\sigma, 5\sigma]$.

Step 3: Use the 2-step reconstruction procedure described in Section 3.1 to recover the signal.

Remark 3.2. For n_q sufficiently large and/or for fast decay functions, $MISE(\widetilde{x}) \approx \tau_q \sigma^2 (2n_q + 1)$. Hence, (3.13) can be re-written as follows:

$$R = \frac{MISE(\widehat{x})}{MISE(\widetilde{x})} \leq 1 - f(G_n, T) = 1 - f\left(\frac{E_0}{\tau_q \sigma^2 (2n_q + 1)}, T\right). \tag{3.14}$$

Figure 3.7 plots the right-hand side of (3.14) as the function of E_0/σ^2 when the duration of measurement $\tau_q(2n_q + 1) = 1$ second, for $T = 0$ and $T = 4\sigma$,

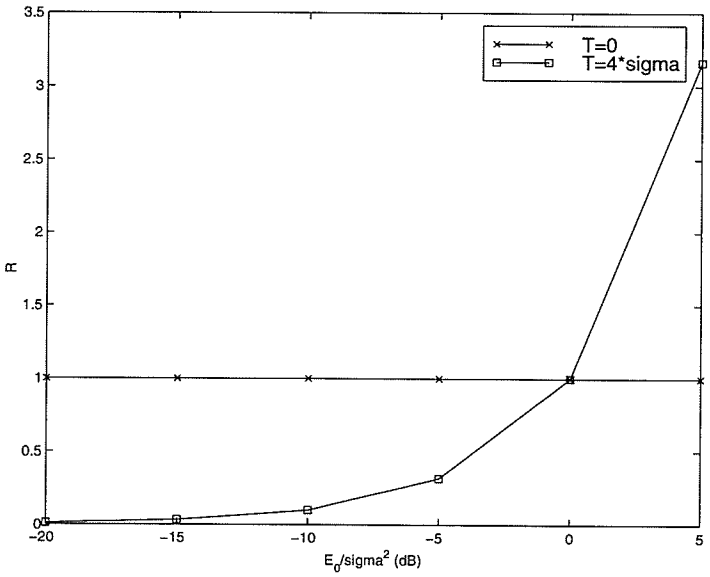

Figure 3.7: Upper bound of R versus E_0/σ^2

respectively. The plot clearly shows the advantage of using the thresholding-based reconstruction scheme with a sub-optimal threshold level for the region of low SNR. On other hand, when SNR is high, it is better to use the classical W-S interpolation scheme of (1.4) for signal reconstruction.

The asymptotic behavior of Δ and R as $n_q \to \infty$ is stated in the following theorem. The proof of the theorem is given in Appendix A. The theorem reveals the fact that the reconstruction accuracy of the proposed reconstruction scheme gets better and better, relative to the standard W-S interpolation scheme of (1.4), as the size of data record increases.

Theorem 3.5. *When* $T = 4\sigma$, *then* $\Delta \to \infty$ *and* $R \to 0$ *as* $n_q \to \infty$

3.4 Simulation Results

The following signals are used for simulations:

Signal 1:

$$x_1(t) = \frac{1}{\sqrt{\pi\Omega}} \cdot \frac{\sin \Omega t}{t} \tag{3.15}$$

Signal 2:

$$x_2(t) = C \cdot \frac{\cos^2 \frac{\Omega}{2} t}{\Omega^2(\pi^2/\Omega^2 - t^2)^2} \tag{3.16}$$

where C is the normalized constant such that the signal's energy $E_0 = \int_{-\infty}^{\infty} x^2(t)dt = = 1$.

Signal 3:

$$x_3(t) = C \cdot \sum_{k=-N}^{N} a_k \frac{\sin \Omega(t - k\tau)}{\Omega^*(t - k\tau)} \tag{3.17}$$

where, $\Omega^* = \pi/\tau \geq \Omega$ and C is the normalized constant such that the signal's energy $E_0 = \int_{-\infty}^{\infty} x^2(t)dt = 1$. With a_k being random variables, (3.17) can be used to model an arbitrary bandlimited signal [27].

The above signals are unit energy $BL(\Omega)$ signals, where $\Omega = 2\pi f_{max}$ is the radian frequency. In the simulation, $f_{max} = 3900$ Hz. Among all bandlimited signals having the same bandwidth, the signal $x_1(t)$ has the lowest rate of decay as $t \to \infty$. Given the fact that the proposed scheme works especially well for fast-decay signals, the use of this signal as a test signal is justified. The signal $x_2(t)$ is the nonnegative band-limited signal whose the normalized moment of inertia $\gamma = \frac{1}{X(0)} \int_{-\infty}^{\infty} t^2 x(t)dt$ is minimum [51]. This signal has various applications in signal processing theory and in spectrum estimation. It was used as a test signal in [3, 4, 28]. The signal $x_3(t)$ is a randomly generated bandlimited signal.

The experiment is repeated $M = 100$ times for various realization of random errors $\{\varepsilon_k\}$. The empirical counterpart of MISE, further called EMISE, is calculated according to the following formula:

$$EMISE(\widehat{x}) = \frac{\bar{\tau}}{M} \sum_{j=1}^{M} \sum_{k=-n}^{n} [\widehat{x}(k\bar{\tau}) - x(k\bar{\tau})]^2 \tag{3.18}$$

where $\bar{\tau} \ll \tau_q$ is the simulation sampling period.

Figure 3.8 and Figure 3.9 plot the EMISE of the proposed reconstruction scheme as a function of E_0/σ^2 when the threshold level is optimally selected. In this simulation, the signal $x_1(t)$ in (3.15) is used as the test signal, $2n_q = 100$ and $\tau_q = 1.25 \cdot 10^{-4}$ seconds (the sampling frequency is just slightly larger than the Nyquist rate). For comparison, the EMISE of the classical W-S interpolation scheme in (1.4), the EMISE of reconstruction schemes based on MA filtering in (2.30) and post-filtering in (2.35) are also plotted. A length-3 MA filter is used. The plots clearly show that the proposed reconstruction scheme gives better reconstruction accuracy than the classical W-S interpolation scheme and the MA filtering reconstruction scheme for every value of SNR. It has better reconstruction accuracy than the oversampling/post-filtering reconstruction scheme in the region of low SNR. On other hand, when SNR is high, the later yields better reconstruction accuracy.

The same simulations are repeated for the test signals $x_2(t)$ and $x_3(t)$ defined in (3.16) and (3.17), respectively. The simulation results are charted in Figure 3.10, Figure 3.11, Figure 3.12, and Figure 3.13, respectively. These results confirm the conclusions made in the previous paragraph about the reconstruction accuracy of the proposed reconstruction scheme. For the test signal $x_2(t)$, the proposed reconstruction scheme yields smaller reconstruction error than the oversampling/post-filtering reconstruction scheme for every value of SNR. The variation of simulation results charted in the above figures reveals the fact that the degree of noise reduction varies from a signal to signal. The accuracy of the proposed reconstruction scheme is signal dependent.

Figure 3.14 plots the EMISE of the proposed reconstruction scheme as a function of E_0/σ^2 when threshold level is sub-optimally chosen, i.e., when $T = 4\sigma$. The signal

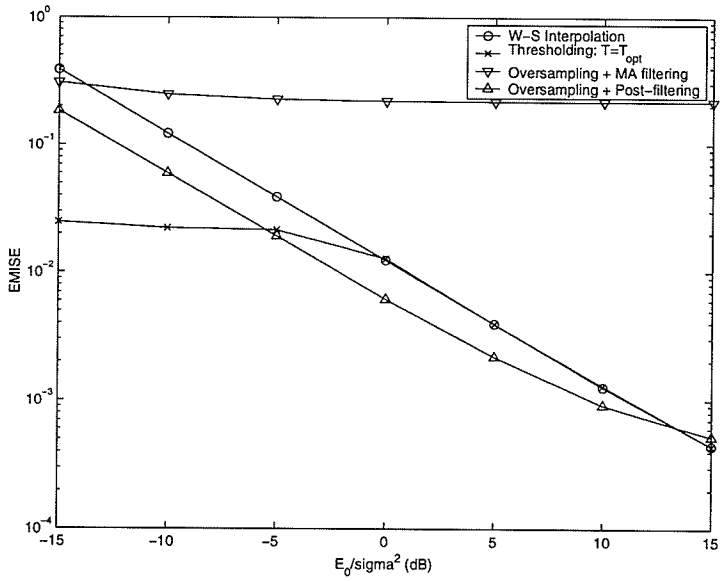

Figure 3.8: $EMISE(\widehat{x})$ versus E_0/σ^2. Test signal $x_1(t)$ is used. The MA filtering and post-filtering reconstruction schemes use the oversampling factor of 2

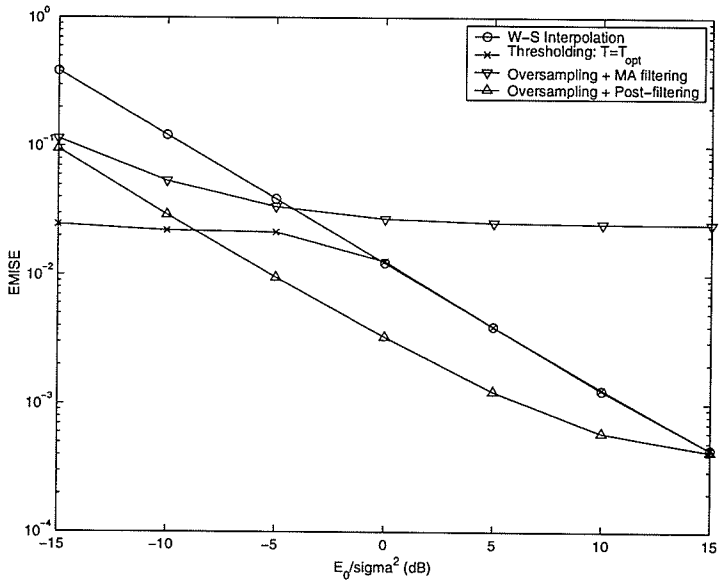

Figure 3.9: $EMISE(\widehat{x})$ versus E_0/σ^2. Test signal $x_1(t)$ is used. The MA filtering and post-filtering reconstruction schemes use the oversampling factor of 4

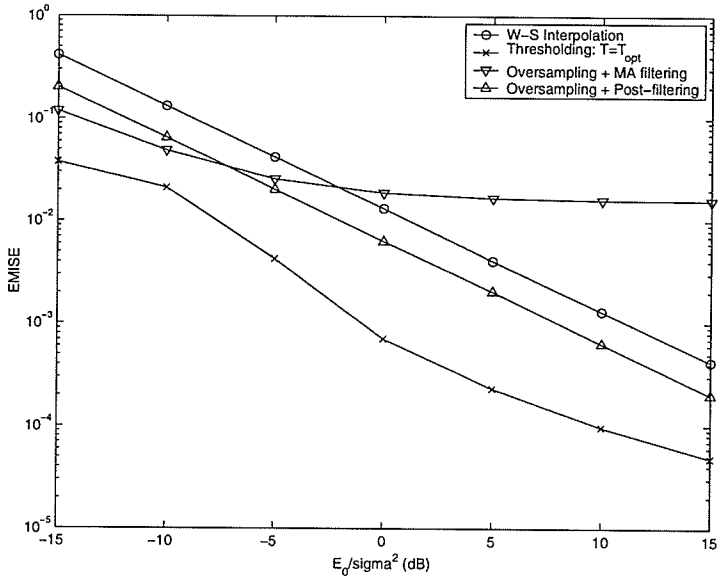

Figure 3.10: $EMISE(\widehat{x})$ versus E_0/σ^2. Test signal $x_2(t)$ is used. The MA filtering and post-filtering reconstruction schemes use the oversampling factor of 2

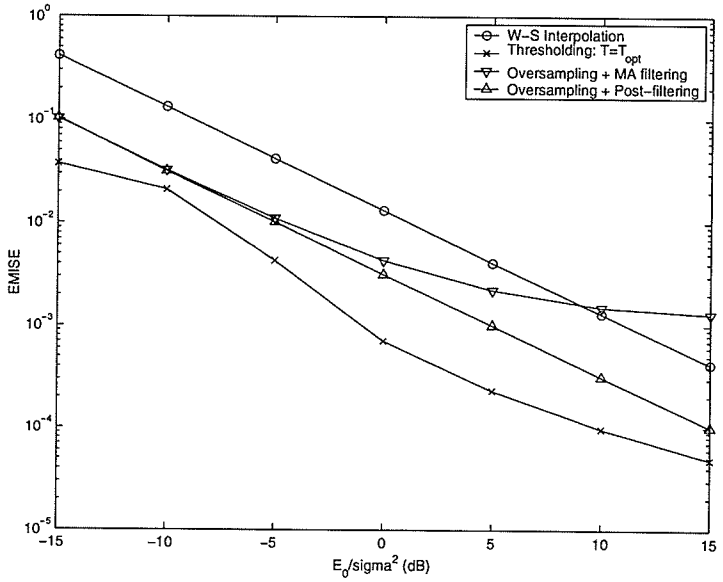

Figure 3.11: $EMISE(\widehat{x})$ versus E_0/σ^2. Test signal $x_2(t)$ is used. The MA filtering and post-filtering reconstruction schemes use the oversampling factor of 4

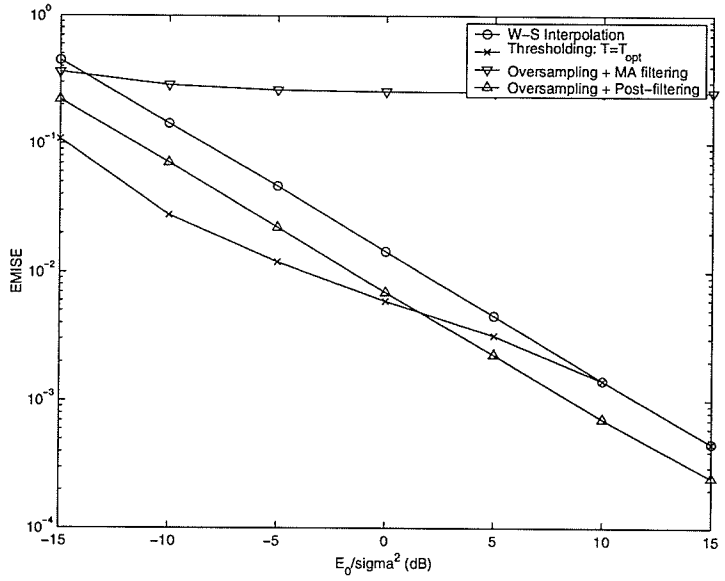

Figure 3.12: $EMISE(\widehat{x})$ versus E_0/σ^2. Test signal $x_3(t)$ is used. The MA filtering and post-filtering reconstruction schemes use the oversampling factor of 2

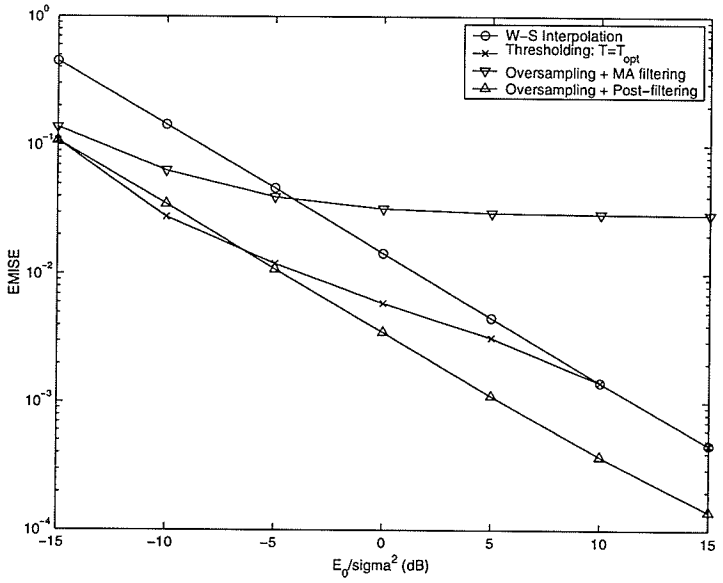

Figure 3.13: $EMISE(\widehat{x})$ versus E_0/σ^2. Test signal $x_3(t)$ is used. The MA filtering and post-filtering reconstruction schemes use the oversampling factor of 4

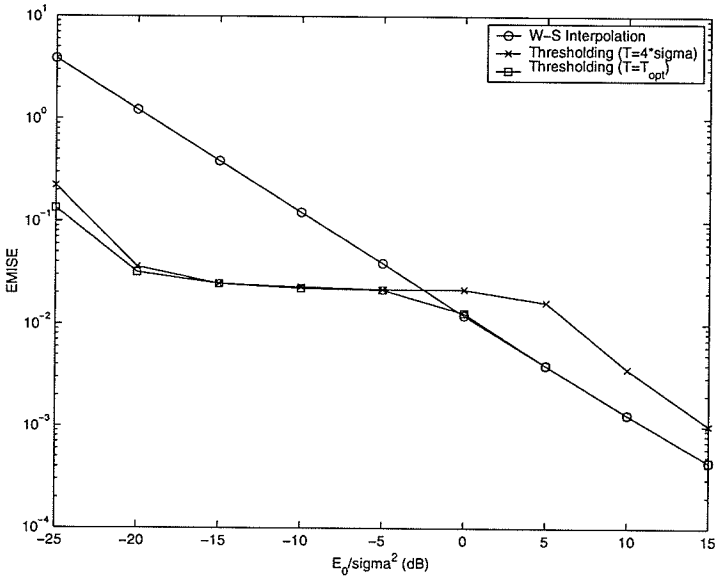

Figure 3.14: $EMISE(\widehat{x})$ versus E_0/σ^2 (Signal $x_1(t)$, Sub-optimal threshold level)

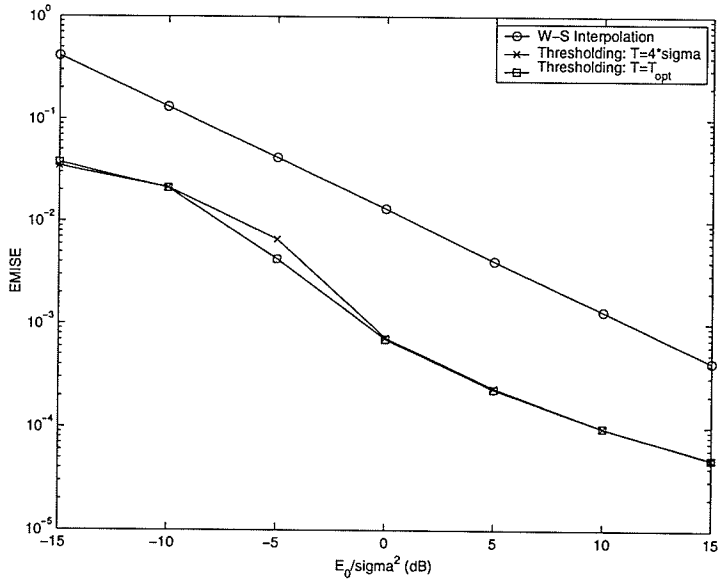

Figure 3.15: $EMISE(\widehat{x})$ versus E_0/σ^2 (Signal $x_2(t)$, Sub-optimal threshold level)

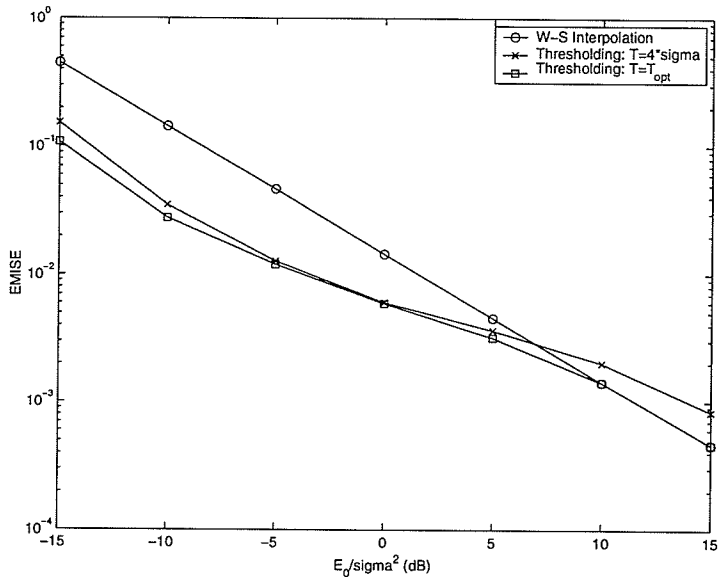

Figure 3.16: $EMISE(\widehat{x})$ versus E_0/σ^2 (Signal $x_3(t)$, Sub-optimal threshold level)

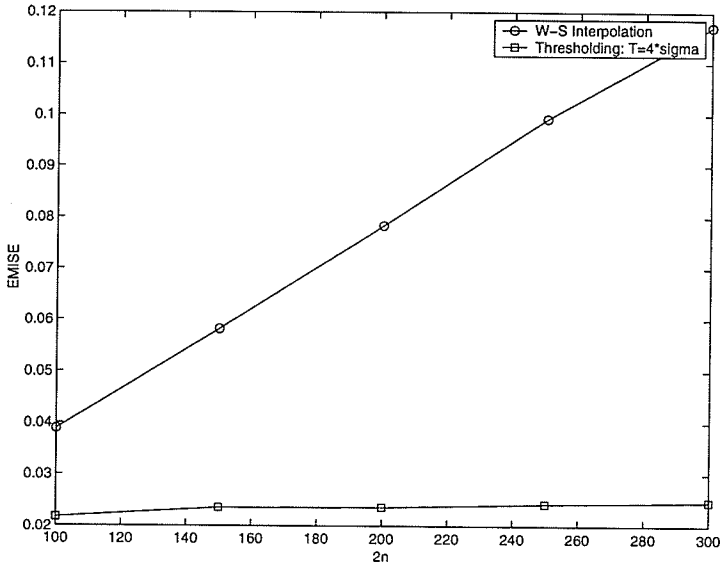

Figure 3.17: $EMISE(\widehat{x})$ versus n_q

$x_1(t)$ defined in (3.15) is used as the test signal, $2n_q = 100$ and $\tau_q = 1.25 \cdot 10^{-4}$ seconds. For comparison, the EMISE of the classical W-S interpolation scheme of (1.4) and the EMISE of the proposed reconstruction scheme with the optimal threshold level T_{opt} are also plotted. The plot clearly shows that when threshold level is set to $T = 4\sigma$, the reconstruction accuracy of the proposed scheme does not seem to be affected in the region of low SNR, but degradation in the reconstruction accuracy is noticed in the region of high SNR. As a result, when $T = 4\sigma$, the proposed reconstruction scheme gives better reconstruction accuracy than the classical W-S interpolation scheme in (1.4) for low SNR only. Recalling that when threshold level is optimally chosen, the proposed reconstruction scheme yields better reconstruction accuracy than the classical W-S interpolation scheme for every values of SNR.

Figure 3.15 and Figure 3.16 plot the EMISE of the proposed reconstruction scheme as a function of E_0/σ^2 for the test signals $x_2(t)$ and $x_3(t)$ defined in (3.16) and (3.17), respectively. The threshold level is sub-optimally selected, i.e., $T = 4\sigma$. These figures confirm the observations made in the preceding paragraph regarding to the accuracy of the proposed reconstruction scheme with a sub-optimal threshold level. For these test signals, the proposed sub-optimal criteria for setting the threshold level yields almost the same reconstruction accuracy as the optimal criteria.

Figure 3.17 plots the EMISE of the proposed reconstruction scheme as a function of n_q when $T = 4\sigma$ is chosen. In this simulation, the test signal $x_1(t)$ defined in (3.15) is used, $E_0/\sigma^2 = -5$ dB and $\tau_q = 1.25 \cdot 10^{-4}$ seconds. For comparison, the EMISE of the classical W-S interpolation scheme in (1.4) is also plotted. The plot clearly shows that the EMISE of the proposed reconstruction scheme is less dependent on n_q compared to that of the classical W-S interpolation scheme in (1.4). It also indicates

that the performance gap between two reconstruction schemes becomes wider as n_q increases. This confirms the observation made earlier in conjunction with theorem 3.5.

The plots of reconstructed waveforms are shown in Appendix F.

3.5 Conclusions

In this chapter, a nonlinear signal reconstruction scheme based on thresholding was proposed for recovering signals from noisy data. The proposed reconstruction scheme does not use oversampling, which is commonly utilized for signal reconstruction from noisy data.

The accuracy of the proposed reconstruction scheme was studied analytically and experimentally. The obtained results showed that when threshold level is optimally chosen, the proposed reconstruction scheme always gives better reconstruction accuracy than the classical W-S interpolation scheme in (1.4), regardless of SNR. A sub-optimal criteria for selection of threshold level, which eliminates the need for delivering the side information (i.e. the optimal threshold level) to the receiver, was suggested. When threshold level is chosen according to this criteria, a slight degradation in reconstruction accuracy is noticed in the region of high SNR. In the region of low SNR, the sub-optimal criteria gives almost the same reconstruction accuracy as the optimal criteria. Therefore, the sub-optimal criteria is recommended for the system operating in highly noisy environments.

The MISE of the proposed reconstruction scheme increases as the size of data record $2n_q + 1$ increases, but at much slower rate than that of the classical W-S interpolation scheme in (1.4). It is worth mentioning that the oversampling/filtering

reconstruction schemes discussed in Section 2.4 converge to the original signal when $n \rightarrow \infty$.

Since the proposed reconstruction scheme works especially well when the SNR is low, it has potential application in designing signal acquisition and reconstruction systems operating under highly noisy environments. For instant, it can be used in wireless communications or sensor networks where a low SNR is likely expected. The proposed reconstruction scheme also has a promising application in speech acquisition and reconstruction. This is due to the fact that, for speech signals, the sampled values near zero are more probable than those far away from zero. Since the proposed technique does not use oversampling, it can be used for acquisition of ultra wideband signals.

Chapter 4

Signal Reconstruction by Adaptive Thresholding

4.1 Introduction

In Chapter 3, a thresholding-based reconstruction scheme for reconstruction of signals from noisy data was proposed. It was observed that this reconstruction scheme does not take into account the transient phenomena of the signal to be reconstructed since all sampled values of the signal are compared to a single threshold level T. Note that the effective noise's power $\tau_q E \sum_{k\in I_i} \varepsilon_k^2$ (here I_i denotes an index set) in equal time intervals are the same, while the signal's energy $\tau_q \sum_{k\in I_i} x_k^2$ in equal time intervals varies with time. A better reconstruction might be obtained by determining threshold level based on the instantaneous SNR measured in a particular time interval, i.e. adaptively. In doing so, one accounts for the localized behavior (in energy sense) of the original signal for signal reconstruction.

The above observation is the motivation for the following adaptive thresholding scheme for reconstruction of signals from noisy data.

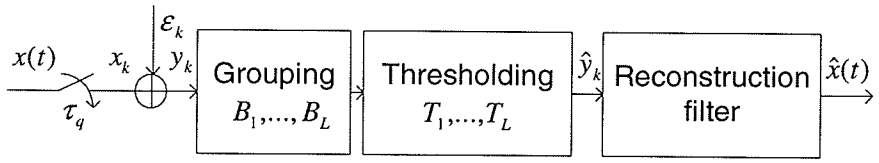

Figure 4.1: Signal reconstruction by adaptive thresholding

Step 1: Partition the observed data set into small, equal-size and disjoint subsets i. e.

$$\bigcup_{i=1}^{L}\{y_k\}_{k\in I_i} = \{y_k\}_{|k|\le n_q}$$

$$\bigcap_{i=1}^{L}\{y_k\}_{k\in I_i} = \emptyset$$

where, I_i denote index sets. L is the number of constituent data sets.

Step 2: Threshold each constituent data sets using different threshold levels T_i, whose values are to be determined later, i. e., for $k \in I_i$:

$$\widehat{y}_k = \begin{cases} y_k & \text{if} \quad |y_k| > T_i \\ \\ 0 & \text{if} \quad |y_k| \le T_i \end{cases} \tag{4.1}$$

Step 3: Use $\{\widehat{y}_k\}$ determined above to form the following estimate:

$$\widehat{x}(t) = \sum_{|k|\le n_q} \widehat{y}_k \cdot \operatorname{sinc}\left(\frac{t}{\tau_q} - k\right) \tag{4.2}$$

A block diagram of the proposed reconstruction scheme is illustrated in Figure 4.1

The subsequent sections present the error analysis of the proposed reconstruction scheme. Also investigated is the influence of the choice of threshold levels T_i on the reconstruction accuracy. Some simulation results are provided to verify the analytical results.

4.2 Error Analysis

The following theorem gives an exact formula for computing the MISE of the proposed reconstruction scheme. The proof of the theorem is given in Appendix B.

Theorem 4.1. *Consider the observation model of (1.3), where ε_k are independent Gaussian random variables with zero mean and variance σ^2. The MISE of estimate $\widehat{x}(t)$ of (4.2) is given by:*

$$MISE(\widehat{x}) = \tau_q \sigma^2 (2n_q + 1) + \tau_q \sum_{|k|>n_q} x_k^2 - \tau_q \sigma^2 \sum_{i=1}^{L} D_i \tag{4.3}$$

with,

$$\begin{aligned} D_i &= f(x_k, \sigma^2, T_i) \\ &= \sum_{\substack{k\in I_i \\ x_k<-T_i}} \frac{1}{\sqrt{\pi}} \left[\gamma\left(\frac{3}{2}, \frac{(x_k - T_i)^2}{2\sigma^2}\right) - \gamma\left(\frac{3}{2}, \frac{(x_k + T_i)^2}{2\sigma^2}\right)\right] \\ &\quad + \sum_{\substack{k\in I_i \\ |x_k|\le T_i}} \frac{1}{\sqrt{\pi}} \left[\gamma\left(\frac{3}{2}, \frac{(x_k - T_i)^2}{2\sigma^2}\right) + \gamma\left(\frac{3}{2}, \frac{(x_k + T_i)^2}{2\sigma^2}\right)\right] \\ &\quad + \sum_{\substack{k\in I_i \\ x_k>T_i}} \frac{1}{\sqrt{\pi}} \left[\gamma\left(\frac{3}{2}, \frac{(x_k + T_i)^2}{2\sigma^2}\right) - \gamma\left(\frac{3}{2}, \frac{(x_k - T_i)^2}{2\sigma^2}\right)\right] \\ &\quad - \sum_{k\in I_i} \frac{x_k^2}{\sigma^2} \left[\frac{1}{2}\mathrm{erf}\left(\frac{x_k + T_i}{\sigma\sqrt{2}}\right) - \frac{1}{2}\mathrm{erf}\left(\frac{x_k - T_i}{\sigma\sqrt{2}}\right)\right] \end{aligned} \tag{4.4}$$

where, $\gamma(\alpha, x)$, $\mathrm{erf}(x)$ are incomplete gamma function and error function, respectively [50].

Remark 4.1. The MISE of the classical W-S interpolation scheme of (1.4) can be expressed as follows [3]:

$$MISE(\widetilde{x}) = \tau_q \sigma^2 (2n_q + 1) + \tau_q \sum_{|k|>n_q} x_k^2$$

Thus, (4.3) can be re-written as:

$$MISE(\widehat{x}) = MISE(\widetilde{x}) - \tau_q \sigma^2 \sum_{i=1}^{L} D_i, \tag{4.5}$$

If the second term in the RHS of (4.5) is positive, it represents the degree of noise reduction of the proposed estimate. Setting threshold levels properly makes $D_i > 0$ for all i.

The following theorem confirms the existence of the optimal threshold levels that minimize the MISE of the proposed reconstruction scheme. The proof of the theorem is given in Appendix B. Since in the proof, it is not assumed that ε_k have Gaussian distribution, the theorem is valid for arbitrary distributions.

Theorem 4.2. *Consider the observation model of (1.3), where ε_k are independent random variables with zero mean and variance σ^2. For a given signal $x(t)$ and noise variance σ^2, there always exist optimal threshold levels $T_{opt,i}$ so that the MISE of estimate $\widehat{x}(t)$ of (4.2) is minimum.*

The following theorem gives exact formulas for computing the IBIAS and the IVAR of the proposed reconstruction scheme. The proof of the theorem is given in the Appendix B.

Theorem 4.3. *Consider the observation model of (1.3), where ε_k are independent Gaussian random variables with zero mean and variances σ^2. The IBIAS and the IVAR of estimate $\widehat{x}(t)$ of (4.2) are given by:*

$$IBIAS(\widehat{x}) = \tau_q \sum_{i=1}^{L} \sum_{k \in I_i} d_k^2 + \tau_q \sum_{|k|>n_q} x_k^2, \tag{4.6}$$

$$IVAR(\widehat{x}) = \tau_q \sigma^2 (2n_q + 1) - \tau_q \sum_{i=1}^{L} \sum_{k \in I_i} d_k^2 - \tau_q \sigma^2 \sum_{i=1}^{L} D_i, \tag{4.7}$$

where D_i is given by (4.4) and,

$$\begin{aligned} d_k &= \frac{\sigma}{\sqrt{2\pi}} \left[e^{-(x_k+T_i)^2/2\sigma^2} - e^{-(x_k-T_i)^2/2\sigma^2} \right] \\ &\quad + \frac{x_k}{2} \left[\operatorname{erf}\left(\frac{x_k + T_i}{\sigma\sqrt{2}} \right) - \operatorname{erf}\left(\frac{x_k - T_i}{\sigma\sqrt{2}} \right) \right]. \end{aligned} \tag{4.8}$$

4.3 Choice of Threshold Levels

In this subsection, the influence of threshold levels T_i on the reconstruction accuracy of the proposed reconstruction scheme is investigated. In particular, it is shown how T_i can be optimally pre-determined during the data acquisition process. A sub-optimal criteria for selection of threshold levels T_i is suggested.

4.3.1 Pre-Determination of the Optimal Threshold Level

Theorem 4.2 shows that there exist optimal threshold levels that minimize the MISE of the proposed reconstruction scheme. Moreover, in Theorem 4.1, one has an exact formula for computing the MISE of the proposed reconstruction scheme. Since the first two terms in the RHS of (4.3) do not depend on threshold levels T_i, one concludes that the optimal threshold levels are the values of T_i, at which the terms D_i defined in (4.4) are maximum.

The terms D_i can be pre-computed during the data acquisition process using (4.4), and the optimal threshold levels $T_{opt,i}$ can be pre-determined accordingly. $T_{opt,i}$ is considered as the side information and can be made available for signal reconstruction by various methods. For example, with $L = 10$, $2n_q = 100$, and test signal $x_1(t)$ defined by (3.15), the optimal threshold levels are given in Table 4.1.

4.3.2 A Sub-Optimal Criteria for Setting Threshold Level

Reconstruction of the signal using the optimal threshold levels $T_{opt,i}$ requires pre-determination of $T_{opt,i}$ and a mechanism for delivering $T_{opt,i}$ to the receiver. Therefore, a sub-optimal method is suggested where the threshold levels T_i are set adaptively based on the noise variance. This criterion is a result of examining the upper bound

Table 4.1: The optimal threshold levels for various E_0/σ^2

E_0/σ^2 (dB)	-15	-10	-5	0	5	10	15
$T_{opt,1}$	50.40	28.50	16.20	9.29	5.40	3.22	0.01
$T_{opt,2}$	50.40	28.60	16.30	9.34	5.45	0.10	0.01
$T_{opt,3}$	51.20	29.30	17.10	0.46	0.01	0.01	0.01
$T_{opt,4}$	51.90	30.00	1.40	0.01	0.01	0.01	1.00
$T_{opt,5}$	52.20	30.40	1.00	1.00	1.00	1.00	1.00
$T_{opt,6}$	45.50	30.40	1.00	1.00	1.00	1.00	1.00
$T_{opt,7}$	52.00	30.20	1.50	0.01	0.01	1.00	1.00
$T_{opt,8}$	51.40	29.60	17.30	0.27	0.01	0.01	0.01
$T_{opt,9}$	50.60	28.80	16.50	9.56	5.68	0.05	0.01
$T_{opt,10}$	50.30	28.40	16.20	9.20	5.32	3.13	0.01

of $MISE(\widehat{x})$ established in the following theorem. The proof of the theorem is given in Appendix B.

Theorem 4.4. *Consider the observation model of (1.3), where ε_k are independent Gaussian random variables with zero mean and variance σ^2. The MISE of estimate $\widehat{x}(t)$ of (4.2) is upper bounded by:*

$$MISE(\widehat{x}) \leq \tau_q\sigma^2(2n_q+1) + \tau_q \sum_{|k|>n_q} x_k^2 - \tau_q\sigma^2 \cdot \frac{2n_q+1}{L}\left[\sum_{i=1}^{L}\left(\frac{2}{\sqrt{\pi}}\gamma\left(\frac{3}{2},\frac{T_i^2}{2\sigma^2}\right) - \right.\right.$$
$$\left.\left. - \frac{\sum_{k\in I_i} x_k^2}{\sigma^2(2n_q+1)/L} \cdot \operatorname{erf}\left(\frac{T_i}{\sigma\sqrt{2}}\right)\right)\right] \tag{4.9}$$

Remark 4.2. When $T_i = T$ for all i, (4.9) reduces to

$$\begin{aligned} MISE(\widehat{x}) \;\leq\; & \tau_q \sigma^2 \left[1 - \frac{2}{\sqrt{\pi}} \gamma\left(\frac{3}{2}, \frac{T^2}{2\sigma^2}\right)\right](2n_q + 1) \\ & + \operatorname{erf}\left(\frac{T}{\sigma\sqrt{2}}\right) E_0 + \left(\tau_q \sum_{|k|>n_q} x_k^2\right) \operatorname{erfc}\left(\frac{T}{\sigma\sqrt{2}}\right) \end{aligned}$$

which is identical to (3.10).

Let

$$f(G_i, T_i) = \frac{2}{\sqrt{\pi}} \gamma\left(\frac{3}{2}, \frac{T_i^2}{2\sigma^2}\right) - G_i \operatorname{erf}\left(\frac{T_i}{\sigma\sqrt{2}}\right) \tag{4.10}$$

where,

$$G_i \triangleq \frac{\frac{L}{2n_q+1} \sum_{k \in I_i} x_k^2}{\sigma^2} \tag{4.11}$$

Re-write (4.9) as follows:

$$\Delta = MISE(\widetilde{x}) - MISE(\widehat{x}) \geq \tau_q \sigma^2 \cdot \frac{2n_q + 1}{L} \cdot \left(\sum_{i=1}^{L} f(G_i, T_i)\right) \tag{4.12}$$

where, $MISE(\widetilde{x})$ is the MISE of the classical W-S interpolation scheme given by (1.4).

Therefore, in order to maximize Δ, one should select T_i such that $f(G_i, T_i)$ is maximum. Similar to Chapter 3, it is observed that:

- For $G_i \geq 1$, one should select $T_i = 0$.
- For $G_i < 1$, $T_i = 0$ is no longer the best choice. In fact, one should select $3\sigma \leq T_i \leq 5\sigma$.

Taking the above observation into account, the following joint detection/estimation scheme for recovering signals from noisy data is proposed:

Step 1: Estimate $P_i \triangleq \sum_{k \in I_i} x_k^2$ from data $\{y_k\}_{k \in I_i}$. Compute G_i using the estimated P_i

Step 2: If $G_i \geq 1$, set $T_i = 0$. Otherwise, set $3\sigma \leq T_i \leq 5\sigma$.

Step 3: Pass the data through the thresholding device, and then, the reconstruction filter to reconstruct the original signal.

4.4 Simulation Results

Figure 4.2, Figure 4.3, and Figure 4.4 plot the EMISE of the proposed reconstruction scheme,(4.2), as a function of E_0/σ^2, when the T_i's are optimally chosen, i.e. when $T_{opt,i}$ is selected according to Table 4.1. In this simulation, signal $x_1(t)$ defined by (3.15) is used as the test signal, $2n_q = 100$ and $\tau_q = 1.25 \cdot 10^{-4}$ seconds. For comparison, the EMISE of the classical W-S interpolation scheme in (1.4) and the EMISE of the thresholding-based reconstruction scheme introduced in Chapter 3 are also plotted. The plots show that the proposed reconstruction scheme gives better reconstruction accuracy than the classical W-S interpolation scheme and the thresholding-based reconstruction scheme for every value of SNR. In addition, it is observed that the reconstruction accuracy of the proposed reconstruction scheme gets better as the size of constituent data sets decreases. This is due to the fact that the smaller the size of constituent data sets, the better adaptation to the local changes in the signal amplitude.

The same simulations were repeated for test signal $x_3(t)$ defined by (3.17). The simulation results are graphed in Figure 4.5, Figure 4.6 and Figure 4.7. It is noticed that the improvement in reconstruction accuracy of the proposed reconstruction scheme over the thresholding-based reconstruction introduced in Chapter 3 is more significant for this test signal than test signal $x_1(t)$. This is due to the fact that test signal $x_3(t)$ has higher degree of variability than test signal $x_1(t)$.

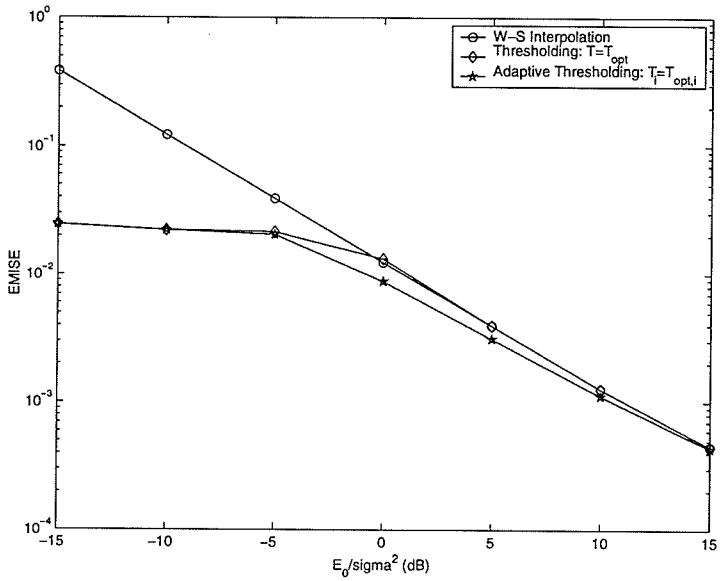

Figure 4.2: $EMISE(\widehat{x})$ versus E_0/σ^2 (Adaptive thresholding, Signal $x_1(t)$, Q=5)

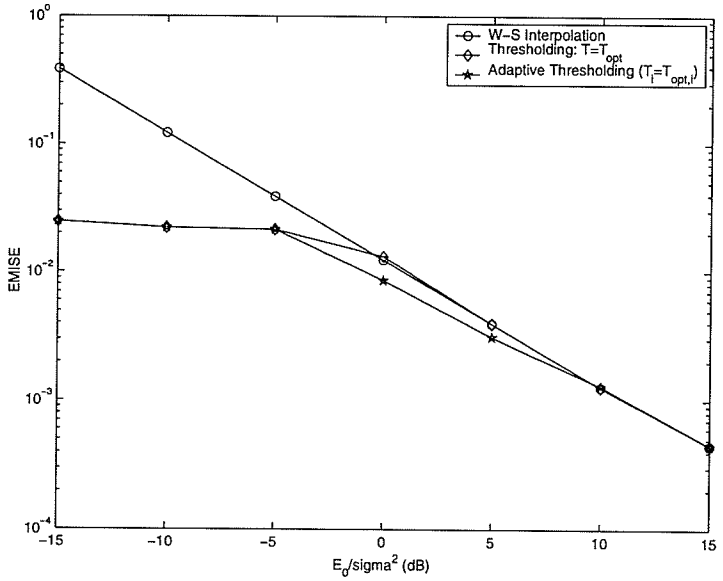

Figure 4.3: $EMISE(\widehat{x})$ versus E_0/σ^2 (Adaptive thresholding, Signal $x_1(t)$, Q=20)

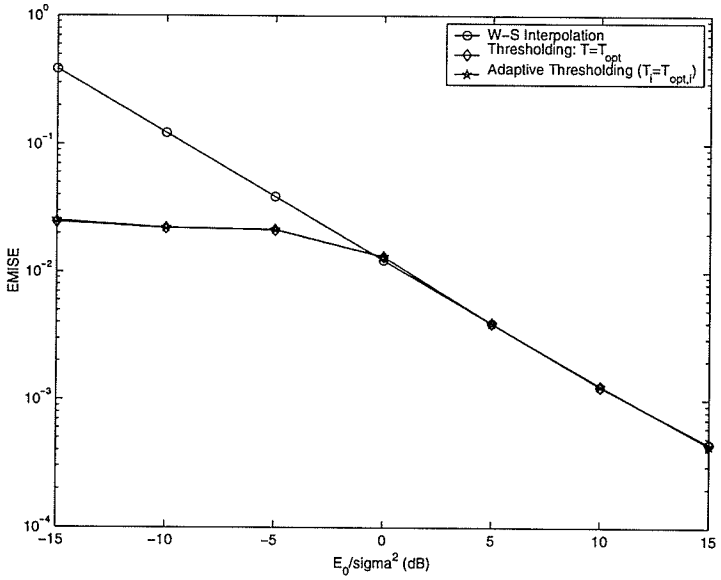

Figure 4.4: $EMISE(\widehat{x})$ versus E_0/σ^2 (Adaptive thresholding, Signal $x_1(t)$, Q=50)

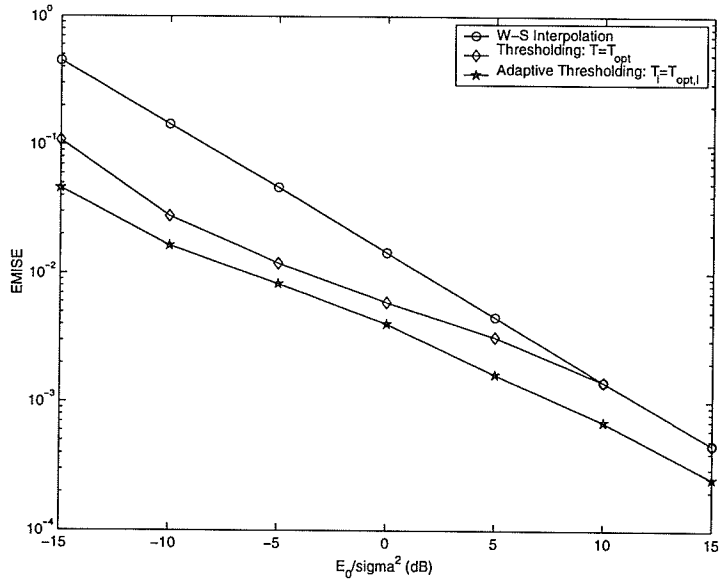

Figure 4.5: $EMISE(\widehat{x})$ versus E_0/σ^2 (Adaptive thresholding, Signal $x_3(t)$, Q=5)

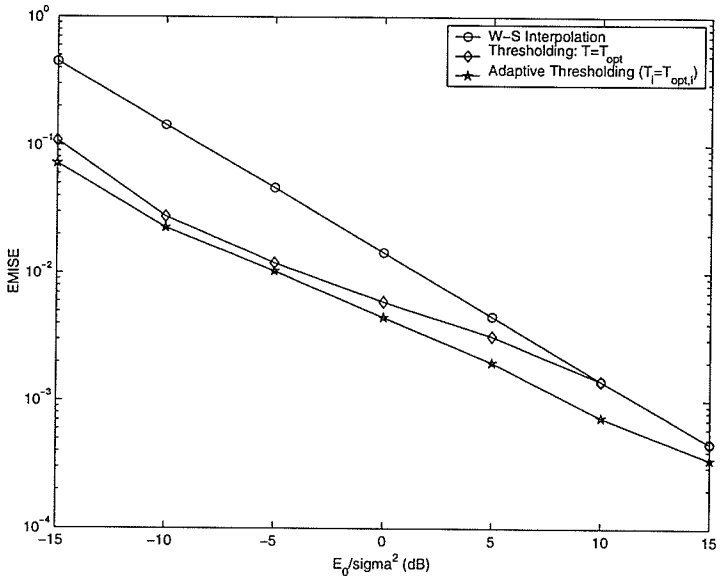

Figure 4.6: $EMISE(\widehat{x})$ versus E_0/σ^2 (Adaptive thresholding, Signal $x_3(t)$, Q=20)

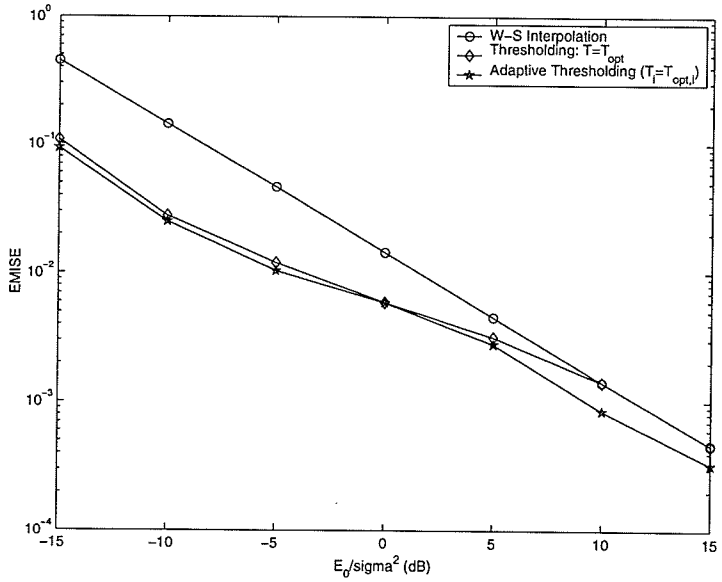

Figure 4.7: $EMISE(\widehat{x})$ versus E_0/σ^2 (Adaptive thresholding, Signal $x_3(t)$, Q=50)

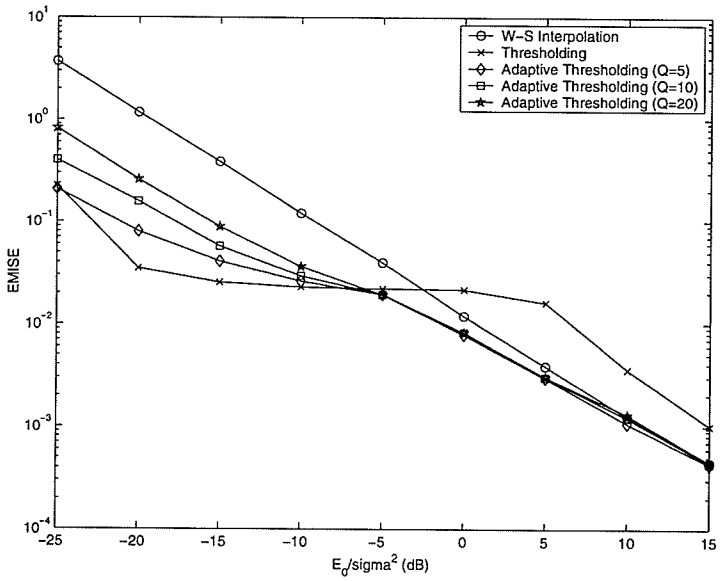

Figure 4.8: $EMISE(\widehat{x})$ versus E_0/σ^2 (Adaptive thresholding, $T_i = 4\sigma$)

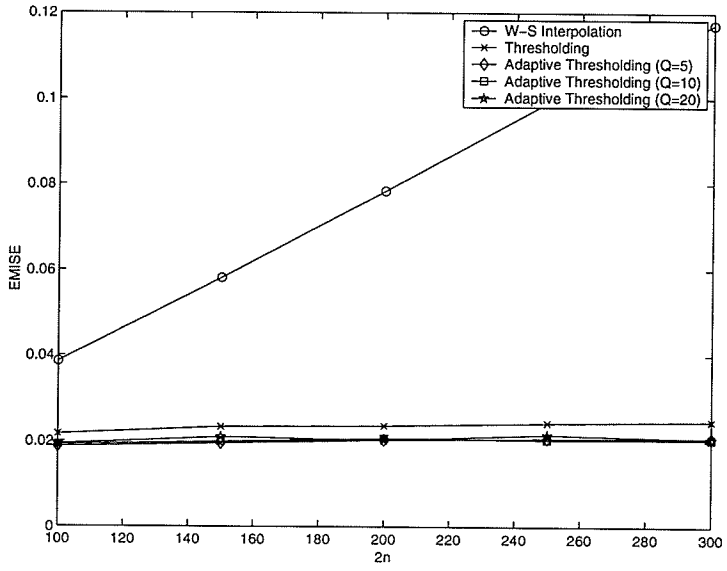

Figure 4.9: $EMISE(\widehat{x})$ versus n_q (Adaptive thresholding)

Figure 4.8 compares the EMISE of the proposed reconstruction scheme to the EMISE of thresholding-based reconstruction scheme in (3.2) when threshold levels are set according to the sub-optimal criteria introduced in the preceding section. Here, it is assumed that the P_i are perfectly estimated. In this simulation, $2n_q = 100$ and $\tau_q = 1.25 \cdot 10^{-4}$ seconds (the sampling frequency is just slightly larger than the Nyquist rate). The figure shows that the proposed reconstruction scheme gives better reconstruction accuracy than the thresholding-based reconstruction scheme introduced in Chapter 3 when SNR is high. On other hand, when SNR is low, the proposed scheme with sub-optimal threshold levels yields higher reconstruction error. Nevertheless, the proposed reconstruction scheme gives better reconstruction accuracy than the classical W-S interpolation scheme in (1.4) for every value of SNR. This can not be obtained with the thresholding-based reconstruction scheme proposed in Chapter 3.

Figure 4.9 plots the EMISE of the proposed reconstruction scheme, (4.2), as a function of n_q. Threshold levels T_i are selected according to the sub-optimal criteria described in the preceding section. Again, it is assumed that the P_i are perfectly estimated. In this simulation, signal $x_1(t)$ defined by (3.15) is used as the test signal, $2n_q = 100$ and $\tau_q = 1.25 \cdot 10^{-4}$ seconds. For comparison, the EMISE of the classical W-S interpolation scheme of (1.4) is also plotted. It shows that the EMISE of the proposed reconstruction scheme is less dependent on the size of data record than that of the W-S interpolation scheme. It also indicates that the performance gap between two reconstruction schemes becomes wider as n_q increases.

The plots of reconstructed waveforms are shown in Appendix F.

4.5 Conclusions

In this Chapter, an adaptive version of the thresholding-based reconstruction scheme introduced in Chapter 3 was proposed to recover signals from noisy data. The proposed reconstruction scheme does not use oversampling, which is commonly utilized for signal reconstruction from noisy data.

The accuracy of the proposed reconstruction scheme was studied analytically and experimentally. The obtained results show that when threshold levels T_i are optimally chosen, the proposed reconstruction scheme yields better reconstruction accuracy than the thresholding-based reconstruction scheme introduced in Chapter 3 for every value of SNR. The better reconstruction accuracy can be achieved with the smaller size of constituent data sets. The proposed reconstruction scheme works especially well for the signals with high degree of variability.

A sub-optimal criteria for selection of threshold levels T_i, which eliminates the need for side information (i.e. the optimal threshold levels) to the receiver, was also suggested. When T_i are chosen according to this criteria, degradation in the reconstruction accuracy is noticed in the region of low SNR.

The MISE of the proposed reconstruction scheme increases as the size of data record $2n_q + 1$ increases, but at much slower rate compared to the classical W-S interpolation scheme of (1.4). It is worth mentioning that the oversampling/filtering reconstruction schemes discussed in Section 2.4 converge to the original signal when $n \rightarrow \infty$.

Since the proposed reconstruction scheme works especially well when SNR is low, it has the potential application in designing signal acquisition and reconstruction systems operating in highly noisy environments. The proposed reconstruction scheme

also has a promising application in speech acquisition and reconstruction. This is due to the fact that, for speech signals, the sampled values near zero are more probable than those far away from zero. Since the proposed technique does not use over-sampling, it can be used for the acquisition of wideband signals.

Chapter 5

A Thresholding-Based Sampling Scheme

5.1 Introduction

In this chapter, a thresholding-based sampling scheme for the acquisition of signals in the presence of noise is proposed and analyzed. The thresholding unit is introduced in the data acquisition (sampling) process, rather than in the signal reconstruction process as in case of Chapter 3 and Chapter 4.

The block diagram of the proposed scheme is illustrated in Figure 5.1. With the use of the thresholding unit in data acquisition process, the set of uniformly-spaced signal's samples is transformed into a set of nonuniformly-spaced signal's samples prior to transmission or storage. A detailed description of the proposed scheme is given in this chapter.

5.1.1 Data Acquisition

The data acquisition process consists of two steps as follows:

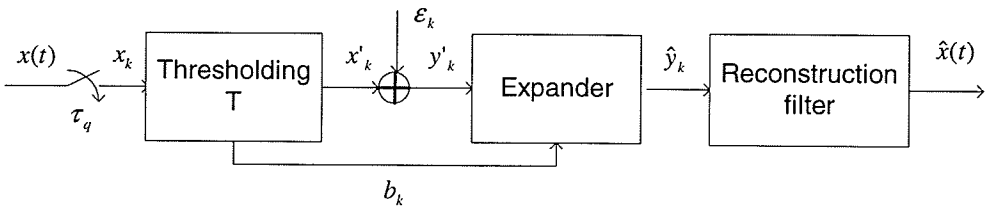

Figure 5.1: The thresholding-based sampling scheme

Step 1: Uniformly sample the signal $x(t)$ at the Nyquist rate to obtain the set of sampled values $\{x_k\}$.

Step 2: Pass $\{x_k\}$ through a threshold device with threshold level T. Only those samples of $\{x_k\}$ for which $|x_k| > T$ are kept. The other samples are destroyed. Therefore, in Figure 5.1, the sequence $\{x'_k\}$ relates to the sequence $\{x_k\}$ by:

$$\{x'_k\} = \{x_k : |x_k| > T\}, \tag{5.1}$$

For signal reconstruction purpose, one needs to know the location at which a particular sample is kept or destroyed. This information is made available at the receiver by using the sequence of binary digits b_k, which are formed as follows.

$$b_k = \begin{cases} 1 & \text{if} \quad |x_k| > T \\ \\ 0 & \text{if} \quad |x_k| \leq T, \end{cases} \tag{5.2}$$

Note that the length of sequence $\{b_k\}$ is $2n_q + 1$, whereas the length of sequence $\{x'_k\}$ is $\eta \leq 2n_q + 1$. Since the length of sequence $\{x'_k\}$ is always shorter than that of sequence $\{x_k\}$, the thresholding unit acts as the compressor. At the receiver side, the expander inserts zeros into the noisy sequence $\{y'_k\}$, at the locations for which $b_k = 0$.

Notice that the compressor (also called decimator) and the expander are the well-known building blocks in digital signal processing theory [52]. They are often used for sampling rate conversion. In Figure 5.1, they serve the purpose of noise reduction. Moreover, the sampling rate conversion process is done in a nonuniform and adaptive

manner. That is, the decision on which samples are kept or destroyed depends on a particular signal and the noise level. The resultant sequence is then a sequence of nonuniformly-spaced signal samples.

5.1.2 Observation Model

Assume $\{b_k\}$ is available for signal reconstruction, while $\{x'_k\}$ is corrupted by noise, i.e.

$$y'_k = x'_k + \varepsilon_k, \quad 1 \leq k \leq \eta \tag{5.3}$$

where $\{\varepsilon_k\}$ is an additive noise process and η is the length of $\{x'_k\}$. Assume further that $\{\varepsilon_k\}$ are independent random variables, independent of $\{x'_k\}$, and having variance σ^2.

It is worth mentioning that the above assumption on the availability of $\{b_k\}$ is a reasonable assumption. Since $\{b_k\}$ is a digital sequence, it is resistant to noise and can be protected by error correcting codes [53].

5.1.3 Signal Reconstruction

The signal reconstruction process consists of two steps as follows:

Step 1: From two sequence $\{b_k\}$ and $\{y'_k\}$, the sequence $\{\widehat{y}_k\}$ is formed according to the procedure described below.

- Set $\{\widehat{y}_k\}$ to the all-zero sequence. Its length is $2n_q + 1$.
- Denote by $k_1, k_2, \ldots, k_\eta$, $(k_1 < k_2 <, \ldots, < k_\eta)$ the locations where $b_k = 1$. Set $\widehat{y}_{k_l} = y_l$, $l = 1, 2, \ldots, \eta$.

For example, if $\{b_k\} = 10110110010$ and $\{y'_k\} = y'_6y'_5y'_4y'_3y'_2y'_1$ then $\{\widehat{y}_k\} = y'_60y'_5y'_40y'_3y'_200y'_10$.

Mathematically, one can also write $\widehat{y}_k = y_k \cdot b_k$, where $y_k = x_k + \varepsilon_k$.

Step 2: Reconstruct the original signal by:

$$\widehat{x}(t) = \sum_{|k| \leq n_q} \widehat{y}_k \cdot \operatorname{sinc}\left(\frac{t}{\tau_q} - k\right), \tag{5.4}$$

5.1.4 Data Storage Reduction Ratio

Assume that an m-bit uniform quantizer is used to obtain the binary representation of the sampled values of signal. In the classical W-S sampling scheme, the total number of bits required to represent the signal is $B_{WS} = (2n_q + 1) \cdot m$. In the proposed sampling scheme, this number is $B_T = \eta \cdot m + (2n_q + 1)$. Let $D_R = B_T / B_{WS}$ denotes the data storage reduction ratio (DSRR), we have:

$$D_R = \frac{\eta}{2n_q + 1} + \frac{1}{m} \tag{5.5}$$

Several conclusions can be drawn from (5.5):

- D_R decreases as m increases. In other word, the finer the quantizer, the higher degree of data storage reduction can be achieved.

- The data storage reduction ratio D_R decreases as η decreases, or equivalently, T increases. However, T can not be made arbitrary large since doing this will effect the reconstruction accuracy.

- For fixed T, the data storage reduction ratio D_R depends on the shape of signal. If the total amount of time that the original signal falls below a threshold level T is large, then D_R is small. In this case, one benefits from using the proposed sampling scheme.

5.2 Error Analysis

The following theorem gives an exact formula for calculation of the MISE of the proposed sampling and reconstruction scheme. The proof of the theorem is given in Appendix C.

Theorem 5.1. *Consider the observation model of (5.3), where ε_k are independent random variables with zero mean and variance σ^2. The MISE of estimate $\widehat{x}(t)$ of (5.4) is given by:*

$$MISE(\widehat{x}) = \tau_q \sigma^2 \eta + \tau_q \sum_{k \in I_d} x_k^2 + \tau_q \sum_{|k| > n_q} x_k^2, \tag{5.6}$$

where, $I_p = \{k : |x_k| > T\}$ and $I_d = \{k : |x_k| \leq T\}$ are two index sets; $\eta = |I_p|$ is the volume (length) of I_p.

The following theorem gives exact formulas for computing the IBIAS and the IVAR of the proposed sampling and reconstruction scheme. The proof of the theorem is given in Appendix C.

Theorem 5.2. *Consider the observation model of (5.3), where ε_k are independent random variables with zero mean and variance σ^2. The IBIAS and the IVAR of estimate $\widehat{x}(t)$ of (5.4) are given by:*

$$IBIAS(\widehat{x}) = \tau_q \sum_{k \in I_d} x_k^2 + \tau_q \sum_{|k| > n_q} x_k^2, \tag{5.7}$$

$$IVAR(\widehat{x}) = \tau_q \sigma^2 \eta, \tag{5.8}$$

From (5.7) and (5.8), one can observe that if T increases, then $IVAR(\widehat{x})$ decreases, but $IBIAS(\widehat{x})$ increases. On other hand, if T decreases, then $IVAR(\widehat{x})$ increases, but $IBIAS(\widehat{x})$ decreases. This trade-off between the IVAR and IBIAS terms is illustrated in Figure 5.2, where $IVAR(\widehat{x})$ and $IBIAS(\widehat{x})$ are plotted as functions of α for the test

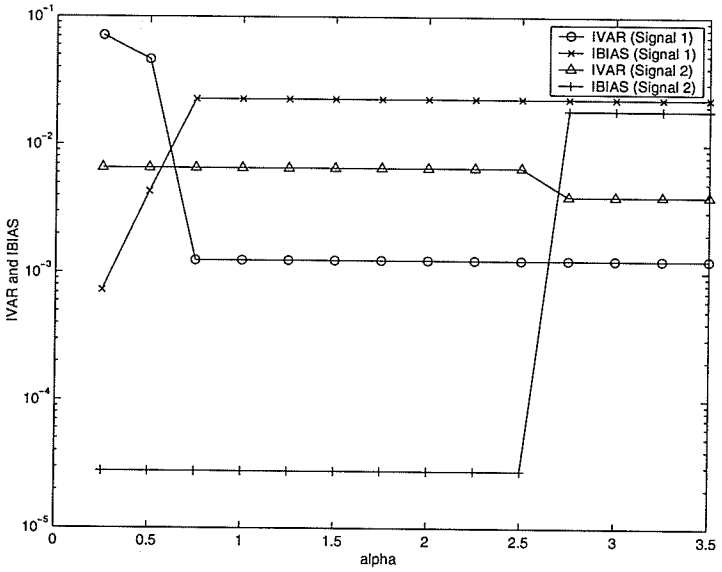

Figure 5.2: $IVAR(\widehat{x})$ and $IBIAS(\widehat{x})$ versus α

signals defined in (3.15) and (3.16), respectively. Here, α relates to T by $T = \alpha\sigma$ and $E_0/\sigma^2 = -10dB$. Due to the trade-off between the IVAR and IBIAS of the proposed sampling and reconstruction scheme, there always exists an optimal threshold level T_{opt} that minimizes $MISE(\widehat{x})$.

For a given noise variance, $MISE(\widehat{x})$ can be pre-computed during data acquisition process using (5.6) and the optimal threshold level T_{opt} can be pre-determined accordingly.

The following corollary compares the reconstruction accuracy of the proposed sampling and reconstruction scheme with the classical W-S interpolation scheme in (1.4). The proof of the corollary is given in Appendix C.

Corollary 5.1. *Selecting $T \leq \sigma$, the proposed estimate $\widehat{x}(t)$ of (5.4) always gives better reconstruction accuracy compared to the W-S interpolation scheme, regardless of noise variance and the size of data record, i.e.*

$$R = \frac{MISE(\widehat{x})}{MISE(\widetilde{x})} \leq 1, \quad \textit{for all} \quad \sigma^2, n_q \tag{5.9}$$

where, $MISE(\widetilde{x})$ is the MISE of the classical W-S interpolation scheme.

Remark 5.1. Corollary 5.1 does not imply that the optimal threshold level must satisfy $T_{opt} \leq \sigma$. However, it does suggest a sub-optimal criteria for setting threshold level, i.e., $T = \sigma$. Here, it is assumed that the noise variance is known.

The MISE of the classical W-S interpolation scheme, (1.4), can be expressed as follows:

$$MISE(\widetilde{x}) = \tau_q \sigma^2 \eta + \tau_q \sum_{k \in I_d} E\varepsilon_k^2 + \tau_q \sum_{|k|>n_q} x_k^2, \tag{5.10}$$

If the threshold level is set to $T = \sigma$, then $|I_d|$ increases as σ^2 increases. But from (5.6) and (5.10), one can see that the ratio R defined in (5.9) decreases as $|I_d|$ increases. This implies that R decreases as σ^2 increases. Therefore, the performance gap between the proposed scheme and the W-S interpolation scheme becomes wider as the noise variance increases. This indicates the advantage of the proposed scheme over the classical W-S sampling and reconstruction scheme when SNR is low.

5.3 Simulation Results

Figure 5.3 and Figure 5.4 plot the EMISE of the proposed sampling and reconstruction scheme as a function of E_0/σ^2 when threshold level is set to $T = \sigma$. In this simulation, signal $x_1(t)$ defined in (3.15) and signal $x_2(t)$ defined in (3.16) are used as the test signal, $2n_q = 100$ and $\tau = 1.25 \cdot 10^{-4}$ seconds (sampling frequency is just slightly larger than the Nyquist rate). For comparison, the EMISE of the classical W-S interpolation scheme and the EMISE of the thresholding-based reconstruction scheme, (3.2), are also plotted. The plot indicates that the proposed sampling and reconstruction scheme gives better reconstruction accuracy than the classical W-S interpolation scheme and the thresholding-based reconstruction scheme proposed in

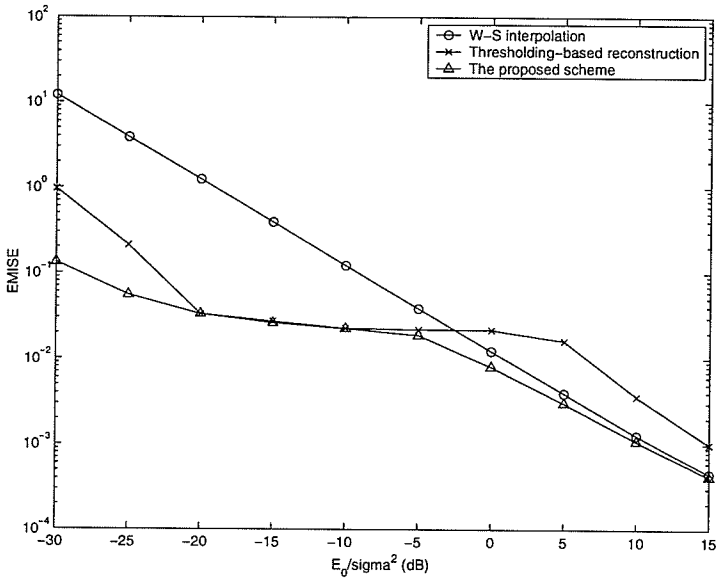

Figure 5.3: $EMISE(\widehat{x})$ versus E_0/σ^2 (Signal $x_1(t)$, $T = \sigma$)

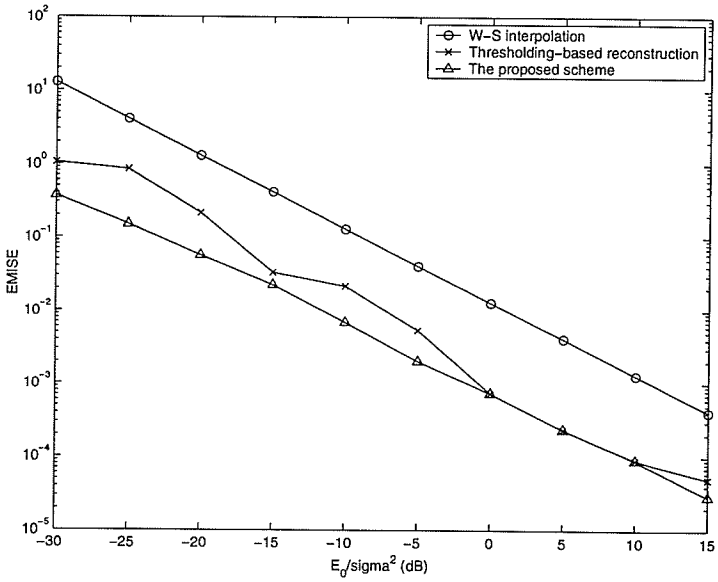

Figure 5.4: $EMISE(\widehat{x})$ versus E_0/σ^2 (Signal $x_2(t)$, $T = \sigma$)

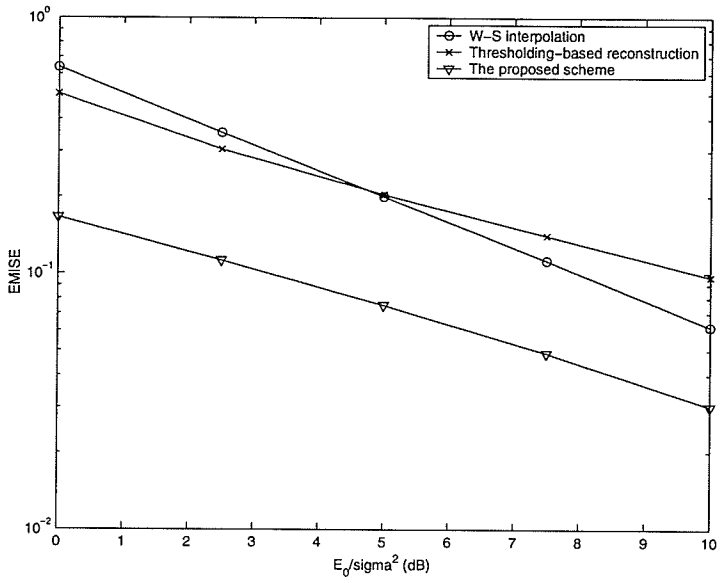

Figure 5.5: $EMISE(\widehat{x})$ versus E_0/σ^2 (Speech signal , $T = \sigma$)

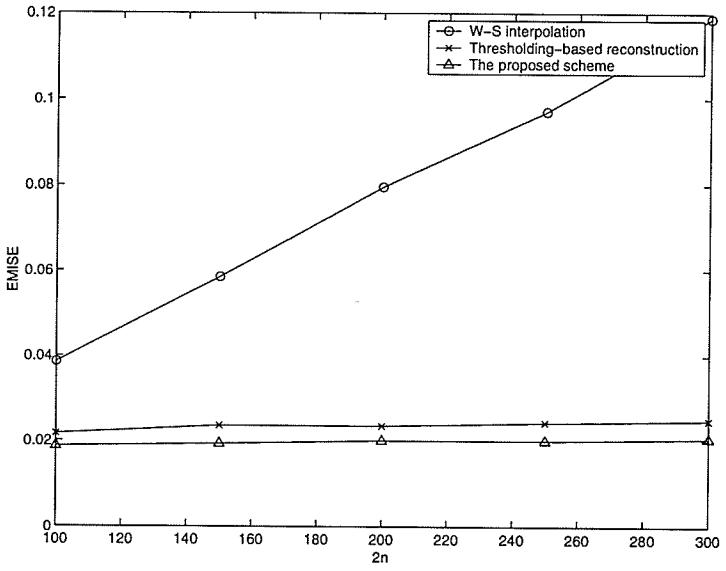

Figure 5.6: $EMISE(\widehat{x})$ versus n_q

Chapter 3 for every value of SNR. This agrees with the observations made in corollary 5.9. Figure 5.5 gives the simulation result when the voice "speech sig" is used as the test signal.

Figure 5.6 plots the EMISE of the proposed sampling and reconstruction scheme as a function of n_q. In this simulation, signal $x_1(t)$ defined in (3.15) is used as the test signal, $E_0/\sigma^2 = -5$ dB and $\tau = 1.25 \cdot 10^{-4}$. The plot clearly shows that the EMISE of the proposed sampling and reconstruction scheme is less dependent on n than the classical W-S interpolation scheme. It also indicates that the performance gap between the two reconstruction schemes becomes wider as n increases.

The plots of the reconstructed waveforms are shown in Appendix F.

The data storage reduction ratio: For test signal $x_1(t)$ defined in (3.15), $T = \sigma$, $2n_q+1 = 101$ and $E_0/\sigma^2 = -5$ dB, we have $\eta = 29$. If 8-bit uniform quantizer is used, then according to (5.5) the data storage reduction ratio is $D_R = 29/101+1/8 \approx 1/2.4$. Table 5.1 shows the computed D_R for various values of E_0/σ^2.

Table 5.1: The Data Storage Reduction Ratio

E_0/σ^2 (dB)	-5	0	5	10
D_R [Signal $x_1(t)$]	1/2.4	1/1.6	1/1.3	1/1.1
D_R [Signal $x_2(t)$]	1/5.7	1/5.7	1/5.7	1/5.1

5.4 Conclusions

This chapter introduced a new sampling and reconstruction scheme for representing and recovering signals from noisy data. The proposed reconstruction scheme does not use oversampling, which is commonly utilized for signal reconstruction from noisy

data.

The accuracy of the proposed reconstruction scheme was studied analytically and experimentally. The obtained results showed that that the proposed scheme always gives better reconstruction accuracy than the classical W-S interpolation scheme, regardless of the SNR, and/or size of data record. It also gives better reconstruction accuracy than the thresholding-based reconstruction scheme proposed in Chapter 3.

The MISE of the proposed reconstruction scheme increases as the size of data record $2n_q+1$ increases, but at much lower rate than that of the classical W-S interpolation scheme. It is worth mentioning that the oversampling/filtering reconstruction schemes discussed in Section 2.4 converge to the original signal when $n \rightarrow \infty$.

For the signals where the small sampled values are more probable (e.g. speech) or for low SNR, the proposed sampling scheme requires smaller number of bits to represent the signals than the classical W-S sampling/reconstruction scheme. As a result, it provides a reduction in data storage.

Since the proposed reconstruction scheme works especially well when SNR is low, it has the potential application in designing signal acquisition and reconstruction systems operating under highly noisy environments. The proposed reconstruction scheme also has a promising application in speech acquisition and reconstruction. This is due to the fact that, for speech signals, the sampled values near zero are more probable than those far away from zero. Since the proposed technique does not use oversampling, it can be used for acquisition of ultra wideband signals.

Chapter 6

Signal Reconstruction via Multiple Observations and Thresholding

As mentioned previously, the signal recovery schemes with smoothing corrections discussed in Section 2.4 depend on the use of a high sampling rate for noise reduction. Therefore, their realizations require costly high-speed electronic circuits. There also exists the potential problem that the correlation between successive samples increases as the sampling rate increases, which leads to unstable reconstruction.

In this chapter, instead of oversampling, a new technique is proposed that collects multiple sets of the sampled values acquired at the Nyquist sampling rate and uses the thresholding-based reconstruction algorithm proposed in Chapter 3 to recover the signal.

The chapter is organized as follows. Section 6.1 introduces a signal recovery scheme that utilizes multiple observations. In Section 6.2, a reconstruction scheme that utilizes both multiple observations and thresholding-based signal recovering algorithm is presented. Section 6.3 discusses several potential applications of the proposed signal recovery schemes. Section 6.4 concludes the Chapter.

6.1 Signal Recovery via Multiple Observations

6.1.1 Introduction

It is well known that if random variables $z_1, z_2, \cdots, z_L$ are mutually uncorrelated with mean μ and variance σ^2, then $z = \frac{1}{L}\sum_{l=1}^{L} z_l$ is a random variable with mean μ and variance $\sigma_1^2 = \sigma^2/L$ [54]. It means that the variance of the new random variance z is reduced by the factor L compared to the variances of individual random variables. In this section, this fact is utilized to improve the reconstruction accuracy of the classical W-S interpolation scheme.

During the data acquisition process, multiple copies of the set of sampled values acquired at the Nyquist rate are collected, i.e., collect the sets $\{x_{lk}\}$, $l = 1, 2, \cdots, L$, where $x_{1k} = x_{2k} = \cdots = x_{Lk} = x(k\tau_q) = x_k$. Here, L is the number of copies of the set of sampled values.

Consider the following observation model :

$$y_{lk} = x_{lk} + \varepsilon_{lk} = x_k + \varepsilon_{lk}, \qquad k = 0, \pm 1, ..., \pm n_q \qquad l = 1, 2, \cdots, L \tag{6.1}$$

where, ε_{lk} are independent random variables with zero-mean and variance σ^2.

From the observed signal samples y_{lk}, the original signal $x(t)$ is reconstructed by:

$$\overline{x}(t) = \sum_{|k| \le n_q} \overline{y}_k \cdot \mathrm{sinc}\left(\frac{t}{\tau_q} - k\right) \tag{6.2}$$

where,

$$\overline{y}_k = \frac{1}{L}\sum_{l=1}^{L} y_{lk} \tag{6.3}$$

is the sample mean of the set $\{y_{lk}\}$, $l = 1, 2, \cdots, L$.

For comparison, assume that the proposed scheme and the oversampling/post-filtering scheme discussed in Section 2.4.2 measure the signal within a fixed interval.

With this assumption, n_q in (6.2) relates to n in (2.35) by:

$$\frac{2n+1}{2n_q+1} = \frac{\tau_q}{\tau} \tag{6.4}$$

If it is assumed further that both schemes use the same number of sampled values for signal reconstruction, then one has the following relationship:

$$L = \frac{2n+1}{2n_q+1} = \frac{\tau_q}{\tau} \tag{6.5}$$

The subsequent subsections provide an error analysis of the proposed scheme and simulation results.

6.1.2 Error Analysis

The following theorem gives an exact formula for computing the MISE of the estimate $\overline{x}(t)$ of (6.2). The proof of the theorem is given in the Appendix D.

Theorem 6.1. *Consider the observation model of (6.1), where ε_{lk} are independent random variables with zero mean and variance σ^2. The MISE of estimate $\overline{x}(t)$ of (6.2) is given by:*

$$MISE(\overline{x}) = \tau_q \sigma_1^2 (2n_q+1) + \tau_q \sum_{|k|>n_q} x_k^2 \tag{6.6}$$

where, $\sigma_1^2 = \sigma^2/L$

Remark 6.1. It can be easily shown that:

$$IVAR(\overline{x}) = \tau_q \sigma_1^2 (2n_q+1) \tag{6.7}$$

$$IBIAS(\overline{x}) = \tau_q \sum_{|k|>n_q} x_k^2 \tag{6.8}$$

From (6.7) and (1.10):

$$\frac{IVAR(\overline{x})}{IVAR(\widetilde{x})} = \frac{1}{L}$$

where, $IVAR(\widetilde{x})$ is the IVAR of the classical W-S interpolation scheme. Therefore, the proposed reconstruction scheme reduces the IVAR of the classical W-S interpolation scheme by a factor L.

Remark 6.2. Assume that the proposed scheme and the oversampling/post-filtering reconstruction scheme defined by (2.35) use the same number of sampled values to recover the original signal. From (2.36), (6.7) and (6.5):

$$IVAR(\overline{x}) = IVAR(\breve{\breve{x}}) \tag{6.9}$$

Thus, the proposed sampling and reconstruction scheme and the oversampling/post-filtering reconstruction scheme have identical IVARs. However, the advantage of the proposed scheme is that it does not require a very high sampling rate as in case of the oversampling/post-filtering reconstruction scheme. Instead, it uses multiple sets of sampled values acquired at the Nyquist rate. Given difficulties in designing high-speed analog-to-digital converters (ADCs with very high sampling rate) [55, 56], the proposed scheme has a clear advantage over the method using oversampling and post-filtering in term of implementation. In addition, the proposed technique avoids the potential problem of increasing correlation between sampled values as the sampling rate increases. Finally, as shall be seen later in Section 6.2, the proposed scheme can be combined nicely with the thresholding-based algorithm proposed in Chapter 3 to provide added reconstruction accuracy.

6.1.3 Simulation Results

Figure 6.1, Figure 6.2 and Figure 6.3 plot the EMISE of the proposed sampling and reconstruction scheme when $L = 2, 4$, and 8, respectively. For comparison, the EMISE of the classical W-S interpolation scheme and the EMISE of the oversampling/post-

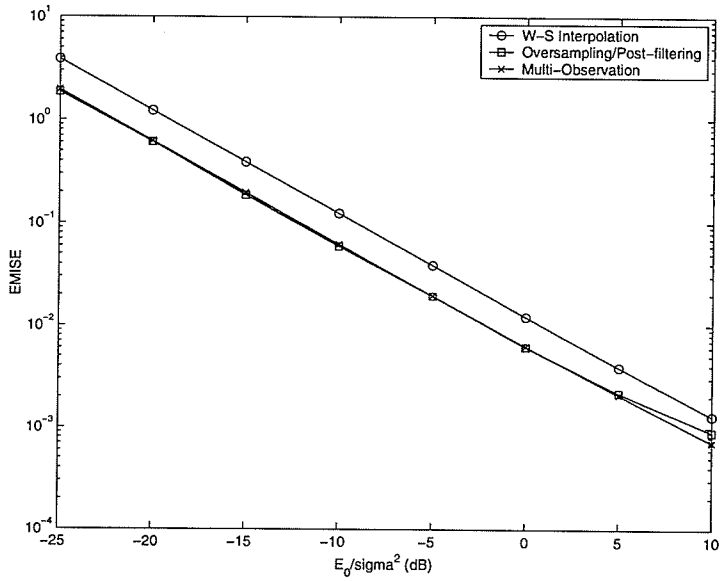

Figure 6.1: $EMISE(\overline{x})$ versus E_0/σ^2 (Signal $x_1(t)$, L=2)

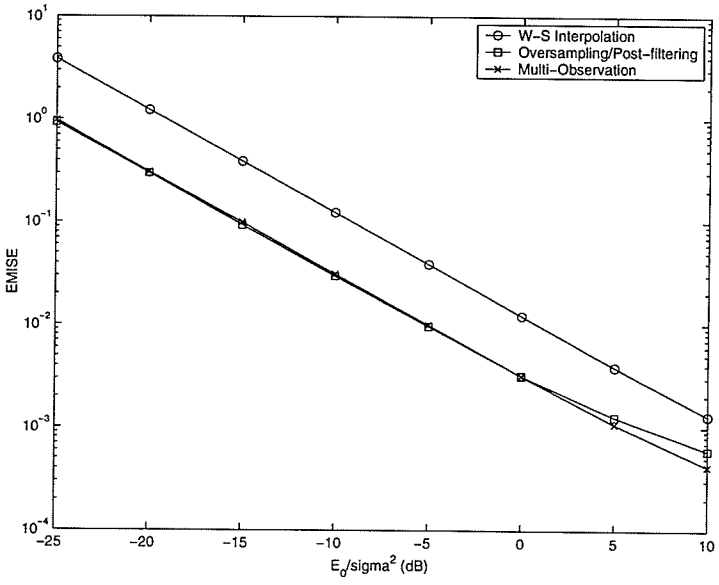

Figure 6.2: $EMISE(\overline{x})$ versus E_0/σ^2 (Signal $x_1(t)$, L=4)

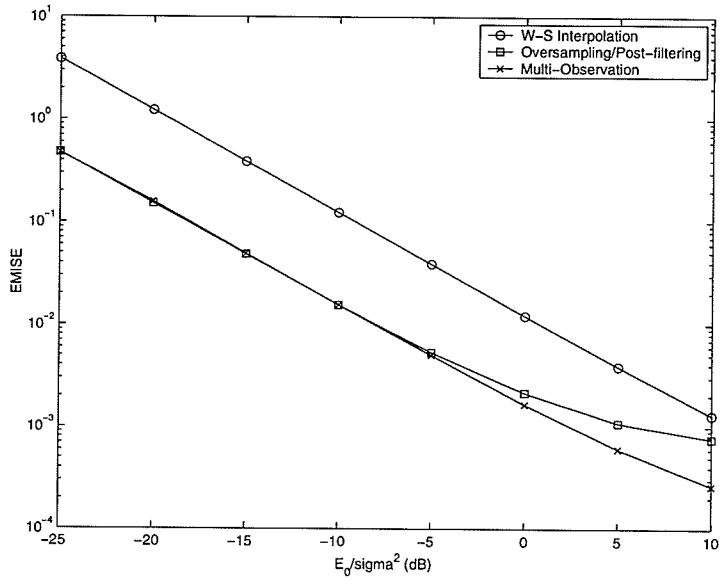

Figure 6.3: $EMISE(\overline{x})$ versus E_0/σ^2 (Signal $x_1(t)$, L=8)

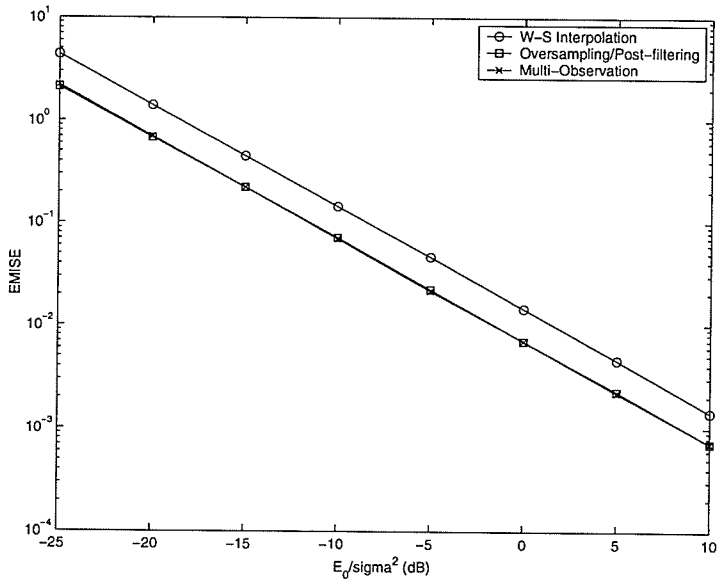

Figure 6.4: $EMISE(\overline{x})$ versus E_0/σ^2 (Signal $x_3(t)$, L=2)

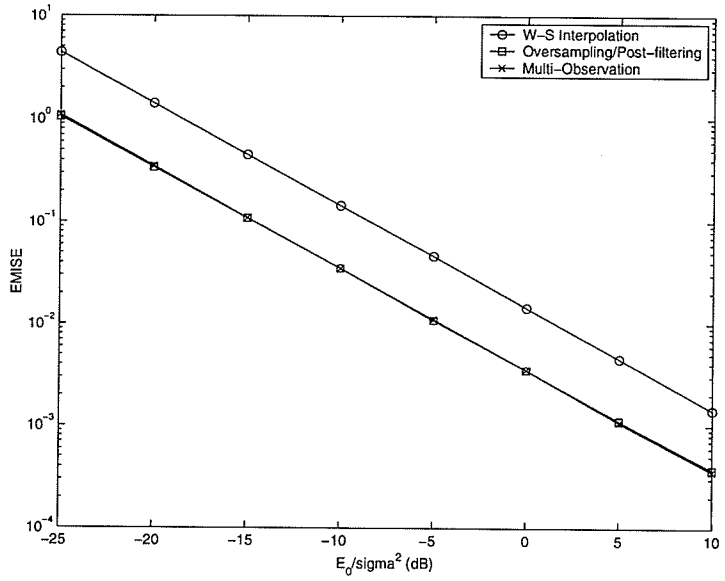

Figure 6.5: $EMISE(\overline{x})$ versus E_0/σ^2 (Signal $x_3(t)$, L=4)

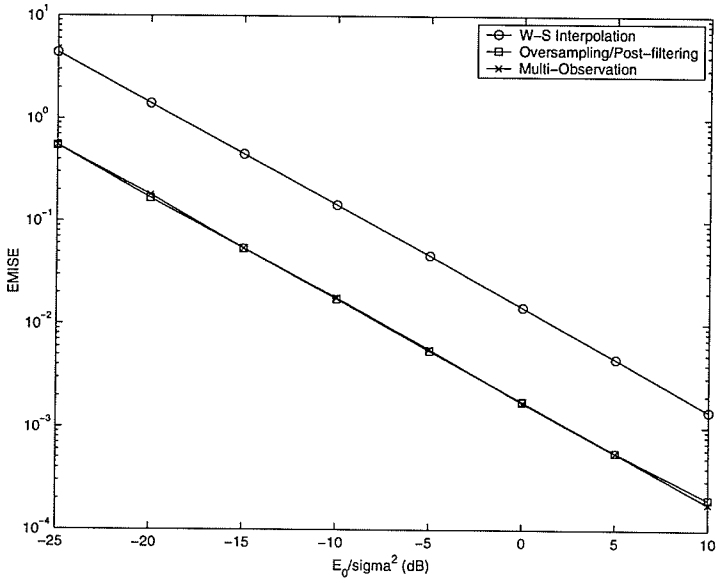

Figure 6.6: $EMISE(\overline{x})$ versus E_0/σ^2 (Signal $x_3(t)$, L=8)

filtering reconstruction method (OSF=2, 4, and 8, respectively) are also plotted. Test signal $x_1(t)$ defined by (3.15) is used for simulation, $2n_q = 100$, $\tau_q = 1.25 \cdot 10^{-4}$ seconds (sampling frequency is just slightly larger than the Nyquist rate). The plots show that the proposed scheme and the oversampling and post-filtering reconstruction scheme have almost identical reconstruction accuracies. However, for high SNR or for large OSF, the former scheme has a better reconstruction accuracy than the latter one. The same simulation is repeated for test signal $x_3(t)$ defined by (3.17). The simulation results are graphed in Figure 6.4, Figure 6.5, and Figure 6.6, respectively.

The plots of reconstructed waveforms are shown in Appendix F.

6.2 Signal Recovery via Multiple Observations and Thresholding

6.2.1 Introduction

The reconstruction accuracy of the signal recovery scheme of (6.1) can be improved further by thresholding the sample means $\overline{y}_k$ defined in (6.3) prior to signal reconstruction. The following 3-step procedure is proposed for reconstruction of the signal $x(t)$ from noisy observations $\{y_{lk}\}$:

Step 1: Calculate the sample means

$$\overline{y}_k = \frac{1}{L} \sum_{l=1}^{L} y_{lk}$$

Step 2: Threshold $\overline{y}_k$ to obtain:

$$\widehat{y}_k = \begin{cases} \overline{y}_k & \text{if} \quad |\overline{y}_k| > T \\ \\ 0 & \text{if} \quad |\overline{y}_k| \leq T. \end{cases} \tag{6.10}$$

where, T is a threshold level. Its value is to be determined later.

Step 3: Use $\widehat{y}_k$ found above to form the following estimate:

$$\widehat{x}(t) = \sum_{|k|\leq n_q} \widehat{y}_k \cdot \text{sinc}\left(\frac{t}{\tau_q} - k\right) \tag{6.11}$$

Consider next the error analysis of the estimate $\widehat{x}(t)$. After this the influence of threshold level T on the performance of the proposed reconstruction scheme is investigated. Finally, simulation results which verify the obtained theoretical results, are provided.

6.2.2 Error Analysis

The following theorem gives an exact formula to compute the MISE of estimate $\widehat{x}(t)$. The proof of the theorem is given in the Appendix D.

Theorem 6.2. *Consider the observation model of (6.1), where ε_{lk} are independent Gaussian random variables with zero mean and variance σ^2. The MISE of estimate $\widehat{x}(t)$ of (6.11) is given by:*

$$MISE(\widehat{x}) = \tau_q \sigma_1^2 (2n_q + 1) + \tau_q \sum_{|k|>n_q} x_k^2 - \tau_q \sigma_1^2 D \tag{6.12}$$

with,

$$\begin{aligned} D &= f(x_k, \sigma_1^2, T) \\ &= \sum_{\substack{|k|\leq n_q \\ x_k<-T}} \frac{1}{\sqrt{\pi}} \left[\gamma\left(\frac{3}{2}, \frac{(x_k - T)^2}{2\sigma_1^2}\right) - \gamma\left(\frac{3}{2}, \frac{(x_k + T)^2}{2\sigma_1^2}\right)\right] \\ &\quad + \sum_{\substack{|k|\leq n_q \\ |x_k|\leq T}} \frac{1}{\sqrt{\pi}} \left[\gamma\left(\frac{3}{2}, \frac{(x_k - T)^2}{2\sigma_1^2}\right) + \gamma\left(\frac{3}{2}, \frac{(x_k + T)^2}{2\sigma_1^2}\right)\right] \\ &\quad + \sum_{\substack{|k|\leq n_q \\ x_k>T}} \frac{1}{\sqrt{\pi}} \left[\gamma\left(\frac{3}{2}, \frac{(x_k + T)^2}{2\sigma_1^2}\right) - \gamma\left(\frac{3}{2}, \frac{(x_k - T)^2}{2\sigma_1^2}\right)\right] \\ &\quad - \sum_{|k|\leq n_q} \frac{x_k^2}{\sigma_1^2} \left[\frac{1}{2}\text{erf}\left(\frac{x_k + T}{\sigma_1\sqrt{2}}\right) - \frac{1}{2}\text{erf}\left(\frac{x_k - T}{\sigma_1\sqrt{2}}\right)\right] \end{aligned} \tag{6.13}$$

where, $\sigma_1^2 = \sigma^2/L$, $\gamma(\alpha, x)$ *and* $\mathrm{erf}(x)$ *are the incomplete gamma function and error function, respectively [50].*

Remark 6.3. From (6.12) and (6.6):

$$MISE(\widehat{x}) = MISE(\overline{x}) - \tau_q \sigma_1^2 D \tag{6.14}$$

where, $MISE(\overline{x})$ is the MISE of the estimate $\overline{x}(t)$ defined by (6.2).

If the second term in the RHS of (6.14) is positive, it represents the degree of noise reduction of the proposed estimate. By setting threshold level properly, one can make $D > 0$.

The following theorem confirms the existence of the optimal threshold level that minimizes the MISE of the proposed reconstruction scheme. The proof of the theorem is given in Appendix D. The theorem is valid for arbitrary distributions.

Theorem 6.3. *Consider the observation model of (6.1), where* ε_k *are independent random variables with zero mean and variance* σ^2. *For a given signal* $x(t)$ *and noise variance* σ^2, *there always exists the optimum threshold level* T_{opt} *so that the MISE of estimate* $\widehat{x}(t)$ *given by (6.11) is minimum.*

The following theorem gives exact formulas for computing the IBIAS and IVAR of the proposed reconstruction scheme. The proof of the theorem is given in Appendix D.

Theorem 6.4. *Consider the observation model of (6.1), where* ε_{lk} *are independent Gaussian random variables with zero mean and variance* σ^2. *The IBIAS and the IVAR of estimate* $\widehat{x}(t)$, *(6.11), is given by:*

$$IBIAS(\widehat{x}) = \tau_q \sum_{|k| \le n_q} d_k^2 + \tau_q \sum_{|k| > n_q} x_k^2, \tag{6.15}$$

$$IVAR(\widehat{x}) = \tau_q \sigma_1^2 (2n_q + 1) - \tau_q \sum_{|k|<n_q} d_k^2 - \tau_q \sigma_1^2 D, \tag{6.16}$$

with D is given by (6.13) and,

$$\begin{aligned} d_k &= \frac{\sigma_1}{\sqrt{2\pi}} \left[e^{-(x_k+T)^2/2\sigma_1^2} - e^{-(x_k-T)^2/2\sigma_1^2} \right] \\ &\quad + \frac{x_k}{2} \left[\text{erf}\left(\frac{x_k + T}{\sigma_1 \sqrt{2}} \right) - \text{erf}\left(\frac{x_k - T}{\sigma_1 \sqrt{2}} \right) \right] \end{aligned} \tag{6.17}$$

6.2.3 Choice of Threshold Level

In this subsection, the influence of the threshold level on the reconstruction accuracy of the proposed reconstruction scheme is investigated. In particular, it is shown how T can be optimally pre-computed during the data acquisition process. A sub-optimal criteria for setting the threshold level is suggested.

Pre-Determination of the Optimal Threshold Level

From Theorem 6.3, one knows that there exists the optimal threshold level that minimizes the MISE of the proposed reconstruction scheme. Moreover, Theorem 6.2 gives an exact formula for computing the MISE of the proposed reconstruction scheme. Since the first two terms in the RHS of (6.12) do not depend on threshold level T, one concludes that the optimal threshold level is the value of T, at which the term D defined by (6.13) is maximum.

The term D can be pre-computed during the data acquisition process and the optimal threshold level T_{opt} can be pre-determined accordingly. T_{opt} is considered as the side information and can be made available for signal reconstruction by various methods. For example, with $L = 4$ and test signal $x_1(t)$ defined by (3.15), the optimal threshold levels are given in the Table 6.1. It is observed from the table that the optimal threshold level increases as noise variance increases, and decreases as noise variance decreases. If $\sigma^2 \to 0$, then $T_{opt} \to 0$.

Table 6.1: The optimal threshold levels at various E_0/σ^2 ($L = 4$)

E_0/σ^2 (dB)	-25	-20	-15	-10	-5	0	5	10
T_{opt}	48.04	46.28	27.00	15.94	1.01	0.107	0.055	0.001

A Sub-Optimal Criteria for Setting Threshold Level

Reconstruction of the signal using the optimal threshold level requires pre-determination of T_{opt} and a mechanism for delivering T_{opt} to the receiver. Therefore, a sub-optimal method is suggested, where the threshold level T is set adaptively according to the noise variance. For instance, one may set $T = \sigma_1\sqrt{a}$, where a is the parameter used to control the reconstruction accuracy. In order to investigate the dependence of $MISE(\widehat{x})$ on parameter a, the following theorem is established. The proof of this theorem is given in Appendix D.

Theorem 6.5. *Consider the observation model of (6.1), where ε_{lk} are independent Gaussian random variables with zero mean and variance σ^2. The MISE of estimate $\widehat{x}(t)$ of (6.11) is upper bounded by:*

$$\begin{aligned} MISE(\widehat{x}) \;\leq\; & \tau_q\sigma_1^2\left[1-\frac{2}{\sqrt{\pi}}\gamma\left(\frac{3}{2},\frac{T^2}{2\sigma_1^2}\right)\right](2n_q+1) \\ & + \operatorname{erf}\left(\frac{T}{\sigma_1\sqrt{2}}\right)E_0 + \left(\tau_q\sum_{|k|>n_q}x_k^2\right)\operatorname{erfc}\left(\frac{T}{\sigma_1\sqrt{2}}\right) \end{aligned} \tag{6.18}$$

where, $\sigma_1^2 = \sigma^2/L$ and $E_0 = \tau_q\sum_{|k|\leq\infty}x_k^2 = \int_{-\infty}^{\infty}x^2(t)dt$ is the signal's energy.

Similar as in Chapter 3, re-write (6.18) as follows:

$$MISE(\widehat{x}) \leq \tau_q\sigma_1^2(2n_q+1) + \tau_q\sum_{|k|>n_q}x_k^2 - \tau_q\sigma_1^2(2n_q+1)f(G_{nq},T)$$

where,

$$f(G_{nq},T) = \frac{2}{\sqrt{\pi}}\gamma\left(\frac{3}{2},\frac{T^2}{2\sigma_1^2}\right) - G_{nq}\operatorname{erf}\left(\frac{T}{\sigma_1\sqrt{2}}\right) \tag{6.19}$$

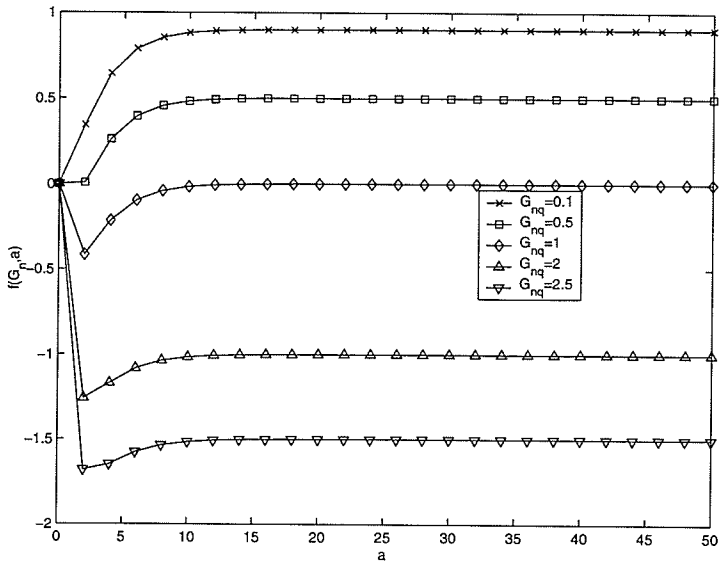

Figure 6.7: $f(G_{nq}, a)$ versus a

and,

$$G_{nq} \triangleq \frac{\frac{1}{2n_q+1}\sum_{|k|\leq n_q} x_k^2}{\sigma_1^2}, \tag{6.20}$$

Equivalently:

$$\Delta \triangleq MISE(\overline{x}) - MISE(\widehat{x}) \geq \tau_q \sigma_1^2 (2n_q + 1) f(G_{nq}, T) \tag{6.21}$$

where, $MISE(\overline{x})$ is the MISE of estimate $\overline{x}(t)$ defined by (6.2).

Consequently, to maximize Δ, we have to choose T such that $f(G_{nq}, T)$ is maximum. Figure 6.7 plots $f(G_{nq}, a)$ as the function of a for various G_{nq}, where a relates to T by $T = \sigma_1\sqrt{a}$. Here, parameter a is used to control the reconstruction accuracy.

The following conclusions can be drawn from the plot:

- For $G_{nq} \geq 1$, one should select $T = 0$. In this case, the reconstruction scheme defined by (6.2) yields better reconstruction accuracy than the proposed reconstruction scheme with sub-optimal threshold level.

- For $G_{nq} < 1$, $T = 0$ is no longer the best choice. In fact, one should select $3\sigma_1 \leq T \leq 5\sigma_1$. In this case, the proposed reconstruction scheme with sub-optimal threshold level yields better reconstruction accuracy than the reconstruction scheme defined by (6.2).

Taking the above observations into account leads to the following proposed joint detection/estimation scheme for reconstruction of bandlimited signals from noisy data:

Step 1: Estimate $P \triangleq \sum_{|k|\leq n_q} x_k^2$ from data. Compute G_{nq} using the estimated P

Step 2: If $G_{nq} \geq 1$, set $T = 0$. Otherwise, set T to lie in the range $[3\sigma_1, 5\sigma_1]$.

Step 3: Follow the 3-step procedure introduced in Subsection 6.2.1 to reconstruct the original signal.

6.2.4 Simulation Results

Figure 6.8, Figure 6.9 and Figure 6.10 plot the EMISE of the proposed sampling and reconstruction scheme using thresholding and multiple observations when $L = 2, 4,$ and 8, respectively. Test signal $x_1(t)$ defined by (3.15) is used for simulation. For comparison, the EMISE of the thresholding-based reconstruction scheme of (3.2) and the EMISE of the oversampling/post-filtering reconstruction scheme of (2.35) are also plotted.

As being indicated in the plots, the proposed sampling and reconstruction scheme gives better reconstruction accuracy than the others for every value of SNR. Comparing with the oversampling/postfiltering reconstruction scheme, the proposed scheme gives significant improvement in reconstruction accuracy when SNR is low or when OSF is large. Compared with the thresholding-based reconstruction scheme,

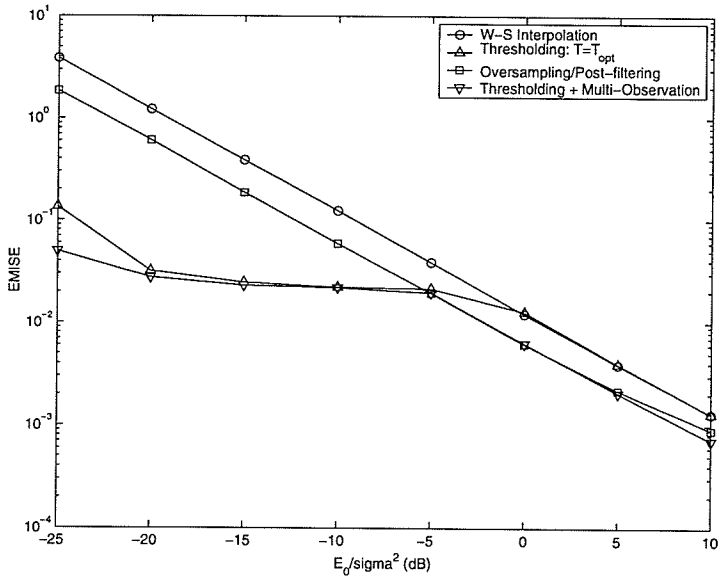

Figure 6.8: $EMISE(\widehat{x})$ versus E_0/σ^2 (Signal $x_1(t)$, L=2)

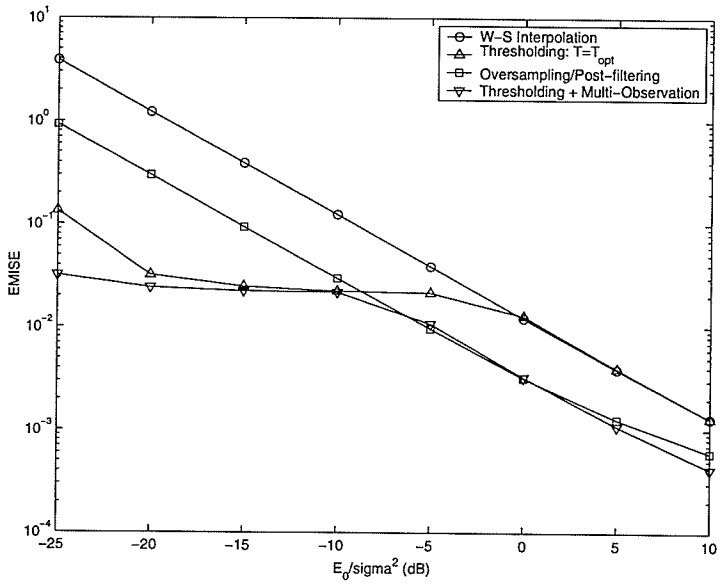

Figure 6.9: $EMISE(\widehat{x})$ versus E_0/σ^2 (Signal $x_1(t)$, L=4)

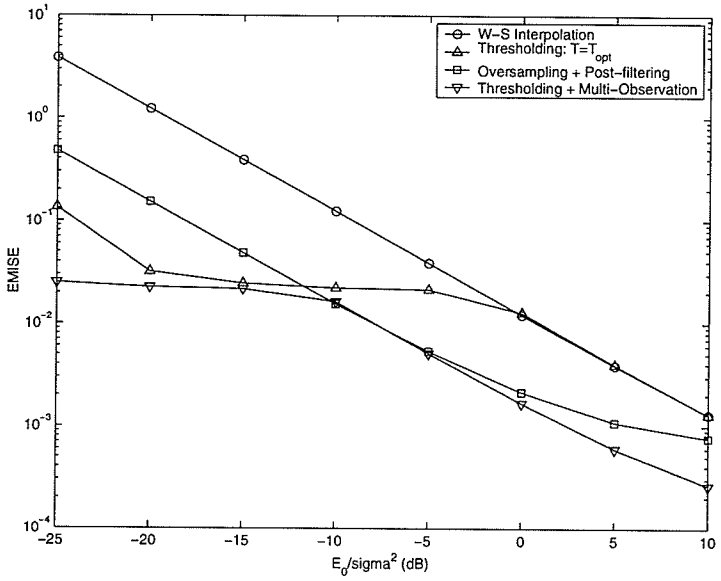

Figure 6.10: $EMISE(\widehat{x})$ versus E_0/σ^2 (Signal $x_1(t)$, L=8)

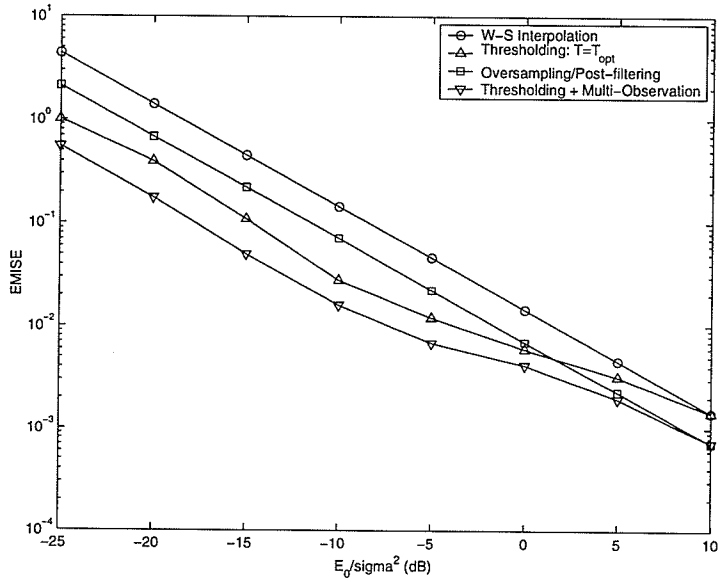

Figure 6.11: $EMISE(\widehat{x})$ versus E_0/σ^2 (Signal $x_3(t)$, L=2)

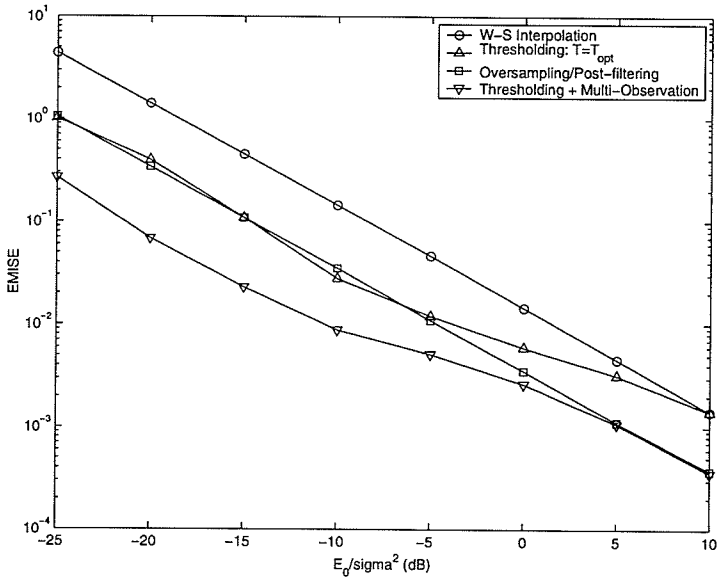

Figure 6.12: $EMISE(\widehat{x})$ versus E_0/σ^2 (Signal $x_3(t)$, L=4)

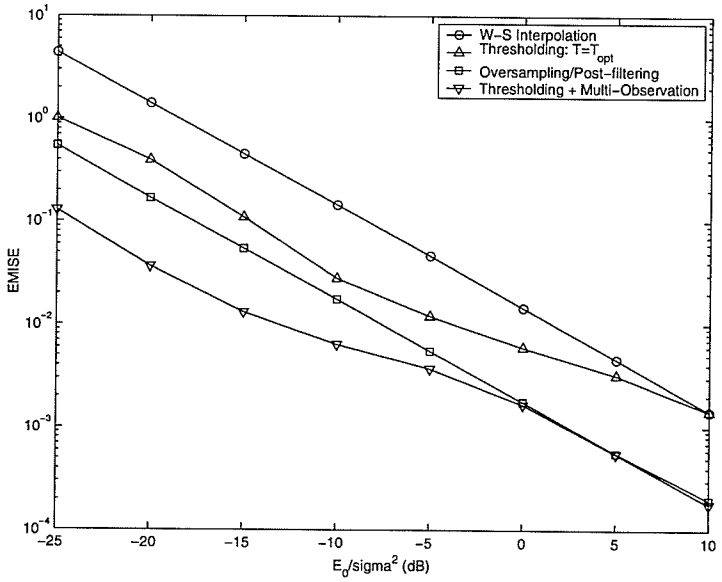

Figure 6.13: $EMISE(\widehat{x})$ versus E_0/σ^2 (Signal $x_3(t)$, L=8)

the proposed scheme yields significant improvement in reconstruction accuracy for high values of SNR. The reconstruction error of the proposed technique decreases as L increases. The same simulation is repeated for test signal $x_3(t)$ defined by (3.17). The simulation results are shown in Figure 6.11, Figure 6.12, and Figure 6.13.

The plots of reconstructed waveforms are shown in Appendix F.

6.3 Applications

The signal sampling and recovery techniques proposed in Sections 6.1 and 6.2 have various applications. For instance, one can apply the proposed techniques to design ADCs with a parallel architecture, see Figure 6.14. Here, instead of increasing the sampling rate to compensate for the noise, one can use a bank of parallel ADCs with the Nyquist sampling rate. The results obtained in the previous sections allow one to claim that this design methodology has better noise reduction property than the method using a single ADC with a very high sampling rate. Moreover, the proposed method has an added advantage taking into account the fact that designing ADCs with very high sampling rate is a challenging task [55, 56]. With the proposed parallel architecture for ADC, one can always add more ADCs into the existing bank of parallel ADCs in order to get better reconstruction accuracy. In contrast, the

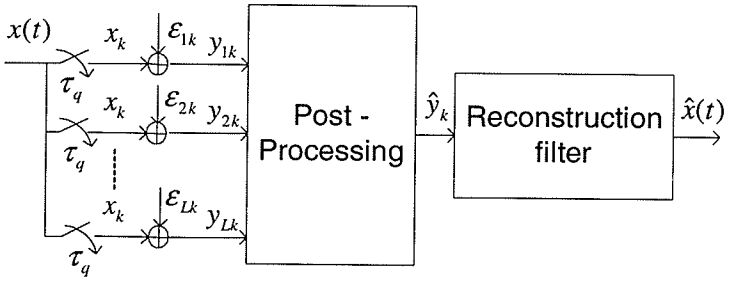

Figure 6.14: ADC with parallel architect

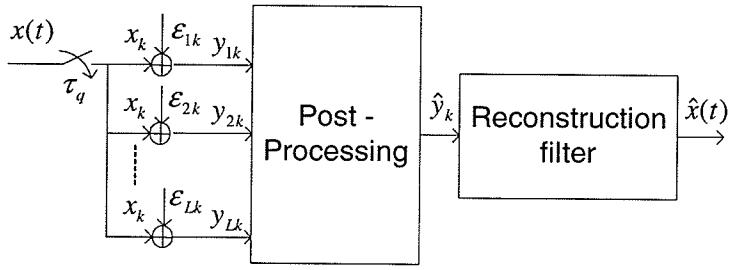

Figure 6.15: Signal reconstruction via multiple access channel

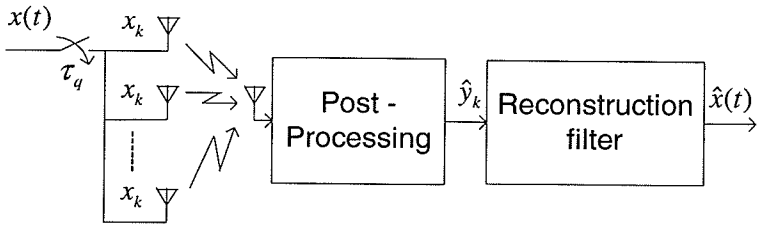

Figure 6.16: Signal reconstruction in multi-antenna communication systems

method using oversampling can not sample the analog signal arbitrary fast. It also has a potential problem of increasing correlation between adjacent samples when the sampling rate increases, which leads to unstable reconstruction.

The signal recovery techniques proposed in Sections 6.1 and 6.2 also have application in reconstruction of signal received via multiple-access channels, see Figure 6.15. This type of channel model can be provided by using multiple transmit antennas, see Figure 6.16. It is worth to mention that designing communication systems with multiple antennas is an active research area in recent years [57].

Two extensions of the model illustrated in Figure 6.14 are shown in Figure 6.17 and Figure 6.18. In these figures d_i and a_i denote unknown delays and gains, respectively. Here, each sensor collects a delayed and distorted version of the sensor field of interest. The objective is to reconstruct the sensor field from a collection of sampled values of the signals acquired at each sensor. These models have potential application in

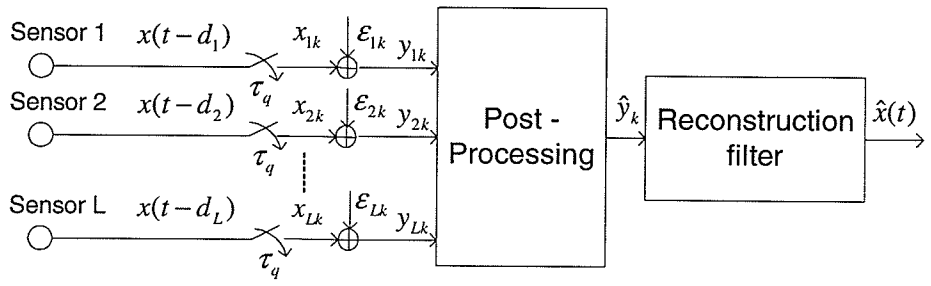

Figure 6.17: Signal acquisition and reconstruction in multi-sensor information systems - Model 1

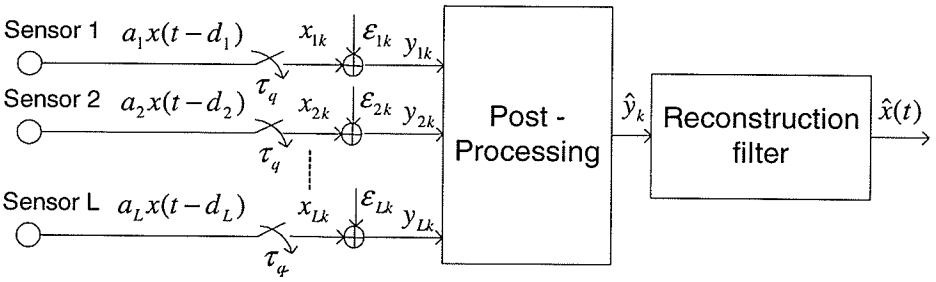

Figure 6.18: Signal acquisition and reconstruction in multi-sensor information systems - Model 2

multi-sensor information systems, where multiple sensors are deployed to enhance the measurement of the surrounding environment or information sources [58].

6.4 Conclusions

In this chapter, new techniques for acquisition and reconstruction of signals in the presence of noise were introduced. The proposed techniques do not use oversampling, which is commonly utilized for signal reconstruction from noisy data.

First, instead of oversampling, the new technique collects multiple sets of signal samples acquired at the Nyquist sampling rate and uses the standard W-S interpolation formula for recovering the signal. It was shown that this sampling and

reconstruction scheme reduces the IVAR of the classical W-S interpolation scheme, (1.4), by the same factor as the oversampling/post-filtering method of (2.35). The obtained results show that for a wide range of SNR or for small OSF, the reconstruction accuracy of the proposed scheme and that of the oversampling/post-filtering method are almost identical. However, for high SNR or for large OSF, the proposed scheme gives better reconstruction accuracy than the oversampling/post-filtering method.

Next, it was shown that added improvement in the reconstruction accuracy can be obtained by acquiring multiple sets of sampled values at the Nyquist sampling rate and using the thresholding-based reconstruction scheme proposed in Chapter 3 to recover the signal. This technique gives better reconstruction accuracy than the thresholding-based reconstruction scheme and the oversampling/post-filtering reconstruction scheme for every value of SNR.

The main advantage of the proposed schemes over the oversampling/filtering method is in term of implementation. Since the proposed techniques do not use oversampling, its realizations do not require costly high-speed electronic circuits. Using the proposed techniques also avoids the potential problem of high correlation between successive samples encountered in the oversampling/filtering method.

Since the proposed techniques work especially well when SNR is low, a potential application is the design of signal acquisition and reconstruction systems which operate in highly noisy environments. The proposed techniques also have applications in ADC, multi-channel communication and multi-sensor information systems. Since the proposed techniques do not use oversampling, its can be used for acquisition of wideband signals.

Chapter 7

A Thresholding-Based Multi-Channel Sampling Scheme

7.1 Introduction

A new signal acquisition technique, which collects multiple sets of the thresholded signal's samples acquired at the Nyquist sampling rate is proposed. The proposed technique is an extension of the thresholding-based sampling scheme introduced in Chapter 5 for the case when multiple channels are available.

The block diagram of the proposed scheme is illustrated in Figure 7.1. It can be

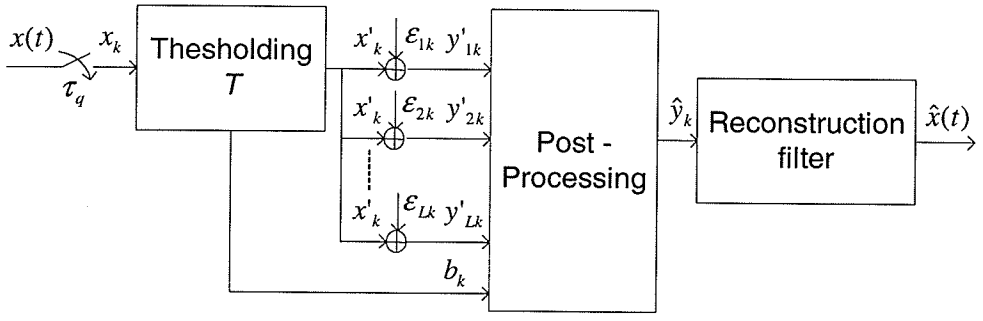

Figure 7.1: The thresholding-based multi-channel sampling scheme

divided into three parts (data acquisition, observation model and reconstruction).

7.1.1 Data Acquisition

The data acquisition process consists of two steps:

Step 1: Uniformly sample the signal $x(t)$ at the Nyquist sampling rate to obtain a sequence of signal samples $\{x_k\}$. Note that the length of $\{x_k\}$ is $2n_q + 1$, where n_q relates to n in (2.35) by $(2n_q + 1)\tau_q = (2n + 1)\tau$. Here, assume that the duration of observation is fixed.

Step 2: Pass $\{x_k\}$ through a threshold device with the threshold level T. Only those samples of $\{x_k\}$ for which $|x_k| > T$ are kept. The other samples are destroyed. Therefore, in Figure 7.1, the sequence $\{x'_k\}$ relates to the sequence $\{x_k\}$ by:

$$\{x'_k\} = \{x_k : |x_k| > T\} \tag{7.1}$$

where, T is a threshold level. Its value is to be determined later.

Instead of using the single set $\{x'_k\}$ as in Chapter 5, in this chapter, L copies of the set $\{x'_k\}$ are collected.

For signal reconstruction purpose, one needs to know the location at which a particular sample is kept or destroyed. This information is made available at the receiver by using the sequence of binary digits $\{b_k\}$, which is formed as follows.

$$b_k = \begin{cases} 1 & \text{if} \quad |x_k| > T \\ 0 & \text{if} \quad |x_k| \leq T \end{cases} \tag{7.2}$$

Note that the length of sequence $\{b_k\}$ is $2n_q + 1$, whereas the length of sequence $\{x'_k\}$ is $\eta \leq 2n_q + 1$. Since the length of sequence $\{x'_k\}$ is always shorter than that of sequence $\{x_k\}$, the thresholding unit acts as a compressor. At the receiver side, the

expander (embedded within post-processing unit) inserts zeros into the noisy sequence $\{\overline{y'}_k\}$ defined by (7.4), at the locations for which $b_k = 0$.

7.1.2 Observation Model

Assume $\{b_k\}$ is available for signal reconstruction while $\{x'_k\}$ is corrupted by noise, i.e.,

$$y'_{lk} = x'_k + \varepsilon_{lk}, \qquad k = 1, ..., \eta \qquad (7.3)$$
$$l = 1, 2, \cdots, L$$

where $\{\varepsilon_{lk}\}$ is an additive noise process and η is the length of $\{x'_k\}$.

7.1.3 Reconstruction

The signal reconstruction process consists of 3 steps as follows.

Step 1: The post-processing unit calculates the sample means

$$\overline{y'}_k = \frac{1}{L}\sum_{l=1}^{L} y'_{lk} \qquad (7.4)$$

Step 2: From the two sequences $\{b_k\}$ and $\{\overline{y'}_k\}$, the sequence $\{\widehat{y}_k\}$ is formed according to the procedure described below.

- Set $\{\widehat{y}_k\}$ to the all-zero sequence. Its length is $2n_q + 1$.
- Denote $k_1, k_2, \ldots, k_\eta$, $(k_1 < k_2 <, \ldots, < k_\eta)$ to be the locations where $b_k = 1$. Set $\widehat{y}_{k_i} = \overline{y'}_i$, $i = 1, 2, \ldots, \eta$.

For example, if $\{b_k\} = 1\ 0\ 1\ 1\ 0\ 1\ 1\ 0\ 0\ 1\ 0$ and $\{\overline{y'}_k\} = \overline{y'}_6\ \overline{y'}_5\ \overline{y'}_4\ \overline{y'}_3\ \overline{y'}_2\ \overline{y'}_1$ then $\{\widehat{y}_k\} = \overline{y'}_6\ 0\ \overline{y'}_5\ \overline{y'}_4\ 0\ \overline{y'}_3\ \overline{y'}_2\ 0\ 0\ \overline{y'}_1\ 0$.

Mathematically:

$$\widehat{y}_k = \begin{cases} \overline{y'}_k & \text{for} \quad k : |x_k| > T \\ \\ 0 & \text{for} \quad k : |x_k| \leq T. \end{cases} \tag{7.5}$$

Step 3: The original signal is reconstructed by:

$$\widehat{x}(t) = \sum_{|k| \leq n_q} \widehat{y}_k \cdot \text{sinc}\left(\frac{t}{\tau_q} - k\right) \tag{7.6}$$

7.1.4 Data Storage Reduction Ratio:

Let assume that a m-bit uniform quantizer is used to obtain binary representation of the sampled values. The oversampling/post-filtering method of (2.35) requires $B_{OS} = (2n+1) \cdot m$ bits for representation of the original signal. On other hand, the proposed technique requires $B_T = L\eta m + (2n_q + 1)$ bits. Denote $D_R = B_T/B_{OS}$ as the data storage reduction ratio (DSRR). Then it can be shown that:

$$D_R = \frac{L\eta}{2n+1} + \frac{\tau}{\tau_q} \cdot \frac{1}{m} \tag{7.7}$$

For comparison with the oversampling/post-filtering method of (2.35), consider the following assumption.

Assumption 7.1. *Assume that the number of copies of the set* $\{x'_k\}$ *in the proposed technique equals to the OSF in the oversampling/post-filtering method, i.e.,* $L = (2n+1)/(2n_q+1) = \tau_q/\tau$.

In this case:

$$D_R = \frac{\eta}{2n_q+1} + \frac{1}{L} \cdot \frac{1}{m} \tag{7.8}$$

Several conclusions can be drawn from (7.8):

- D_R decreases as m increases. In other word, the finer the quantizer, the smaller amount of data storage is required by the proposed technique in comparison with the oversampling/post-filtering method.

- D_R decreases as η decreases, or equivalently, T increases. However, T can not be set arbitrary large since this will effect the reconstruction accuracy.

- For the fixed T, D_R depends on the shape of signal. If the total amount of time that the signal's amplitude falls below threshold level T is large, then D_R is small. In this case, there is a benefit to use the proposed sampling and reconstruction scheme.

- D_R decreases as L increases, or equivalently, τ_q/τ increases. In other word, if very accurate signal reconstruction is expected, then using the proposed technique requires smaller amount of bits for representation and reconstruction of the original signal than using the oversampling/post-filtering method.

7.2 Error Analysis

The following theorem gives an exact formula for the MISE of the proposed sampling and reconstruction scheme. The proof of the theorem is given in Appendix E.

Theorem 7.1. *Consider the observation model of (7.3), where ε_{lk} are independent random variables with zero mean and variance σ^2. The MISE of the estimate $\widehat{x}(t)$ of (7.6) is given by:*

$$MISE(\widehat{x}) = \tau_q \sigma_1^2 \eta + \tau_q \sum_{k \in I_d} x_k^2 + \tau_q \sum_{|k| > n_q} x_k^2 \tag{7.9}$$

where, $\sigma_1^2 = \sigma^2/L$; $I_p = \{k : |x_k| > T\}$ and $I_d = \{k : |x_k| \leq T\}$ are two index sets; $\eta = |I_p|$ is the volume (length) of I_p.

The following theorem gives exact formulas for computing the IBIAS and the IVAR of the proposed sampling and reconstruction scheme. The proof of the theorem is given in Appendix E.

Theorem 7.2. *Consider the observation model of (7.3), where ε_{lk} are independent random variables with zero mean and variance σ^2. The IBIAS and the IVAR of estimate $\widehat{x}(t)$ of (7.6) are given by:*

$$IBIAS(\widehat{x}) = \tau_q \sum_{k \in I_d} x_k^2 + \tau_q \sum_{|k|>n_q} x_k^2, \tag{7.10}$$

$$IVAR(\widehat{x}) = \tau_q \sigma_1^2 \eta, \tag{7.11}$$

where $\sigma_1^2 = \sigma^2/L$; $I_p = \{k : |x_k| > T\}$ and $I_d = \{k : |x_k| \leq T\}$ are two index sets; $\eta = |I_p|$ is the volume (length) of I_p.

Remark 7.1. From (2.36) and (7.11), one can easily show that:

$$\frac{IVAR(\widehat{x})}{IVAR(\breve{\breve{x}})} = \frac{\eta}{2n_q + 1} \leq 1 \tag{7.12}$$

Thus, the proposed scheme reduces the IVAR of the oversampling/post-filtering method defined by (2.35) by a factor $(2n_q + 1)/\eta$.

Similar to Chapter 5, one can observe from (7.10) and (7.11) that if T increases, then $IVAR(\widehat{x})$ decreases, but $IBIAS(\widehat{x})$ increases. On other hand, if T decreases, then $IVAR(\widehat{x})$ increases, but $IBIAS(\widehat{x})$ decreases. This trade-off between the IVAR and IBIAS of the proposed scheme reveals the fact that there always exists an optimal threshold level T_{opt} which minimizes $MISE(\widehat{x})$.

For a given noise variance, $MISE(\widehat{x})$ can be pre-computed during data acquisition process using (7.9) and the optimal threshold level T_{opt} can be pre-determined accordingly.

Corollary 7.1. *If* $T \leq \sigma_1$, *then*

$$R = \frac{MISE(\widehat{x})|_{T \leq \sigma_1}}{MISE(\widehat{x})|_{T=0}} \leq 1, \quad \textit{for all} \quad n, \sigma^2 \tag{7.13}$$

Remark 7.2. Corollary 7.1 does not imply that the optimal threshold level must satisfy $T_{opt} \leq \sigma_1$. However, it does suggest a sub-optimal criteria for setting the threshold level, i.e., $T = \sigma_1$. Here, it is assumed that the noise variance is known. With the threshold level set to $T = \sigma_1$, one can observe that R decreases if σ^2 increases. This indicates the advantage of using the proposed technique when SNR is low.

Remark 7.3. It can be observed that when $T = 0$, the proposed estimate and the estimate $\overline{x}(t)$ defined in (6.2) are the same. Therefore, it follows that if the threshold level is selected such that $T \leq \sigma_1$, then $MISE(\widehat{x}) \leq MISE(\overline{x})$. Another advantage of the proposed estimate over the estimate $\overline{x}(t)$ is the reduction in amount of data storage. Refer to (7.8) and at the same time observe that the estimate $\overline{x}(t)$ and the estimate based on oversampling/post-filtering require the same amount of data storage.

7.3 Simulation Results

Figure 7.2 and Figure 7.3 plot the EMISE of the proposed sampling and reconstruction scheme when $L = 4$ and $L = 8$, respectively. In this simulation, signal $x_1(t)$ defined by (3.15) is used as the test signal; $T = \sigma_1 = \sigma/\sqrt{L}$; $2n_q = 100$ and $\tau_q = 1.25 \cdot 10^{-4}$ seconds (the sampling frequency is just slightly larger than the Nyquist rate). For comparison, the EMISE of the thresholding-based sampling scheme proposed in chapter 5 and the EMISE of the oversampling/post-filtering reconstruction scheme of (2.35) are also plotted. As indicated by the plots, the proposed scheme

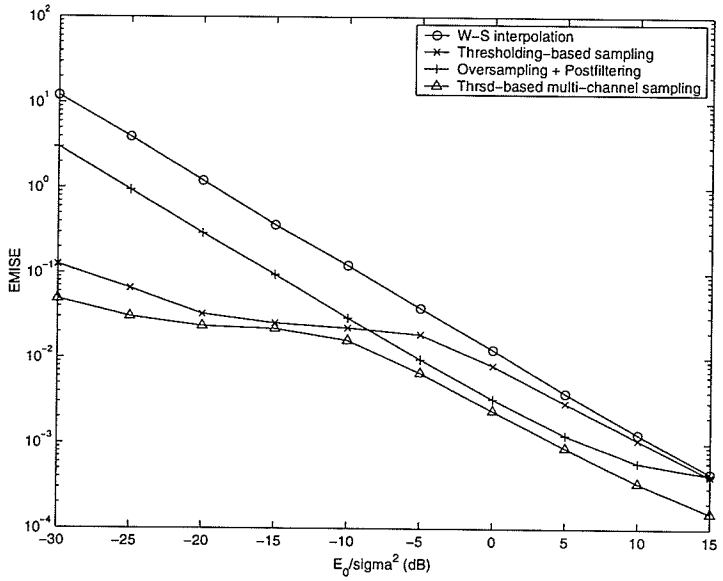

Figure 7.2: $EMISE(\widehat{x})$ versus E_0/σ^2 (Signal $x_1(t)$, L=4)

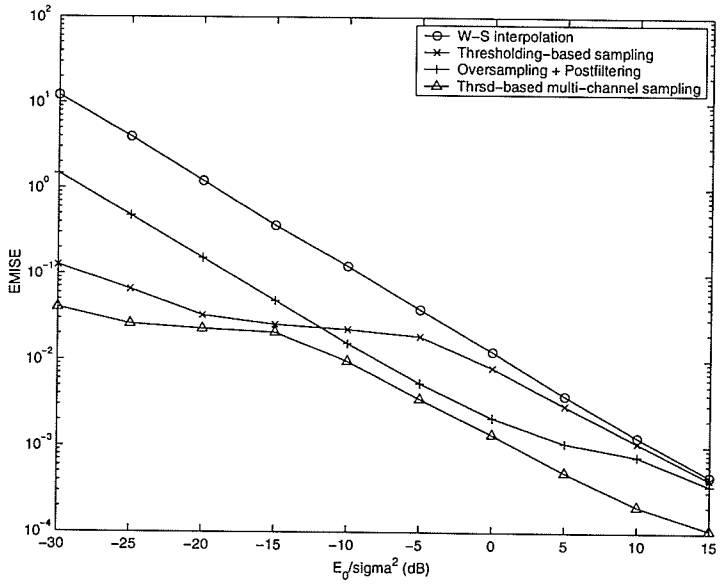

Figure 7.3: $EMISE(\widehat{x})$ versus E_0/σ^2 (Signal $x_1(t)$, L=8)

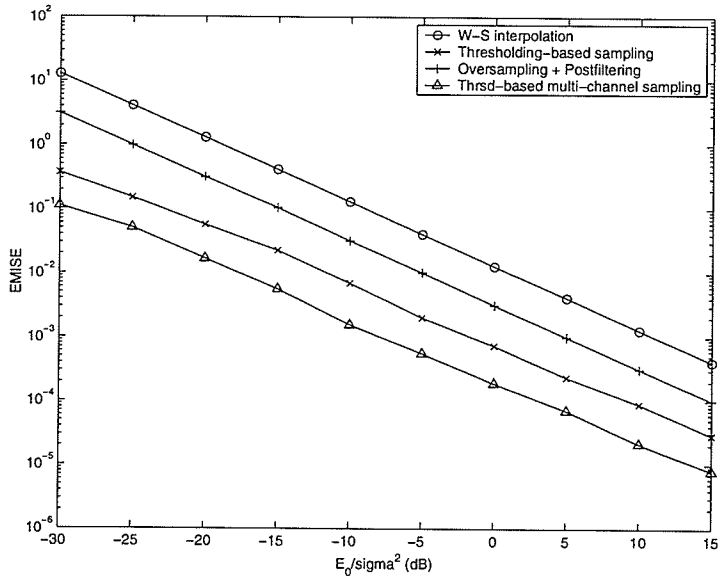

Figure 7.4: $EMISE(\widehat{x})$ versus E_0/σ^2 (Signal $x_2(t)$, L=4)

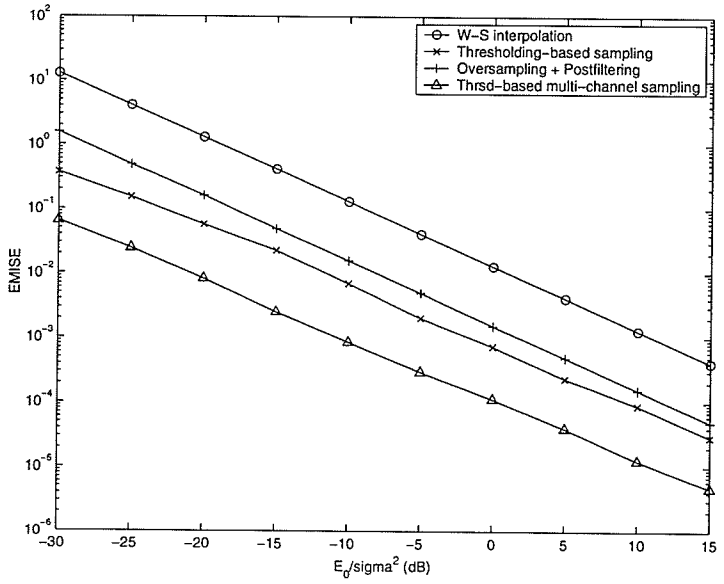

Figure 7.5: $EMISE(\widehat{x})$ versus E_0/σ^2 (Signal $x_2(t)$, L=8)

gives better reconstruction accuracy than the others for every value of SNR. However, significant improvement in the reconstruction accuracy is observed in the region of low SNR.

The same simulation was repeated for test signal $x_2(t)$ defined by (3.16). The simulation results are given in Figure 7.4 and Figure 7.5.

The data storage reduction ratio: For test signal $x_1(t)$ defined by (3.15); $L = 4$; $T = \sigma_1 = \sigma/\sqrt{L}$; $2n_q + 1 = 101$ and $E_0/\sigma^2 = -5$ dB, and therefore, $\eta = 55$. If a 8-bit uniform quantizer is used then according to (7.8) the DSRR is $D_R = 55/101 + (1/4) \cdot (1/8) \approx 1/1.7$. Table 7.1 shows the computed D_R for various values of E_0/σ^2.

Table 7.1: The Data Storage Reduction Ratio

E_0/σ^2 (dB)	-10	-5	0	5
D_R [Signal $x_1(t)$]	1/2.5	1/1.7	1/1.5	1/1.2
D_R [Signal $x_2(t)$]	1/12.4	1/12.4	1/12.4	1/9.9

7.4 Conclusions

A new method for acquisition and reconstruction of signals in the presence of noise was proposed. The proposed technique does not use over-sampling, which is commonly utilized for signal reconstruction from noisy data. It was shown that the proposed technique gives better reconstruction accuracy than the oversampling/post-filtering method for every value of SNR.

For the signals where the small sampled values are more probable (e.g. speeches) or for low SNR, the proposed technique requires smaller amount of bits for representation

of the signals than the oversampling/filtering method. As a result, it provides a reduction in data storage.

Another advantage of the proposed technique over the oversampling/filtering method is in term of implementation. Since the proposed technique does not use oversampling, its realization does not require costly high-speed electronic circuits. Using the proposed technique also avoids the potential problem of high correlation between successive samples encountered in the oversampling/filtering method.

Since the proposed technique works especially well when SNR is low, it has the potential application in designing signal acquisition and reconstruction systems operating in highly noisy environments. It also has applications in ADC, multi-channel communication and multi-sensor information systems. Since the proposed technique does not use oversampling, it can be used for acquisition of ultra wideband signals. It also has application in acquisition and reconstruction of speech. This is due to the fact that, for speech signals, small sampled values are more probable.

Chapter 8

Conclusions

In this thesis, several methods for sampling and recovering signals from noisy observations were proposed. The proposed methods do not use oversampling, which is commonly utilized for recovering signal from noisy data. These techniques were developed based on the observation that small-value samples are denominated by noise, hence, should be removed. This is especially true when noise level is high. This explains why the proposed techniques give significant improvement over the classical W-S interpolation scheme and the oversampling/post-filtering methods when the signal-to-noise ratio is low.

By having the small sampled values deleted, some information is lost about the signal to be reconstructed. As a result, the bias of the proposed techniques is increased. Nevertheless, since these samples are small, they contribute less to the quality of signal reconstruction and the amount of information loss is tolerable. The results reported in the thesis showed that a small number of high-value samples would be sufficient for recovering the signal with acceptable precision. The benefit gained from reducing the variance, however, is great. This trade-off between the variance and bias of the proposed methods reveals the fact that there exists the optimal threshold

level that minimizes the overall reconstruction error.

Obviously, the number of small-value samples that may be deleted depends on the noise level and the signal itself. Therefore, the optimal threshold level depends on the signal-to-noise ratio and the shape of signal. This is why the reconstruction accuracy of the proposed techniques is signal dependent. This property is actually a desirable one since it allows the proposed signal recovery schemes to work adaptively and selectively to the signal they suppose to reconstruct.

The dependency of the reconstruction accuracy on the signal's shape makes the task of identifying the optimal threshold level difficult. The good news is that when the noise level is high, the reconstruction accuracy of the proposed techniques is not so sensitive to the error in identifying the optimal threshold level. It means that one may set the threshold level to lie within a certain range not just the optimal value.

Even though this thesis considered only the classical uniform sampling scheme due to W-S sampling theorem, the observations that made above apply to other sampling schemes as well. These observations should be taken into account when noise is presented. Very often, a signal representation which is exact for the noise-free case will not work in the noisy case, and over-modelling signals results in a lack of robustness.

In Chapter 3, a thresholding-based reconstruction scheme was proposed that gives better reconstruction accuracy than the classical W-S interpolation scheme without utilizing oversampling. The results were extended in Chapter 4, where an adaptive thresholding-based reconstruction scheme was proposed. It was shown that this adaptive thresholding scheme yields better reconstruction accuracy than the thresholding-based reconstruction scheme proposed in Chapter 3. The improvement in the reconstruction accuracy of the proposed reconstruction schemes over the

classical W-S interpolation scheme is significant in the region of low SNR. Therefore, the proposed schemes have potential applications in designing signal acquisition and reconstruction systems operating in highly noisy environments.

As an extension of the above mentioned techniques, a thresholding-based sampling scheme is proposed in Chapter 5. That is, a threshold unit is introduced in the data acquisition process, rather than in the signal reconstruction process as in Chapter 3 and Chapter 4. It was shown that this sampling scheme always gives better reconstruction accuracy than the classical W-S sampling interpolation scheme regardless of SNR, and the size of data set. Moreover, for the signals where the small sampled values are more probable (e.g. speech) or for low SNR, the proposed sampling scheme requires fewer bits to represent the signals compared with the classical W-S sampling/reconstruction scheme. As a result, it provides a reduction in data storage. The proposed sampling scheme has a promising application in speech acquisition and reconstruction. This is due to the fact that for speech signals, the sampled values near zero are more probable.

Chapter 6 proposed a signal sampling and recovering method that utilizes multiple observations and threshold-based signal recovering algorithm for noise reduction. Here, instead of oversampling, one collects multiple sets of sampled values acquired at the Nyquist sampling rate and uses a thresholding-based algorithm for reconstructing the signal. The proposed technique offers better reconstruction accuracy than the oversampling/filtering method. Since the proposed technique does not use oversampling, its realization does not require costly high-speed electronic circuits. It also avoids the potential problem of high correlation between successive samples encountered in the oversampling/filtering method. Several potential applications of this method to ADC, multiple access communication systems and multi-sensor infor-

mation systems were discussed.

Finally, in Chapter 7, a thresholding-based multi-channel sampling scheme was proposed, which is an extension of the thresholding-based sampling scheme introduced in Chapter 5 for multi-channel. It gave a better reconstruction accuracy than the methods proposed in Chapter 6. For the signals where the small sampled values are more probable (e.g. speech) or for low SNR, the proposed sampling scheme requires fewer bits to represent the signals compared with the oversampling/filtering method. As a result, it provides a reduction in data storage. Since the proposed technique does not use oversampling, its realization does not require costly high-speed electronic circuits. It also avoids the potential problem of high correlation between successive samples encountered in the oversampling/filtering method. The proposed technique have potential applications in multi-channel communication and multi-sensor information systems.

The thesis can be extended in several directions. Firstly, the method for estimating the optimal threshold level directly from the noisy data would be worth to investigate. This will eliminate the need for transmission of side information (i.e. the optimal threshold levels) to the receiver for signal reconstruction. A well-known technique in statistical literature called bootstrapping might be used to solve this problem. It is also worth to tabulate the optimal threshold levels for the subclasses of signals having similar features. For example, one may want to tabulate the optimal threshold levels for the signals of practical interest such as speech, audio, bird's sounds, electrical signals in the human body, and so on. Note that when the noise level is high, the reconstruction accuracy of the proposed techniques is not so sensitive to the error in identifying the optimal threshold level. It means that we can estimate a certain range of the threshold level, not just the optimal value.

Secondly, since the thresholded data set is a set of non-uniformly spaced signal samples, one may apply non-linear or iterative signal recovering algorithms for improving the reconstruction accuracy. Refer to [18] for a detailed description of these algorithms. On other hand, the problem of recovering signals from thresholded data is equivalent to the problem of recovering signals from missing data. Therefore, one can apply the techniques developed for reconstructing signals from missing data for improving the reconstruction accuracy. Reference [5] gives a detailed description of these algorithms.

Next, it is noticed that, in Chapter 4, a simple grouping strategy was used, i.e., the observed signal samples were grouped from left to right. It would be of interest to develop more intelligent grouping strategies that selectively group sampled values with the same characteristics together. The optimal threshold levels are then determined for each group accordingly. This approach seems to provide promising results. One can also utilize the concept of block thresholding introduced in the wavelet literature to develop new adaptive thresholding-based reconstruction schemes [59].

In Section 6.3 of Chapter 6, two system models were introduced in Figure 6.17 and Figure 6.18, respectively. These models have potential applications in multi-sensor information systems, where multiple sensors are deployed to enhance the measurement of the surrounding environment or information sources. It is worth to develop signal recovery algorithms for these models.

Thresholding can also be used in the "noise residual" domain. In this method, the noisy data $\{y_k\}$ is passed through a smoothing filter to obtain the smoothed data $\{\widehat{y}_k\}$. The difference $|y_k - \widehat{y}_k|$ between the smoothed data and the noisy data is compared to a threshold level T for making a decision about the noise level. If $|y_k - \widehat{y}_k| > T$, it is likely that the noise level is high. In this case, the smoothed data $\{\widehat{y}_k\}$ should be used

for signal reconstruction. On other hand, if $|y_k - \widehat{y}_k| \leq T$, it is likely that the noise level is low. In this case, one should use $\{y_k\}$ for signal reconstruction. It is worth mentioning that this technique is a particular case of the more general technique that combines thresholding and smoothing for recovering signals from noisy data. One can propose different techniques under this framework.

Finally, it is useful to study the statistical aspects of sampling and reconstruction of other signal classes such as power signals and signals in shift-invariant signal spaces. Shift-invariant signal spaces may be more suitable for modelling the real-world signals than the bandlimited signal model considered in this thesis, see Chapter 2. For instance, one may want consider the model of Figure 2.1 with $c(k)$ being replaced with their noisy versions $y(k) = c(k) + \varepsilon_k$, where $\{\varepsilon_k\}$ is an additive noise process. Similar to the bandlimited signal space studied in the thesis, in the presence of noise, the algorithms for recovering the signals in shift-invariant spaces must incorporate certain smoothing schemes for noise reduction.

Appendix A

Proofs of Theorems in Chapter 3

A.1 Proof of Theorem 3.1

Consider,

$$MISE(\widehat{x}) = E\int_{-\infty}^{\infty}(\widehat{x}(t) - x(t))^2 dt$$

Due to Paseval's formula, $MISE(\widehat{x})$ can be expressed as follows:

$$MISE(\widehat{x}) = \tau_q \sum_{|k|\leq n_q} E(\widehat{y}_k - x_k)^2 + \tau_q \sum_{|k|>n_q} x_k^2 \tag{A.1}$$

Therefore,

$$\begin{aligned}
E(\widehat{y}_k - x_k)^2 &= \int_{-\infty}^{\infty}(\widehat{y}_k - x_k)^2 f_{y_k}(y_k)dy_k \\
&= \int_{-\infty}^{-T}(y_k - x_k)^2 f_{y_k}(y_k)dy_k + \int_{T}^{\infty}(y_k - x_k)^2 f_{y_k}(y_k)dy_k \\
&\quad + \int_{-T}^{T} x_k^2 f_{y_k}(y_k)dy_k \\
&= E(y_k - x_k)^2 - \int_{-T}^{T}(y_k - x_k)^2 f_{y_k}(y_k)dy_k + \int_{-T}^{T} x_k^2 f_{y_k}(y_k)dy_k \\
&= \sigma^2 - \int_{-x_k-T}^{-x_k+T} \varepsilon_k^2 f_{\varepsilon_k}(\varepsilon_k)d\varepsilon_k + x_k^2 \int_{-x_k-T}^{-x_k+T} f_{\varepsilon_k}(\varepsilon_k)d\varepsilon_k
\end{aligned}$$

where,

$$f_{y_k}(y_k) = \frac{1}{\sigma\sqrt{2\pi}} e^{-(y_k - x_k)^2/2\sigma^2}$$

and,

$$f_{\varepsilon_k}(\varepsilon_k) = \frac{1}{\sigma\sqrt{2\pi}} e^{-\varepsilon_k^2/2\sigma^2}$$

are the probability density functions (pdf) of random variables y_k and ε_k, respectively.

Replacing $E(\widehat{y}_k - x_k)^2$ found above into (A.1) gives:

$$\begin{aligned} MISE(\widehat{x}) &= \tau_q\sigma^2(2n_q+1) + \tau_q \sum_{|k|>n_q} x_k^2 - \tau_q \sum_{|k|\le n_q} \int_{-x_k-T}^{-x_k+T} \varepsilon_k^2 f_{\varepsilon_k}(\varepsilon_k) d\varepsilon_k \\ &\quad + \tau_q \sum_{|k|\le n_q} x_k^2 \int_{-x_k-T}^{-x_k+T} f_{\varepsilon_k}(\varepsilon_k) d\varepsilon_k \\ &= \tau_q\sigma^2(2n_q+1) + \tau_q \sum_{|k|>n_q} x_k^2 - \tau_q \sum_{|k|\le n_q} [A(x_k,T) - B(x_k,T)] \quad \text{(A.2)} \end{aligned}$$

where,

$$A(x_k,T) = \int_{-x_k-T}^{-x_k+T} \varepsilon_k^2 f_{\varepsilon_k}(\varepsilon_k) d\varepsilon_k = \frac{1}{\sigma\sqrt{2\pi}} \int_{x_k-T}^{x_k+T} \varepsilon_k^2 e^{-\varepsilon_k^2/2\sigma^2} d\varepsilon_k \qquad \text{(A.3)}$$

and,

$$B(x_k,T) = x_k^2 \int_{-x_k-T}^{-x_k+T} f_{\varepsilon_k}(\varepsilon_k) d\varepsilon_k = \frac{x_k^2}{\sigma\sqrt{2\pi}} \int_{x_k-T}^{x_k+T} e^{-\varepsilon_k^2/2\sigma^2} d\varepsilon_k \qquad \text{(A.4)}$$

It can be shown that:

$$A(x_k,T) = \begin{cases} \frac{\sigma^2}{\sqrt{\pi}} \left[\gamma\left(\frac{3}{2}, \frac{(x_k-T)^2}{2\sigma^2}\right) - \gamma\left(\frac{3}{2}, \frac{(x_k+T)^2}{2\sigma^2}\right) \right] & \text{for} \quad x_k < -T \\ \frac{\sigma^2}{\sqrt{\pi}} \left[\gamma\left(\frac{3}{2}, \frac{(x_k-T)^2}{2\sigma^2}\right) + \gamma\left(\frac{3}{2}, \frac{(x_k+T)^2}{2\sigma^2}\right) \right] & \text{for} \quad |x_k| \le T \\ \frac{\sigma^2}{\sqrt{\pi}} \left[\gamma\left(\frac{3}{2}, \frac{(x_k+T)^2}{2\sigma^2}\right) - \gamma\left(\frac{3}{2}, \frac{(x_k-T)^2}{2\sigma^2}\right) \right] & \text{for} \quad x_k > T \end{cases}$$

and,

$$B(x_k,T) = \frac{x_k^2}{2} \left[\text{erf}\left(\frac{x_k+T}{\sigma\sqrt{2}}\right) - \text{erf}\left(\frac{x_k-T}{\sigma\sqrt{2}}\right) \right]$$

where, $\gamma(\alpha, z)$ and $\text{erf}(x)$ are the incomplete gamma function and the error function, respectively. They are defined as follows [50]:

$$\gamma(\alpha, x) = \int_0^x z^{\alpha-1} e^{-z} dz, \qquad \text{Re}(\alpha) > 0$$

$$\text{erf}(x) = \frac{2}{\sqrt{\pi}} \int_0^x e^{-z^2} dz.$$

Replacing $A(x_k,T)$ and $B(x_k,T)$ founded above into (A.2), we obtain (3.3). The proof is complete.

A.2 Proof of Theorem 3.2

It was found in (A.1) that:

$$MISE(\widehat{x}) = \tau_q \sum_{|k|\leq n_q} E(\widehat{y}_k - x_k)^2 + \tau_q \sum_{|k|>n_q} x_k^2$$

But,

$$\begin{aligned} E(\widehat{y}_k - x_k)^2 &= \int_{-\infty}^{\infty} (\widehat{y}_k - x_k)^2 f_{y_k}(y_k) dy_k \\ &= \int_{-\infty}^{-T} (y_k - x_k)^2 f_{y_k}(y_k) dy_k + \int_{T}^{\infty} (y_k - x_k)^2 f_{y_k}(y_k) dy_k \\ &\quad + \int_{-T}^{T} x_k^2 f_{y_k}(y_k) dy_k \\ &= E(y_k - x_k)^2 - \int_{-T}^{T} (y_k - x_k)^2 f_{y_k}(y_k) dy_k + \int_{-T}^{T} x_k^2 f_{y_k}(y_k) dy_k \\ &= \sigma^2 + \left(- \int_{-T}^{T} (y_k - x_k)^2 f_{y_k}(y_k) dy_k \right) + \int_{-T}^{T} x_k^2 f_{y_k}(y_k) dy_k \end{aligned}$$

Therefore,

$$\begin{aligned} MISE(\widehat{x}) &= \tau_q \sigma^2 (2n_q + 1) + \tau_q \sum_{|k|>n_q} x_k^2 + \left(-\tau_q \sum_{|k|\leq n_q} \int_{-T}^{T} (y_k - x_k)^2 f_{y_k}(y_k) dy_k \right) \\ &\quad + \tau_q \sum_{|k|\leq n_q} \int_{-T}^{T} x_k^2 f_{y_k}(y_k) dy_k \end{aligned} \tag{A.5}$$

Since $(y_k - x_k)^2 f_{y_k}(y_k)$ and $x_k^2 f_{y_k}(y_k)$ are positive functions of y_k, the third term in the RHS of (A.5) is a monotonically decreasing function of T, whereas the forth term is monotonically increasing function of T. Hence, $MISE(\widehat{x})$ is a relatively regular function of T. Moreover, for a finite n_q, $MISE(\widehat{x})$ is finite. Therefore, there always exists an optimal threshold level T_{opt} which minimizes $MISE(\widehat{x})$. The proof is complete.

It is worth noticing that if the noise has Gaussian distribution, the third term in the RHS of (A.5) behaves like C_1/T^{α}, whereas the forth term behaves like $C_2 T^{\beta}$, where $\alpha, \beta > 0$ and $C_1, C_2 > 0$ are positive constants. In this case, it can be shown that the optimal threshold level T_{opt} is the value of T, for which these terms are equal.

A.3 Proof of Theorem 3.3

Parseval's formula yields the following decompositions of the errors:

$$IBIAS(\widehat{x}) = \tau_q \sum_{|k|\le n_q} (E\widehat{y}_k - x_k)^2 + \tau_q \sum_{|k|>n_q} x_k^2. \tag{A.6}$$

But,

$$\begin{aligned}
E\widehat{y}_k &= \int_{-\infty}^{-T} y_k f_{y_k}(y_k)dy_k + \int_{T}^{\infty} y_k f_{y_k}(y_k)dy_k \\
&= Ey_k - \int_{-T}^{T} y_k f_{y_k}(y_k)dy_k = x_k - \frac{1}{\sigma\sqrt{2\pi}} \int_{-T}^{T} y_k e^{-(y_k-x_k)^2/2\sigma^2} dy_k \\
&= x_k - \frac{1}{\sigma\sqrt{2\pi}} \int_{-x_k-T}^{-x_k+T} \varepsilon_k e^{-\varepsilon_k^2/2\sigma^2} d\varepsilon_k - \frac{x_k}{\sigma\sqrt{2\pi}} \int_{-x_k-T}^{-x_k+T} e^{-\varepsilon_k^2/2\sigma^2} d\varepsilon_k \\
&= x_k - \frac{\sigma}{\sqrt{2\pi}} \left[e^{-(x_k+T)^2/2\sigma^2} - e^{-(x_k-T)^2/2\sigma^2} \right] - \frac{x_k}{2} \left[\mathrm{erf}\left(\frac{x_k+T}{\sigma\sqrt{2}} \right) - \mathrm{erf}\left(\frac{x_k-T}{\sigma\sqrt{2}} \right) \right]
\end{aligned}$$

Replacing $E\widehat{y}_k$ founded above into (A.6), one obtains (3.6) with d_k computed as in (3.8).

But, $IVAR(\widehat{x}) = MISE(\widehat{x}) - IBIAS(\widehat{x})$, where $MISE(\widehat{x})$ and $IBIAS(\widehat{x})$ are given in (3.3) and (3.6), respectively. Thus, (3.7) is immediately followed. The proof is complete.

A.4 Proof of Theorem 3.4

Observing that the function $f(\varepsilon_k) = \varepsilon_k^2 e^{-\varepsilon_k^2/2\sigma^2}$ is always positive, symmetric around zero. It has the minimums at $\varepsilon_k = 0$ and $\varepsilon_k = \pm\infty$, respectively. Consequently, for the fixed T, $A(x_k, T)$ defined in (A.3)has the minimums at $x_k = 0$ and $x_k = \pm\infty$, respectively. Since the function $x(t)$ of interest is bounded, one can ignore the case $x_k = \pm\infty$ and establish the following inequality:

$$A(x_k, T) \ge \frac{1}{\sigma\sqrt{2\pi}} \int_{-T}^{T} \varepsilon_k^2 e^{-\varepsilon_k^2/2\sigma^2} d\varepsilon_k, \qquad \forall x_k$$

Or equivalently,

$$A(x_k, T) \geq \frac{2\sigma^2}{\sqrt{\pi}}\gamma\left(\frac{3}{2}, \frac{T^2}{2\sigma^2}\right) \tag{A.7}$$

Similarly, observing that the function $f(\varepsilon_k) = e^{-\varepsilon_k^2/2\sigma^2}$ is always positive, symmetric around zero. It has the maximum at at $\varepsilon_k = 0$ and it decreases as $|\varepsilon_k|$ decreases. Consequently, for the fixed T, $B(x_k, T)$ defined in (A.4) has the maximum at $x_k = 0$. The following inequality can be established.

$$B(x_k, T) \leq \frac{x_k^2}{\sigma\sqrt{2\pi}} \int_{-T}^{T} e^{-\varepsilon_k^2/2\sigma^2} d\varepsilon_k, \quad \forall x_k$$

Or equivalently,

$$B(x_k, T) \leq x_k^2 \text{erf}\left(\frac{T}{\sigma\sqrt{2}}\right) \tag{A.8}$$

From (A.2), (A.7) and (A.8), one can easily obtain (3.10). The proof is completed.

A.5 Proof of Theorem 3.5

If $T = 4\sigma$, then $f(G_n, T) \approx 1 - G_n$. Replacing this into (3.13) gives:

$$\Delta \geq \tau_q \sigma^2 (2n_q + 1)\left[1 - \frac{\sum_{|k|\leq n_q} x_k^2}{\sigma^2(2n_q + 1)}\right] = \tau_q \sigma^2 (2n_q + 1) - \tau_q \sum_{|k|\leq n_q} x_k^2$$

As $n_q \to \infty$, the first term in the right-hand side of the preceding inequality approaches ∞, whereas the second term approaches E_0. This implies that $\Delta \to \infty$ as $n_q \to \infty$.

On other hand, since $f(G_n, T) \approx 1 - G_n$ if selecting $T = 4\sigma$, (3.14) reduces to:

$$R \leq G_n = \frac{\tau_q \sum_{|k|\leq n_q} x_k^2}{\tau_q \sigma^2 (2n_q + 1)}$$

As $n_q \to \infty$, the numerator of the right-hand side of the preceding inequality approaches E_0, whereas the denominator approaches infinity. This implies that $R \to 0$ as $n_q \to \infty$. The proof is complete.

Appendix B

Proofs of Theorems in Chapter 4

B.1 Proof of Theorem 4.1

Consider,

$$MISE(\widehat{x}) = E\int_{-\infty}^{\infty}(\widehat{x}(t) - x(t))^2 dt$$

Due to Paseval's formula, $MISE(\widehat{x})$ can be expressed as follows:

$$MISE(\widehat{x}) = \tau_q \sum_{|k|\leq n_q} E(\widehat{y}_k - x_k)^2 + \tau_q \sum_{|k|>n_q} x_k^2$$

Since the original data set is partitioned into disjoint data sets, one can write:

$$\begin{aligned} MISE(\widehat{x}) &= \tau_q \sum_{i=1}^{L}\sum_{k\in I_i} E(\widehat{y}_k - x_k)^2 + \tau_q \sum_{|k|>n_q} x_k^2 \\ &= \sum_{i=1}^{L} MISE_i(\widehat{x}) + \tau_q \sum_{|k|>n_q} x_k^2 \end{aligned} \tag{B.1}$$

where,

$$MISE_i(\widehat{x}) \triangleq \tau_q \sum_{k\in I_i} E(\widehat{y}_k - x_k)^2$$

Similar to the proof of Theorem 3.1 in Appendix A, one can write:

$$\begin{aligned} MISE_i(\widehat{x}) &= \tau_q\sigma^2 \cdot \frac{2n_q+1}{L} - \tau_q \sum_{k\in I_i} \int_{-x_k-T_i}^{-x_k+T_i} \varepsilon_k^2 f_{\varepsilon_k}(\varepsilon_k) d\varepsilon_k \\ &\quad + \tau_q \sum_{k\in I_i} x_k^2 \int_{-x_k-T_i}^{-x_k+T_i} f_{\varepsilon_k}(\varepsilon_k) d\varepsilon_k \\ &= \tau_q\sigma^2 \cdot \frac{2n_q+1}{L} - \tau_q \sum_{k\in I_i} [A(x_k,T_i) - B(x_k,T_i)] \end{aligned} \tag{B.2}$$

where,

$$A(x_k,T_i) = \int_{-x_k-T_i}^{-x_k+T_i} \varepsilon_k^2 f_{\varepsilon_k}(\varepsilon_k) d\varepsilon_k = \frac{1}{\sigma\sqrt{2\pi}} \int_{x_k-T_i}^{x_k+T_i} \varepsilon_k^2 e^{-\varepsilon_k^2/2\sigma^2} d\varepsilon_k$$

and,

$$B(x_k,T_i) = x_k^2 \int_{-x_k-T_i}^{-x_k+T_i} f_{\varepsilon_k}(\varepsilon_k) d\varepsilon_k = \frac{x_k^2}{\sigma\sqrt{2\pi}} \int_{x_k-T_i}^{x_k+T_i} e^{-\varepsilon_k^2/2\sigma^2} d\varepsilon_k$$

From (B.1) and (B.2):

$$MISE(\widehat{x}) = \tau_q\sigma^2(2n_q+1) + \tau_q \sum_{|k|>n_q} x_k^2 - \tau_q \sum_{i=1}^{L} \sum_{k\in I_i} [A(x_k,T_i) - B(x_k,T_i)] \tag{B.3}$$

But,

$$A(x_k,T_i) = \begin{cases} \frac{\sigma^2}{\sqrt{\pi}} \left[\gamma\left(\frac{3}{2}, \frac{(x_k-T_i)^2}{2\sigma^2}\right) - \gamma\left(\frac{3}{2}, \frac{(x_k+T_i)^2}{2\sigma^2}\right) \right] & \text{for} \quad x_k < -T_i \\ \frac{\sigma^2}{\sqrt{\pi}} \left[\gamma\left(\frac{3}{2}, \frac{(x_k-T_i)^2}{2\sigma^2}\right) + \gamma\left(\frac{3}{2}, \frac{(x_k+T_i)^2}{2\sigma^2}\right) \right] & \text{for} \quad |x_k| \le T_i \\ \frac{\sigma^2}{\sqrt{\pi}} \left[\gamma\left(\frac{3}{2}, \frac{(x_k+T_i)^2}{2\sigma^2}\right) - \gamma\left(\frac{3}{2}, \frac{(x_k-T_i)^2}{2\sigma^2}\right) \right] & \text{for} \quad x_k > T_i \end{cases}$$

and,

$$B(x_k,T_i) = \frac{x_k^2}{2} \left[\text{erf}\left(\frac{x_k+T_i}{\sigma\sqrt{2}}\right) - \text{erf}\left(\frac{x_k-T_i}{\sigma\sqrt{2}}\right) \right]$$

Substituting $A(x_k,T_i)$ and $B(x_k,T_i)$ found above into (B.3) gives (4.3). The proof is complete.

B.2 Proof of Theorem 4.2

It was found in (B.1) that:

$$MISE(\widehat{x}) = \sum_{i=1}^{L} MISE_i(\widehat{x}) + \tau_q \sum_{|k|>n_q} x_k^2$$

where $MISE_i(\widehat{x}) = \tau_q \sum_{k\in I_i} E(\widehat{y}_k - x_k)^2$.

From the proof of Theorem 3.2 given in Appendix A, one has:

$$E(\widehat{y}_k - x_k)^2 = \sigma^2 + \left(- \int_{-T}^{T} (y_k - x_k)^2 f_{y_k}(y_k) dy_k \right) + \int_{-T}^{T} x_k^2 f_{y_k}(y_k) dy_k$$

Therefore:

$$\begin{aligned} MISE_i(\widehat{x}) &= \tau_q \sigma^2 \frac{2n_q + 1}{L} + \left(-\tau_q \sum_{k\in I_i} \int_{-T}^{T} (y_k - x_k)^2 f_{y_k}(y_k) dy_k \right) \\ &\quad + \tau_q \sum_{k\in I_i} \int_{-T}^{T} x_k^2 f_{y_k}(y_k) dy_k \end{aligned} \tag{B.4}$$

Similar to the proof of Theorem 3.2 given in Appendix A, it is observed from (B.4) that there always exists optimal threshold levels $T_{opt,i}$ which minimize $MISE_i(\widehat{x})$. The proof is complete.

B.3 Proof of Theorem 4.3

Parseval's formula yields the following decompositions of the errors:

$$IBIAS(\widehat{x}) = \tau_q \sum_{|k|\le n_q} (E\widehat{y}_k - x_k)^2 + \tau_q \sum_{|k|>n_q} x_k^2$$

Since the original data set is partitioned into disjoint data sets, one can write:

$$\begin{aligned} IBIAS(\widehat{x}) &= \tau_q \sum_{i=1}^{L} \sum_{k\in I_i} (E\widehat{y}_k - x_k)^2 + \tau_q \sum_{|k|>n_q} x_k^2 \\ &= \sum_{i=1}^{L} IBIAS_i(\widehat{x}) + \tau_q \sum_{|k|>n_q} x_k^2 \end{aligned} \tag{B.5}$$

where,

$$IBIAS_i(\widehat{x}) \triangleq \tau_q \sum_{k \in I_i} (E\widehat{y}_k - x_k)^2$$

From the proof of Theorem 3.3 in Appendix A:

$$IBIAS_i(\widehat{x}) = \tau_q \sum_{k \in I_i} d_k^2 \tag{B.6}$$

where,

$$\begin{aligned} d_k &= \frac{\sigma}{\sqrt{2\pi}} \left[e^{-(x_k+T_i)^2/2\sigma^2} - e^{-(x_k-T_i)^2/2\sigma^2} \right] \\ &\quad + \frac{x_k}{2} \left[\text{erf}\left(\frac{x_k + T_i}{\sigma\sqrt{2}} \right) - \text{erf}\left(\frac{x_k - T_i}{\sigma\sqrt{2}} \right) \right] \end{aligned} \tag{B.7}$$

Substituting (B.6) into (B.5) gives (4.6) with d_k computed as in (4.8).

But, $IVAR(\widehat{x}) = MISE(\widehat{x}) - IBIAS(\widehat{x})$, where $MISE(\widehat{x})$ and $IBIAS(\widehat{x})$ are given in (4.3) and (4.6), respectively. Thus, (4.7) is immediately followed. The proof is complete.

B.4 Proof of Theorem 4.4

In the proof of Theorem 3.4 in Appendix A, the following inequalities were established:

$$A(x_k, T_i) \geq \frac{2\sigma^2}{\sqrt{\pi}} \gamma\left(\frac{3}{2}, \frac{T_i^2}{2\sigma^2} \right) \tag{B.8}$$

and

$$B(x_k, T_i) \leq x_k^2 \text{erf}\left(\frac{T_i}{\sigma\sqrt{2}} \right) \tag{B.9}$$

From (B.8),(B.9) and (B.2):

$$MISE_i(\widehat{x}) \leq \tau_q \sigma^2 \cdot \frac{2n_q + 1}{L} - \tau_q \cdot \frac{2n_q + 1}{L} \cdot \frac{2\sigma^2}{\sqrt{\pi}} \gamma\left(\frac{3}{2}, \frac{T_i^2}{2\sigma^2} \right) + \tau_q \cdot \text{erf}\left(\frac{T_i}{\sigma\sqrt{2}} \right) \cdot \sum_{k \in I_i} x_k^2$$

Substituting the above upper bound for $MISE_i(\widehat{x})$ into (B.1) gives (4.9). The proof is complete.

Appendix C

Proofs of Theorems in Chapter 5

C.1 Proof of Theorem 5.1

Consider,

$$MISE(\widehat{x}) = E\int_{-\infty}^{\infty}(\widehat{x}(t) - x(t))^2 dt$$

Due to Paseval's formula, $MISE(\widehat{x})$ can be expressed as follows.

$$MISE(\widehat{x}) = \tau_q \sum_{|k|\leq n_q} E(\widehat{y}_k - x_k)^2 + \tau_q \sum_{|k|>n_q} x_k^2,$$

Since,

$$\widehat{y}_k = \begin{cases} x_k + \varepsilon_k & \text{for} \quad k \in I_p \\ \\ 0 & \text{for} \quad k \in I_d, \end{cases} \tag{C.1}$$

One has,

$$\begin{aligned} MISE(\widehat{x}) &= \tau_q \sum_{k\in I_p} E\varepsilon_k^2 + \tau_q \sum_{k\in I_d} x_k^2 + \tau_q \sum_{|k|>n_q} x_k^2 \\ &= \tau_q \sigma^2 \eta + \tau_q \sum_{k\in I_d} x_k^2 + \tau_q \sum_{|k|>n_q} x_k^2, \end{aligned}$$

This completes the proof.

C.2 Proof of Theorem 5.2

Due to Paseval's formula, the IBIAS of the proposed sampling and reconstruction scheme can be written as follows, see [3].

$$IBIAS(\widehat{x}) = \tau_q \sum_{|k|\le n_q} (E\widehat{y}_k - x_k)^2 + \tau_q \sum_{|k|>n_q} x_k^2,$$

From (C.1):

$$\begin{aligned} IBIAS(\widehat{x}) &= \tau_q \sum_{k\in I_p} [E(x_k+\varepsilon_k) - x_k]^2 + \tau_q \sum_{k\in I_d} x_k^2 + \tau_q \sum_{|k|>n_q} x_k^2 \\ &= \tau_q \sum_{k\in I_d} x_k^2 + \tau_q \sum_{|k|>n_q} x_k^2, \end{aligned}$$

Hence, (5.7) has been proven.

Since $MISE(\widehat{x}) = IBIAS(\widehat{x}) + IVAR(\widehat{x})$, one can easily obtain (5.8) from (5.6) and (5.7). The proof is complete.

C.3 Proof of Corollary 5.1

Due to Paseval's formula, the MISE of the classical W-S interpolation scheme of (1.4) can be expressed as follows.

$$MISE(\widetilde{x}) = \tau_q \sum_{|k|\le n_q} E(y_k - x_k)^2 + \tau_q \sum_{|k|>n_q} x_k^2,$$

Equivalently,

$$\begin{aligned} MISE(\widetilde{x}) &= \tau_q \sum_{k\in I_p} E\varepsilon_k^2 + \tau_q \sum_{k\in I_d} E\varepsilon_k^2 + \tau_q \sum_{|k|>n_q} x_k^2 \\ &= \tau_q \sigma^2 \eta + \tau_q \sum_{k\in I_d} E\varepsilon_k^2 + \tau_q \sum_{|k|>n_q} x_k^2, \end{aligned} \tag{C.2}$$

If $T \le \sigma$, then for any $k \in I_d$, then $x_k^2 \le T^2 \le E\varepsilon_k^2 = \sigma^2$. This together with (5.6) and (C.2) implies that $MISE(\widehat{x}) \le MISE(\widetilde{x})$, regardless of σ^2 and n_q. And (5.9) is immediately followed.

Appendix D

Proofs of Theorems in Chapter 6

D.1 Proof of Theorem 6.1

It is well known that if random variables $z_1, z_2, \cdots, z_L$ are marginally Gaussian and independent, then they are jointly Gaussian. And, if they are jointly Gaussian, then their sum $z = z_1 + z_2 + \cdots + z_L$ is also Gaussian [54]. It is also well known that if random variables $z_1, z_2, \cdots, z_L$ are independent with the same mean μ and variance σ^2, then $z = \frac{1}{L}\sum_{l=1}^{L} z_l$ is a random variable with the mean μ and variance σ^2/L [54]. Therefore, the probability density function of $\overline{y}_k$ can be written as follows:

$$f_{\overline{y}_k}(\overline{y}_k) = \frac{1}{\sigma_1\sqrt{2\pi}} e^{-(\overline{y}_k - x_k)^2/2\sigma_1^2} \tag{D.1}$$

where, $\sigma_1^2 = \sigma^2/L$. It means that $\overline{y}_k$ is a Gaussian random variable with mean x_k and variance σ_1^2.

Consider,

$$MISE(\overline{x}) = E\int_{-\infty}^{\infty} (\overline{x}(t) - x(t))^2 dt$$

Due to Paseval's formula, $MISE(\overline{x})$ can be expressed as follows:

$$MISE(\overline{x}) = \tau_q \sum_{|k|\leq n_q} E(\overline{y}_k - x_k)^2 + \tau_q \sum_{|k|>n_q} x_k^2$$

Since, $E(\overline{y}_k - x_k)^2 = \text{var}[\overline{y}_k] = \sigma_1^2 = \sigma^2/L$, one has

$$MISE(\overline{x}) = \tau_q \sigma_1^2 (2n_q + 1) + \tau_q \sum_{|k|>n_q} x_k^2$$

The proof is complete.

D.2 Proof of Theorem 6.2

Due to Paseval's formula, $MISE(\widehat{x})$ can be expressed as follows:

$$MISE(\widehat{x}) = \tau_q \sum_{|k|\leq n_q} E(\widehat{y}_k - x_k)^2 + \tau_q \sum_{|k|>n_q} x_k^2 \tag{D.2}$$

One can write:

$$\begin{aligned}
E(\widehat{y}_k - x_k)^2 &= \int_{-\infty}^{\infty} (\widehat{y}_k - x_k)^2 f_{\overline{y}_k}(\overline{y}_k) d\overline{y}_k \\
&= \int_{-\infty}^{-T} (\overline{y}_k - x_k)^2 f_{\overline{y}_k}(\overline{y}_k) d\overline{y}_k + \int_{T}^{\infty} (\overline{y}_k - x_k)^2 f_{\overline{y}_k}(\overline{y}_k) d\overline{y}_k \\
&\quad + \int_{-T}^{T} x_k^2 f_{\overline{y}_k}(\overline{y}_k) d\overline{y}_k \\
&= E(\overline{y}_k - x_k)^2 - \int_{-T}^{T} (\overline{y}_k - x_k)^2 f_{\overline{y}_k}(\overline{y}_k) d\overline{y}_k + \int_{-T}^{T} x_k^2 f_{\overline{y}_k}(\overline{y}_k) d\overline{y}_k \\
&= \sigma_1^2 - \frac{1}{\sigma_1\sqrt{2\pi}} \int_{-T}^{T} (\overline{y}_k - x_k)^2 e^{-(\overline{y}_k - x_k)^2/2\sigma_1^2} d\overline{y}_k \\
&\quad + \frac{x_k^2}{\sigma_1\sqrt{2\pi}} \int_{-T}^{T} e^{-(\overline{y}_k - x_k)^2/2\sigma_1^2} d\overline{y}_k
\end{aligned}$$

Let $\varepsilon = \overline{y}_k - x_k$:

$$\begin{aligned}
E(\widehat{y}_k - x_k)^2 &= \sigma_1^2 - \frac{1}{\sigma_1\sqrt{2\pi}} \int_{-x_k-T}^{-x_k+T} \varepsilon^2 e^{-\varepsilon^2/2\sigma_1^2} d\varepsilon + \frac{x_k^2}{\sigma_1\sqrt{2\pi}} \int_{-x_k-T}^{-x_k+T} e^{-\varepsilon^2/2\sigma_1^2} d\varepsilon \\
&= \sigma_1^2 - \frac{1}{\sigma_1\sqrt{2\pi}} \int_{x_k-T}^{x_k+T} \varepsilon^2 e^{-\varepsilon^2/2\sigma_1^2} d\varepsilon + \frac{x_k^2}{\sigma_1\sqrt{2\pi}} \int_{x_k-T}^{x_k+T} e^{-\varepsilon^2/2\sigma_1^2} d\varepsilon
\end{aligned}$$

Replacing $E(\widehat{y}_k - x_k)^2$ found above into (D.2) gives:

$$MISE(\widehat{x}) = \tau_q \sigma_1^2 (2n_q + 1) + \tau_q \sum_{|k|>n_q} x_k^2 - \tau_q \sum_{|k|\leq n_q} [A(x_k, T) - B(x_k, T)] \tag{D.3}$$

where,

$$A(x_k, T) = \frac{1}{\sigma_1\sqrt{2\pi}} \int_{x_k-T}^{x_k+T} \varepsilon^2 e^{-\varepsilon^2/2\sigma_1^2} d\varepsilon \tag{D.4}$$

and,

$$B(x_k, T) = \frac{x_k^2}{\sigma_1\sqrt{2\pi}} \int_{x_k-T}^{x_k+T} e^{-\varepsilon^2/2\sigma_1^2} d\varepsilon \tag{D.5}$$

It can be shown that:

$$A(x_k, T) = \begin{cases} \frac{\sigma_1^2}{\sqrt{\pi}} \left[\gamma\left(\frac{3}{2}, \frac{(x_k-T)^2}{2\sigma_1^2}\right) - \gamma\left(\frac{3}{2}, \frac{(x_k+T)^2}{2\sigma_1^2}\right)\right] & \text{for} \quad x_k < -T \\ \frac{\sigma_1^2}{\sqrt{\pi}} \left[\gamma\left(\frac{3}{2}, \frac{(x_k-T)^2}{2\sigma_1^2}\right) + \gamma\left(\frac{3}{2}, \frac{(x_k+T)^2}{2\sigma_1^2}\right)\right] & \text{for} \quad |x_k| \le T \\ \frac{\sigma_1^2}{\sqrt{\pi}} \left[\gamma\left(\frac{3}{2}, \frac{(x_k+T)^2}{2\sigma_1^2}\right) - \gamma\left(\frac{3}{2}, \frac{(x_k-T)^2}{2\sigma_1^2}\right)\right] & \text{for} \quad x_k > T \end{cases}$$

and,

$$B(x_k, T) = \frac{x_k^2}{2} \left[\text{erf}\left(\frac{x_k+T}{\sigma_1\sqrt{2}}\right) - \text{erf}\left(\frac{x_k-T}{\sigma_1\sqrt{2}}\right)\right]$$

where, $\gamma(\alpha, z)$ and $\text{erf}(x)$ are the incomplete gamma function and the error function, respectively. They are defined as follows [50]:

$$\gamma(\alpha, x) = \int_0^x z^{\alpha-1} e^{-z} dz, \qquad \text{Re}(\alpha) > 0$$

$$\text{erf}(x) = \frac{2}{\sqrt{\pi}} \int_0^x e^{-z^2} dz.$$

Replacing $A(x_k, T)$ and $B(x_k, T)$ found above into (D.3) gives (6.12). The proof is complete.

D.3 Proof of Theorem 6.3

It was found in (D.2) that:

$$MISE(\widehat{x}) = \tau_q \sum_{|k|\le n_q} E(\widehat{y}_k - x_k)^2 + \tau_q \sum_{|k|>n_q} x_k^2$$

But,

$$\begin{aligned} E(\widehat{y}_k - x_k)^2 &= \int_{-\infty}^{\infty} (\widehat{y}_k - x_k)^2 f_{\overline{y}_k}(\overline{y}_k) d\overline{y}_k \\ &= \int_{-\infty}^{-T} (\overline{y}_k - x_k)^2 f_{\overline{y}_k}(\overline{y}_k) d\overline{y}_k + \int_{T}^{\infty} (\overline{y}_k - x_k)^2 f_{\overline{y}_k}(\overline{y}_k) d\overline{y}_k \\ &\quad + \int_{-T}^{T} x_k^2 f_{\overline{y}_k}(\overline{y}_k) d\overline{y}_k \\ &= E(\overline{y}_k - x_k)^2 - \int_{-T}^{T} (\overline{y}_k - x_k)^2 f_{\overline{y}_k}(\overline{y}_k) d\overline{y}_k + \int_{-T}^{T} x_k^2 f_{\overline{y}_k}(\overline{y}_k) d\overline{y}_k \\ &= \sigma_1^2 + \left(- \int_{-T}^{T} (\overline{y}_k - x_k)^2 f_{\overline{y}_k}(\overline{y}_k) d\overline{y}_k \right) + \int_{-T}^{T} x_k^2 f_{\overline{y}_k}(\overline{y}_k) d\overline{y}_k \end{aligned}$$

Therefore,

$$\begin{aligned} MISE(\widehat{x}) &= \tau_q \sigma_1^2 (2n_q + 1) + \tau_q \sum_{|k|>n_q} x_k^2 + \left(-\tau_q \sum_{|k|\le n_q} \int_{-T}^{T} (\overline{y}_k - x_k)^2 f_{\overline{y}_k}(\overline{y}_k) d\overline{y}_k \right) \\ &\quad + \tau_q \sum_{|k|\le n_q} \int_{-T}^{T} x_k^2 f_{\overline{y}_k}(\overline{y}_k) d\overline{y}_k \end{aligned} \tag{D.6}$$

Similar to the proof of Theorem 3.2 given in Appendix A, it is observed from (D.6) that there always exists an optimal threshold level T_{opt} which minimizes $MISE(\widehat{x})$. The proof is complete.

D.4 Proof of Theorem 6.4

Parseval's formula yields the following decompositions of the errors:

$$IBIAS(\widehat{x}) = \tau_q \sum_{|k|\le n_q} (E\widehat{y}_k - x_k)^2 + \tau_q \sum_{|k|>n_q} x_k^2. \tag{D.7}$$

But,

$$\begin{aligned} E\widehat{y}_k &= \int_{-\infty}^{-T} \overline{y}_k f_{\overline{y}_k}(\overline{y}_k) d\overline{y}_k + \int_{T}^{\infty} \overline{y}_k f_{\overline{y}_k}(\overline{y}_k) d\overline{y}_k \\ &= E\overline{y}_k - \int_{-T}^{T} \overline{y}_k f_{\overline{y}_k}(\overline{y}_k) d\overline{y}_k = x_k - \frac{1}{\sigma_1 \sqrt{2\pi}} \int_{-T}^{T} \overline{y}_k e^{-(\overline{y}_k - x_k)^2 / 2\sigma_1^2} d\overline{y}_k \end{aligned}$$

Let $\varepsilon = \overline{y}_k - x_k$:

$$\begin{aligned} E\widehat{y}_k &= x_k - \frac{1}{\sigma_1\sqrt{2\pi}} \int_{-x_k-T}^{-x_k+T} \varepsilon e^{-\varepsilon^2/2\sigma_1^2} d\varepsilon - \frac{x_k}{\sigma_1\sqrt{2\pi}} \int_{-x_k-T}^{-x_k+T} e^{-\varepsilon^2/2\sigma_1^2} d\varepsilon \\ &= x_k - \frac{\sigma_1}{\sqrt{2\pi}} \left[e^{-(x_k+T)^2/2\sigma_1^2} - e^{-(x_k-T)^2/2\sigma_1^2} \right] - \frac{x_k}{2} \left[\text{erf}\left(\frac{x_k+T}{\sigma_1\sqrt{2}} \right) - \text{erf}\left(\frac{x_k-T}{\sigma_1\sqrt{2}} \right) \right] \end{aligned}$$

Replacing $E\widehat{y}_k$ found above into (D.7) gives (6.15) with d_k computed as in (6.17).

But, $IVAR(\widehat{x}) = MISE(\widehat{x}) - IBIAS(\widehat{x})$, where $MISE(\widehat{x})$ and $IBIAS(\widehat{x})$ are given in (6.12) and (6.15), respectively. Thus, (6.16) is immediately followed. The proof is complete.

D.5 Proof of Theorem 6.5

Observing that the function $f(\varepsilon) = \varepsilon^2 e^{-\varepsilon^2/2\sigma_1^2}$ is always positive, symmetric around zero. It has the minimums at $\varepsilon = 0$ and $\varepsilon = \pm\infty$, respectively. Consequently, for the fixed T, $A(x_k, T)$ defined in (D.4) has the minimums at $x_k = 0$ and $x_k = \pm\infty$, respectively. Since the function $x(t)$ of interest is bounded, one can ignore the case $x_k = \pm\infty$ and establish the following inequality:

$$A(x_k, T) \geq \frac{1}{\sigma_1\sqrt{2\pi}} \int_{-T}^{T} \varepsilon^2 e^{-\varepsilon^2/2\sigma_1^2} d\varepsilon, \qquad \forall x_k$$

Or equivalently,

$$A(x_k, T) \geq \frac{2\sigma_1^2}{\sqrt{\pi}} \gamma\left(\frac{3}{2}, \frac{T^2}{2\sigma_1^2} \right) \tag{D.8}$$

Similarly, observing that the function $f(\varepsilon) = e^{-\varepsilon^2/2\sigma_1^2}$ is always positive, symmetric around zero. It has the maximum at at $\varepsilon = 0$ and it decreases as $|\varepsilon|$ decreases. Consequently, for the fixed T, $B(x_k, T)$ defined in (D.5) has the maximum at $x_k = 0$. The following inequality can be established.

$$B(x_k, T) \leq \frac{x_k^2}{\sigma_1\sqrt{2\pi}} \int_{-T}^{T} e^{-\varepsilon^2/2\sigma_1^2} d\varepsilon, \quad \forall x_k$$

Or equivalently,

$$B(x_k, T) \leq x_k^2 \text{erf}\left(\frac{T}{\sigma_1\sqrt{2}}\right) \tag{D.9}$$

From (D.3), (D.8) and (D.9), one can easily obtain (6.18). The proof is complete.

Appendix E

Proofs of Theorems in Chapter 7

E.1 Proof of Theorem 7.1

Consider,

$$MISE(\widehat{x}) = E\int_{-\infty}^{\infty}(\widehat{x}(t) - x(t))^2 dt$$

Due to Paseval's formula, $MISE(\widehat{x})$ can be expressed as follows.

$$MISE(\widehat{x}) = \tau_q \sum_{|k|\leq n_q} E(\widehat{y}_k - x_k)^2 + \tau_q \sum_{|k|>n_q} x_k^2,$$

But,

$$\widehat{y}_k = \begin{cases} \overline{y'}_k & \text{for} \quad k \in I_p \\ \\ 0 & \text{for} \quad k \in I_d, \end{cases} \tag{E.1}$$

Hence,

$$MISE(\widehat{x}) = \tau_q \sum_{k\in I_p} E(\overline{y'}_k - x_k)^2 + \tau_q \sum_{k\in I_d} x_k^2 + \tau_q \sum_{|k|>n_q} x_k^2$$

Since y'_{lk} in (7.3) are independent random variables with mean x'_k and variance σ^2, the random variables $\overline{y'}_k$ defined in (7.4) are random variables with mean x'_k and

variance $\sigma_1^2 = \sigma^2/L$. Thus, the preceding equality can be re-written as follows:

$$\begin{aligned} MISE(\widehat{x}) &= \tau_q \sum_{k\in I_p} \mathrm{var}(\overline{y'}_k) + \tau_q \sum_{k\in I_d} x_k^2 + \tau_q \sum_{|k|>n_q} x_k^2 \\ &= \tau_q \sigma_1^2 \eta + \tau_q \sum_{k\in I_d} x_k^2 + \tau_q \sum_{|k|>n_q} x_k^2, \end{aligned}$$

This completes the proof.

E.2 Proof of Theorem 7.2

Consider,

$$IBIAS(\widehat{x}) \triangleq \int_{-\infty}^{\infty} (E\widehat{x}(t) - x(t))^2 dt$$
$$IVAR(\widehat{x}) \triangleq E \int_{-\infty}^{\infty} (\widehat{x}(t) - E\widehat{x}(t))^2 dt.$$

Parseval's formula yields the following decompositions of the errors [3]:

$$IBIAS(\widehat{x}) = \tau_q \sum_{|k|\le n_q} (E\widehat{y}_k - x_k)^2 + \tau_q \sum_{|k|>n_q} x_k^2$$
$$IVAR(\widehat{x}) = \tau_q \sum_{|k|\le n_q} \mathrm{var}(\widehat{y}_k).$$

Taking (E.1) into account gives:

$$\begin{aligned} IBIAS(\widehat{x}) &= \tau_q \sum_{k\in I_p} (E\overline{y'}_k - x'_k)^2 + \tau_q \sum_{k\in I_d} x_k^2 + \tau_q \sum_{|k|>n_q} x_k^2 \\ &= \tau_q \sum_{k\in I_d} x_k^2 + \tau_q \sum_{|k|>n_q} x_k^2 \\ IVAR(\widehat{x}) &= \tau_q \sum_{k\in I_p} \mathrm{var}(\overline{y'}_k) = \tau_q \sigma_1^2 \eta. \end{aligned}$$

The proof is complete.

E.3 Proof of Corollary 7.1

If $T \le \sigma_1$, then for any $k \in I_d$, one has $x_k^2 \le T^2 \le \sigma_1^2$. Consequently, $\sum_{k\in I_d} x_k^2 \le \sigma_1^2 |I_d| = \sigma_1^2[(2n_q + 1) - \eta]$. Here, $|I_d|$ denotes the volume (size) of the index set I_d.

This together with (7.9) implies:

$$MISE(\widehat{x})|_{T\leq\sigma_1} \leq \tau_q\sigma_1^2(2n_q+1) + \tau_q \sum_{|k|>n_q} x_k^2 = MISE(\widehat{x})|_{T=0}.$$

The proof is complete.

Appendix F

Plots of Reconstructed Waveforms

Figure F.1 and Figure F.2 plot test signal $x_1(t)$ defined by (3.15) and the reconstructed signals when $E_0/\sigma^2 = -15$ dB and 0 dB, respectively. Figure F.3 and Figure F.4 plot test signal $x_2(t)$ defined by (3.16) and the reconstructed signals when $E_0/\sigma^2 = -15$ dB and 0 dB, respectively. Figure F.5 and Figure F.6 plot test signal $x_3(t)$ defined by (3.17) and the reconstructed signals when $E_0/\sigma^2 = -15$ dB and 0 dB, respectively. These figures compare the reconstruction accuracy of the thresholding-based reconstruction scheme introduced in Chapter 3 with the other reconstruction schemes.

Figure F.7 and Figure F.8 plot test signal $x_1(t)$ defined by (3.15) and the reconstructed signals when $E_0/\sigma^2 = -15$ dB and 0 dB, respectively. These figures compare the reconstruction accuracy of the adaptive thresholding-based reconstruction scheme introduced in Chapter 4 with the other reconstruction schemes.

Figure F.9 and Figure F.10 plot test signal $x_1(t)$ defined by (3.15) and the reconstructed signals when $E_0/\sigma^2 = -25$ dB and 0 dB, respectively. These figures compare the reconstruction accuracy of the thresholding-based sampling scheme introduced in Chapter 5 with the other sampling and reconstruction schemes. Figure F.11, Figure

F.12 and Figure F.13 plot the voice "speech sig" and the reconstructed speech when $E_0/\sigma^2 = 0$ dB, 5 dB and 10 dB, respectively.

Figure F.14 and Figure F.15 plot test signal $x_1(t)$ defined by (3.15) and the reconstructed signals when $E_0/\sigma^2 = -25$ dB and 0 dB, respectively. These figures compare the reconstruction accuracy of the reconstruction schemes proposed in Chapter 6 with the classical W-S interpolation scheme and the oversampling/post-filtering reconstruction scheme.

Figure F.16 and Figure F.17 plot test signal $x_1(t)$ defined by (3.15) and the reconstructed signals when $E_0/\sigma^2 = -25$ dB and 0 dB, respectively. These figures compare the reconstruction accuracy of the reconstruction scheme proposed in Chapter 7 with the classical W-S interpolation scheme and the reconstruction schemes proposed in Chapter 6.

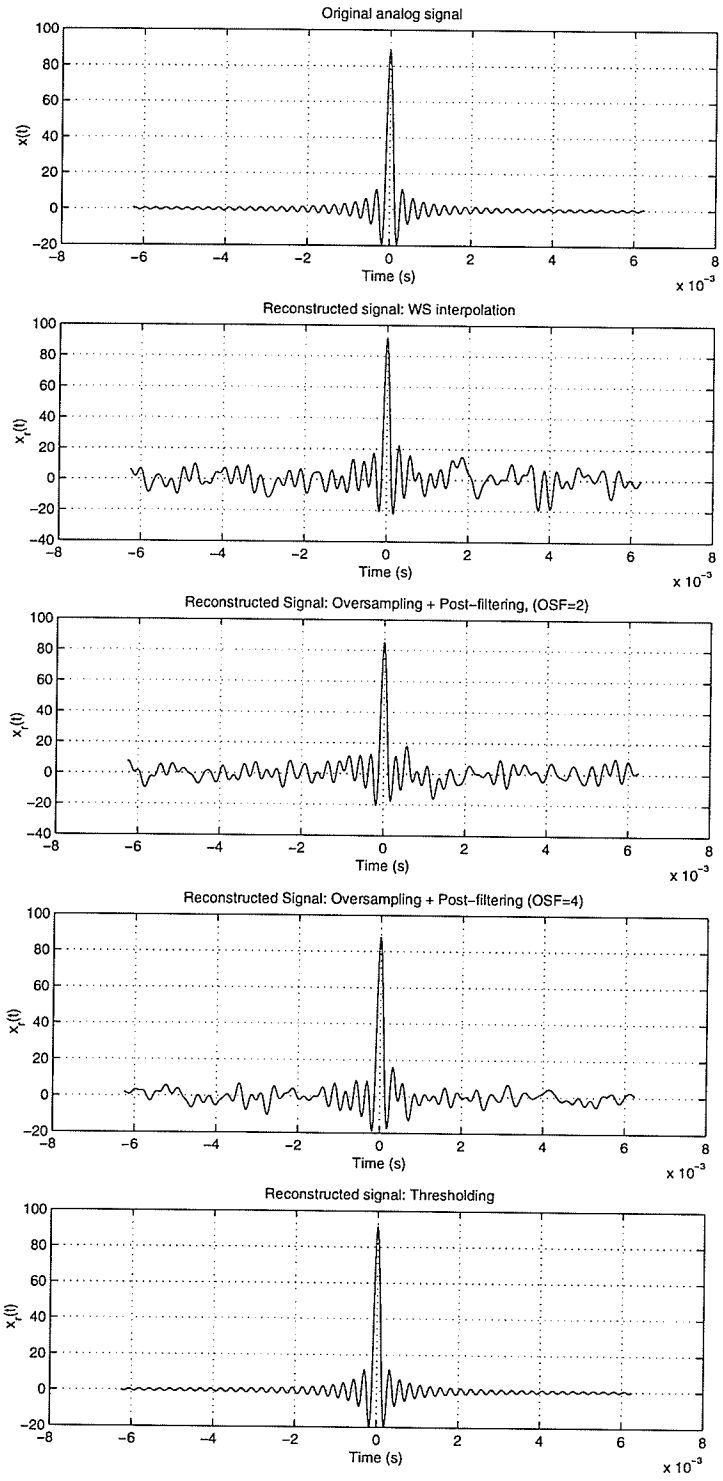

Figure F.1: Reconstructed signals in Chapter 3 (Test signal $x_1(t)$, $E_0/\sigma^2 = -15$ dB)

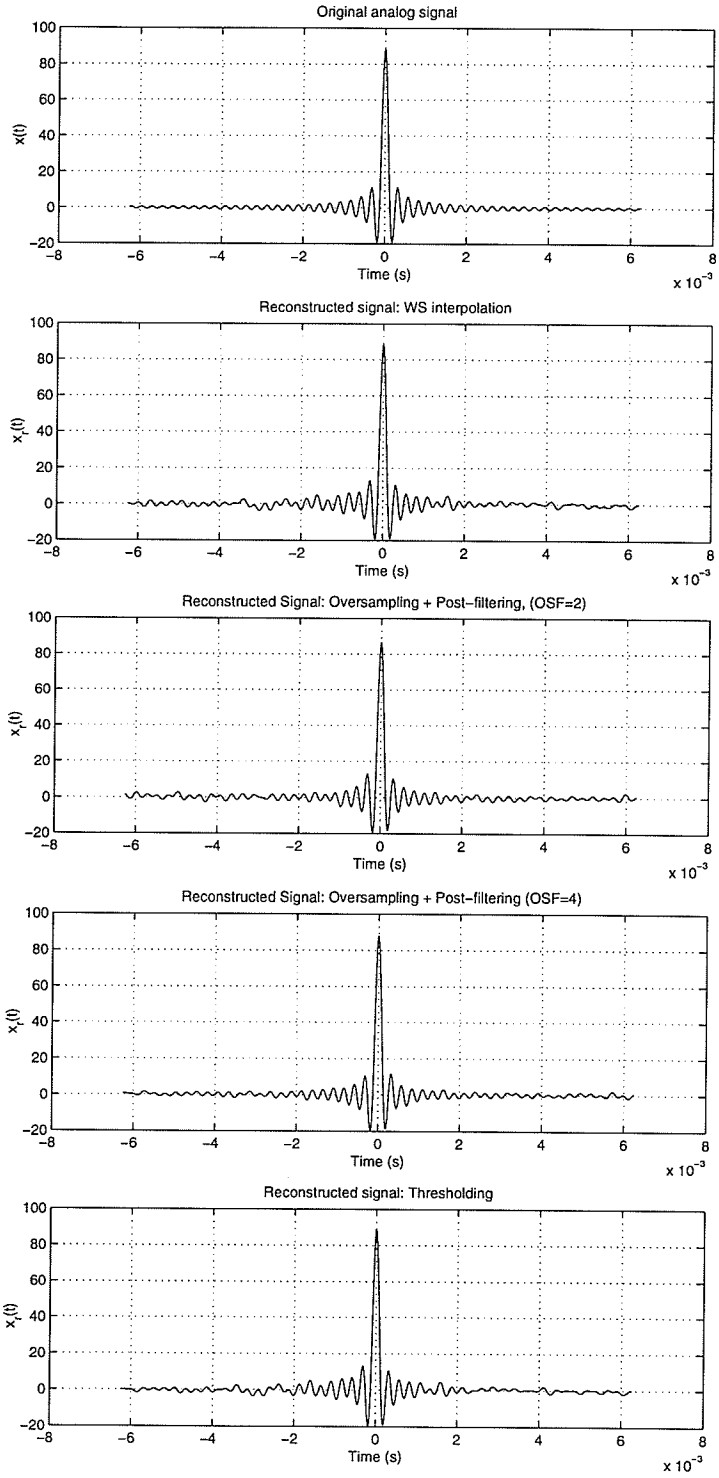

Figure F.2: Reconstructed signals in Chapter 3 (Test signal $x_1(t)$, $E_0/\sigma^2 = 0$ dB)

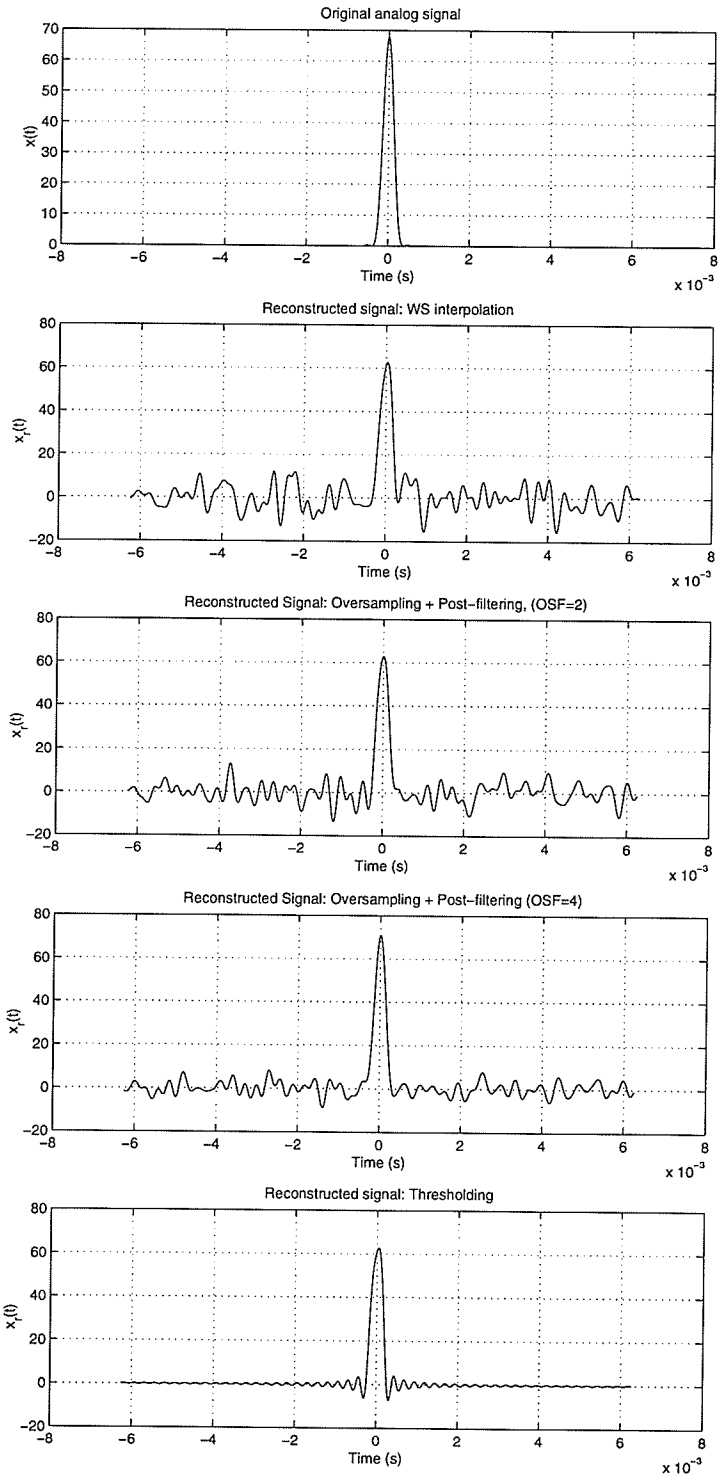

Figure F.3: Reconstructed signals in Chapter 3 (Test signal $x_2(t)$, $E_0/\sigma^2 = -15$ dB)

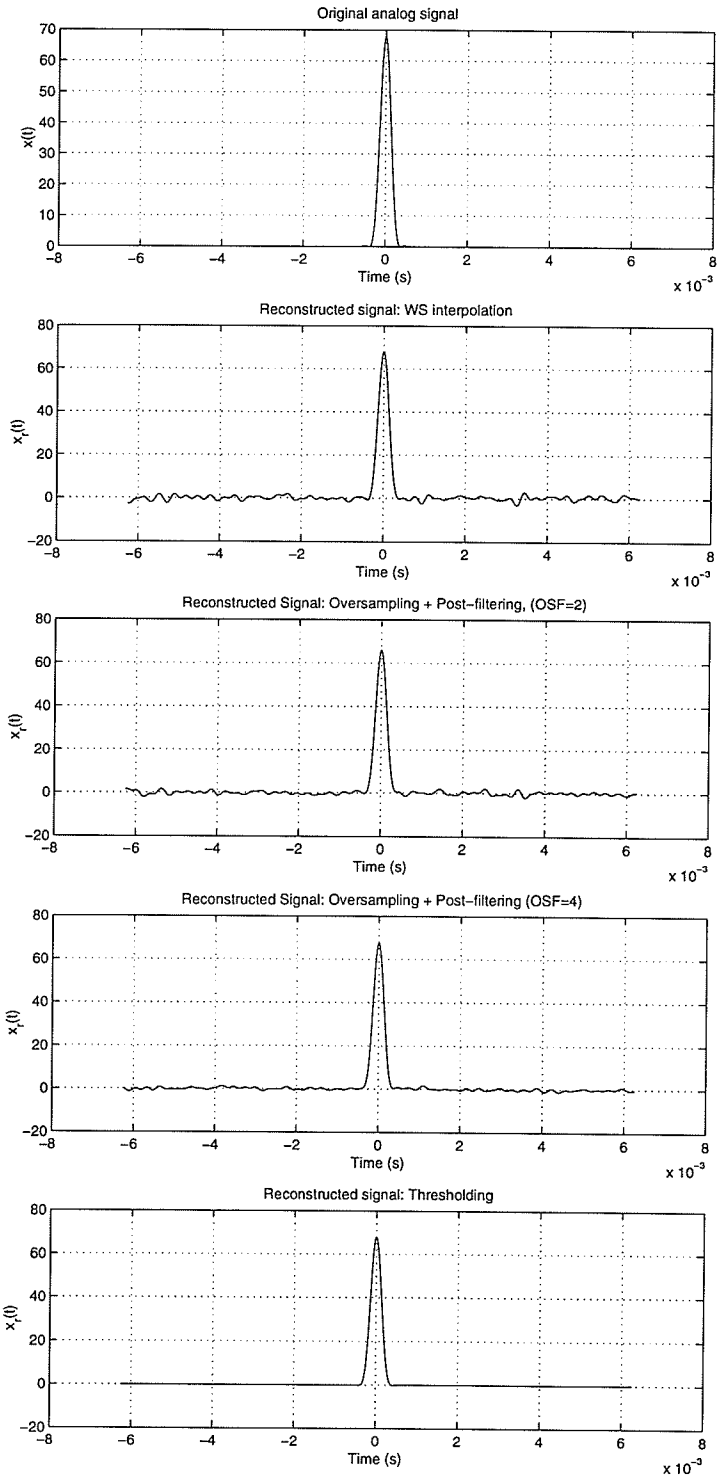

Figure F.4: Reconstructed signals in Chapter 3 (Test signal $x_2(t)$, $E_0/\sigma^2 = 0$ dB)

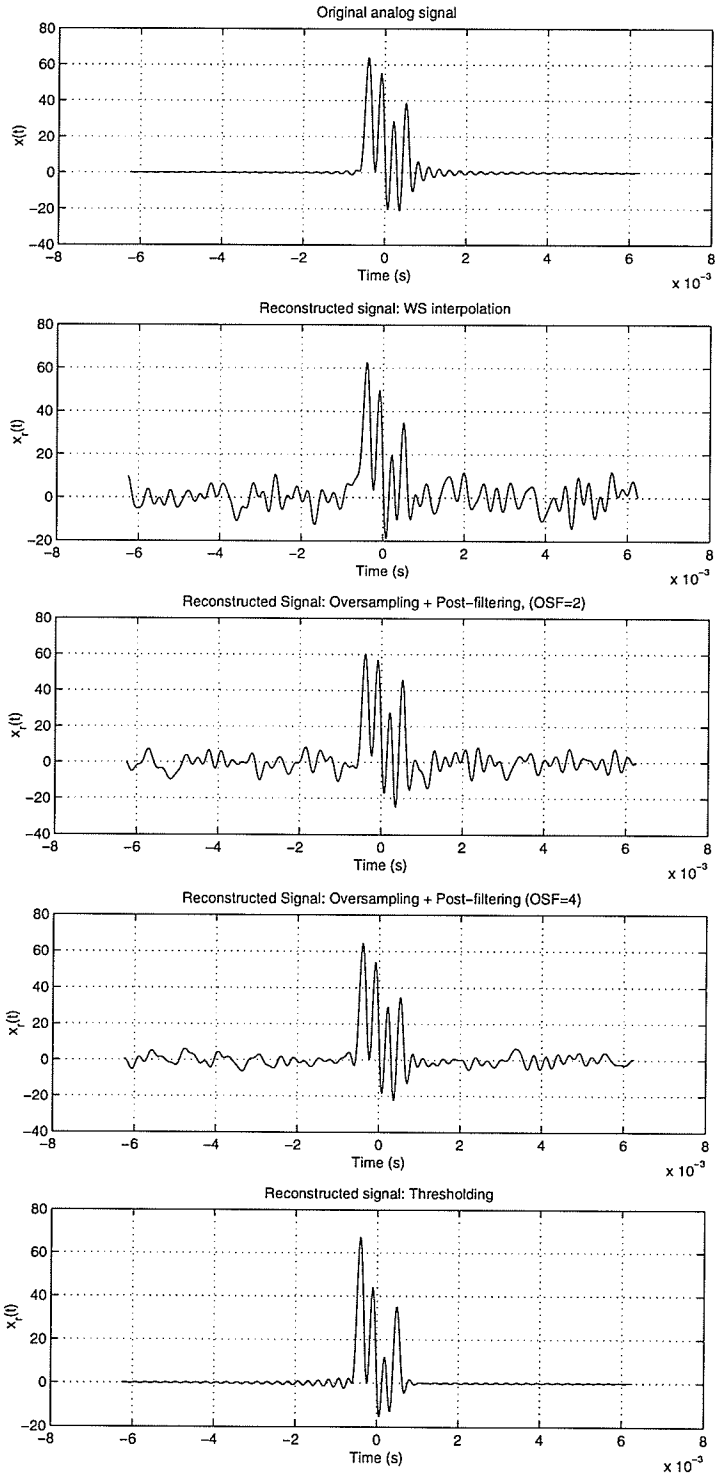

Figure F.5: Reconstructed signals in Chapter 3 (Test signal $x_3(t)$, $E_0/\sigma^2 = -15$ dB)

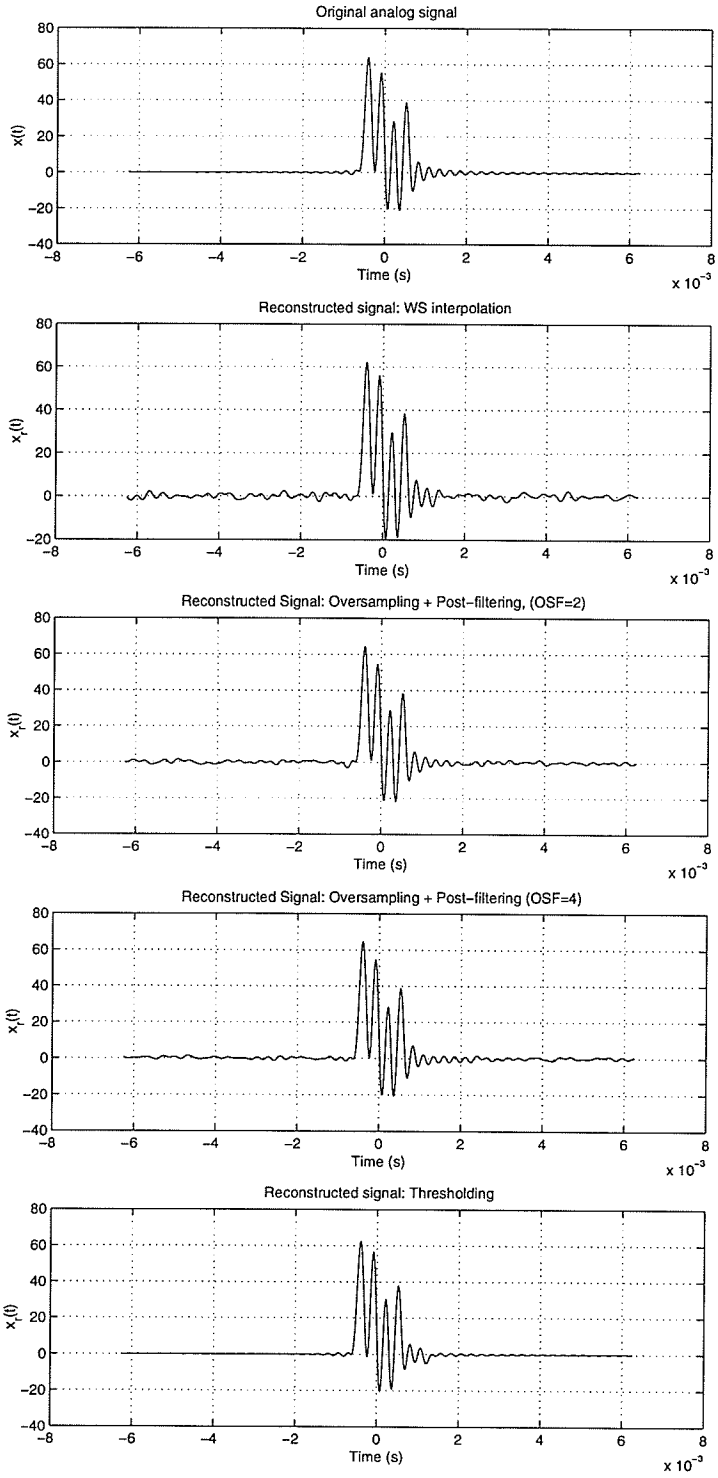

Figure F.6: Reconstructed signals in Chapter 3 (Test signal $x_3(t)$, $E_0/\sigma^2 = 0$ dB)

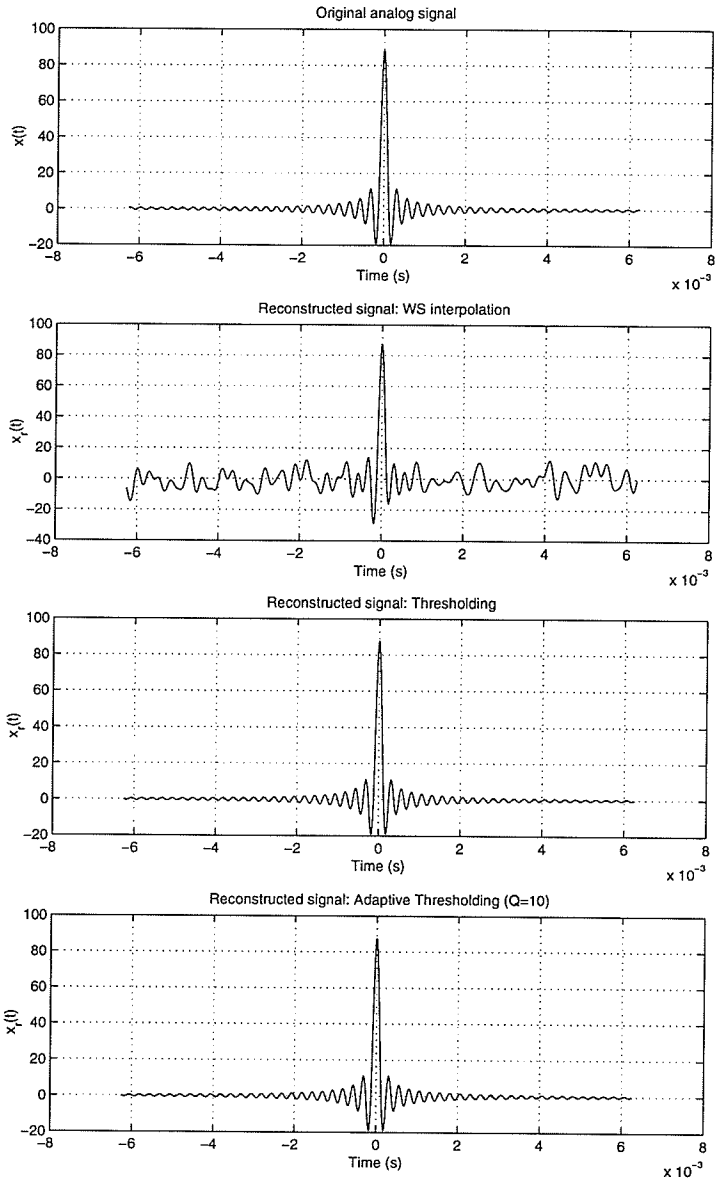

Figure F.7: Reconstructed signals in Chapter 4 (Test signal $x_1(t)$, $E_0/\sigma^2 = -15$ dB)

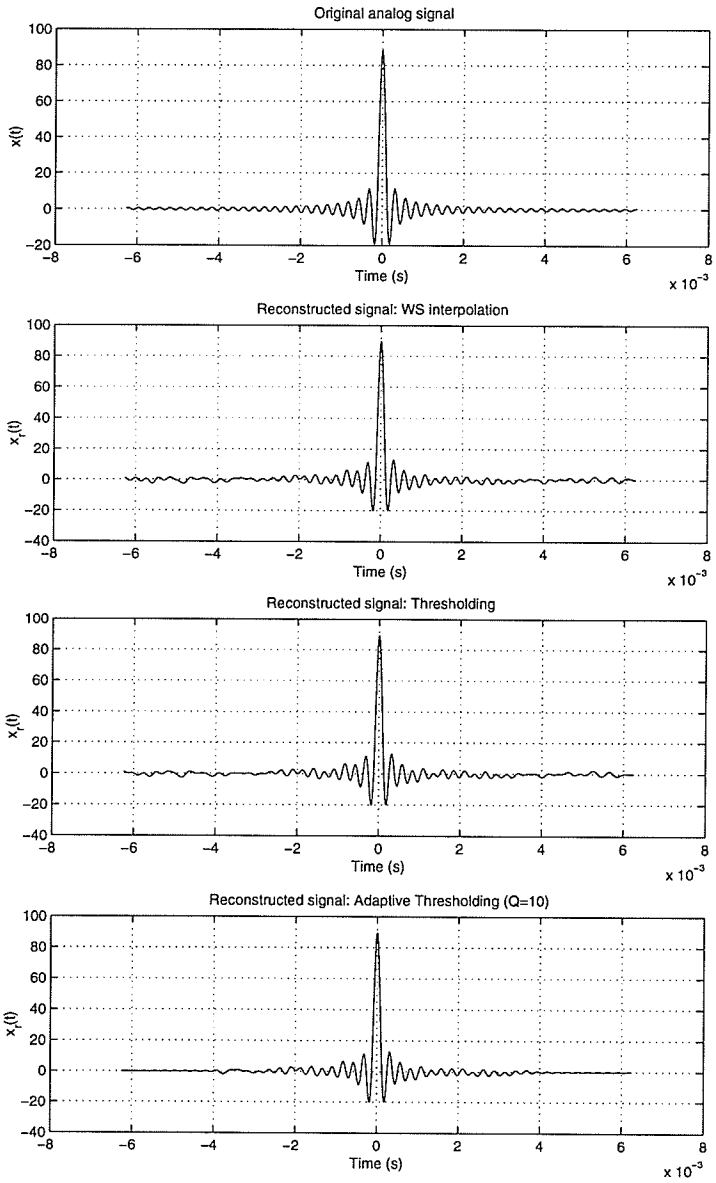

Figure F.8: Reconstructed signals in Chapter 4 (Test signal $x_1(t)$, $E_0/\sigma^2 = 0$ dB)

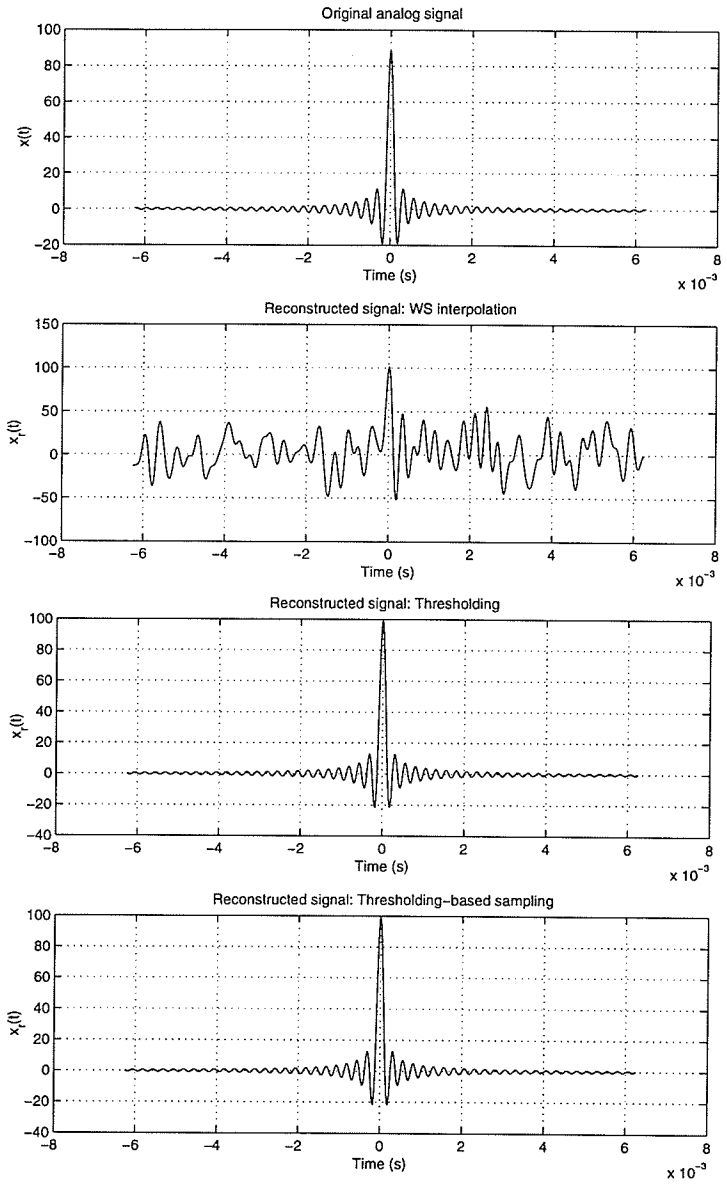

Figure F.9: Reconstructed signals in Chapter 5 (Test signal $x_1(t)$, $E_0/\sigma^2 = -25$ dB)

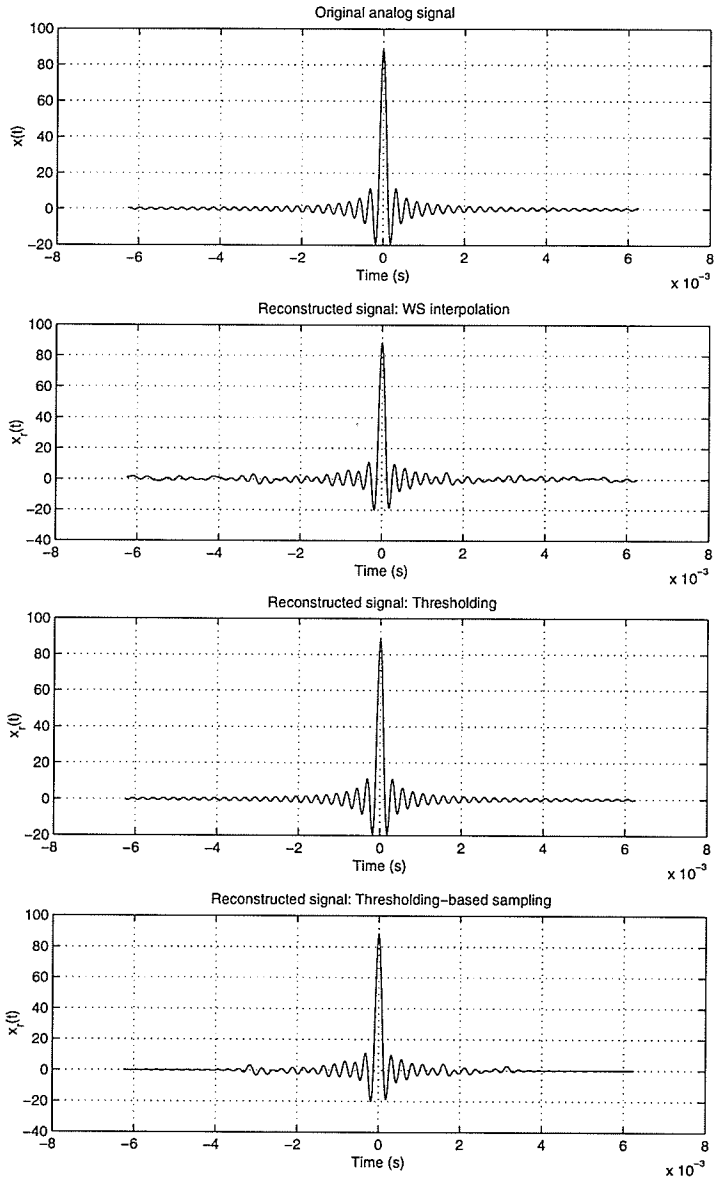

Figure F.10: Reconstructed signals in Chapter 5 (Test signal $x_1(t)$, $E_0/\sigma^2 = 0$ dB)

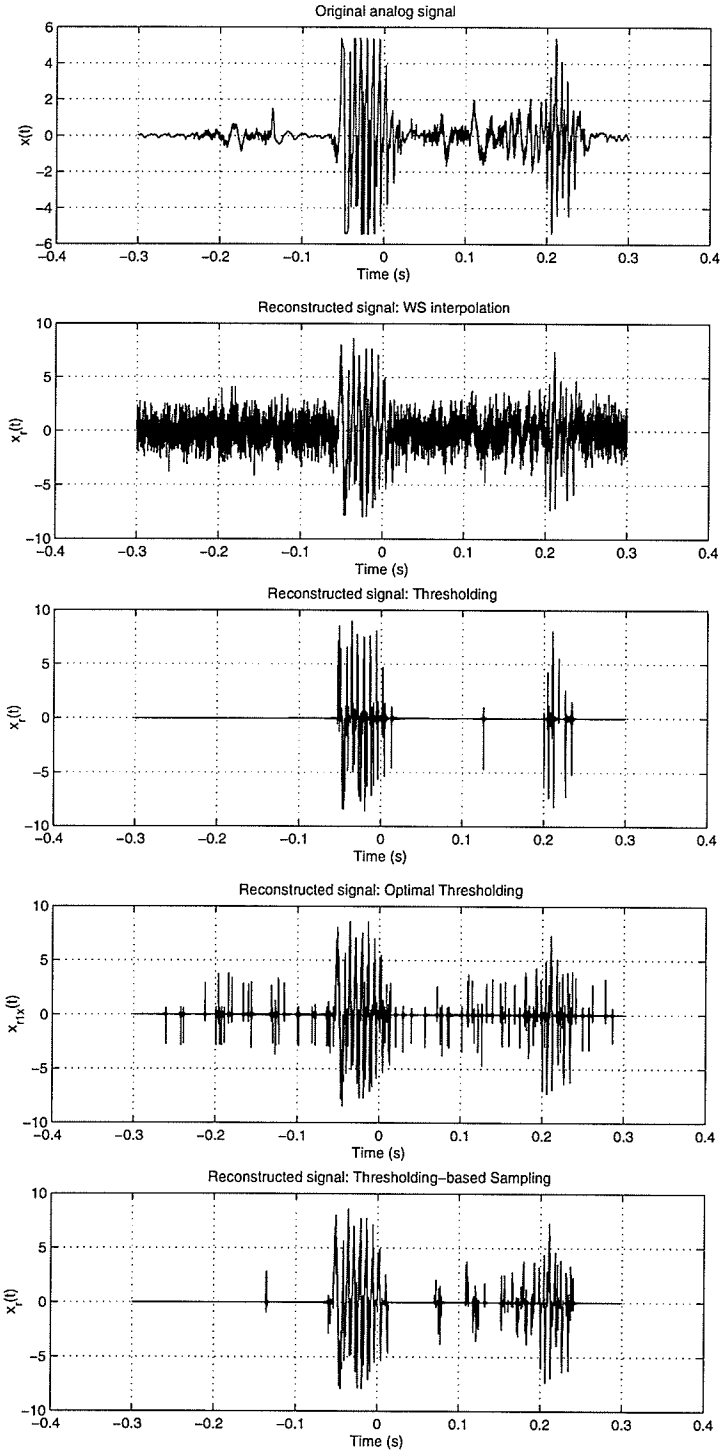

Figure F.11: Reconstructed signals in Chapter 3 and Chapter 5 (Speech signal, $E_0/\sigma^2 = 0$ dB)

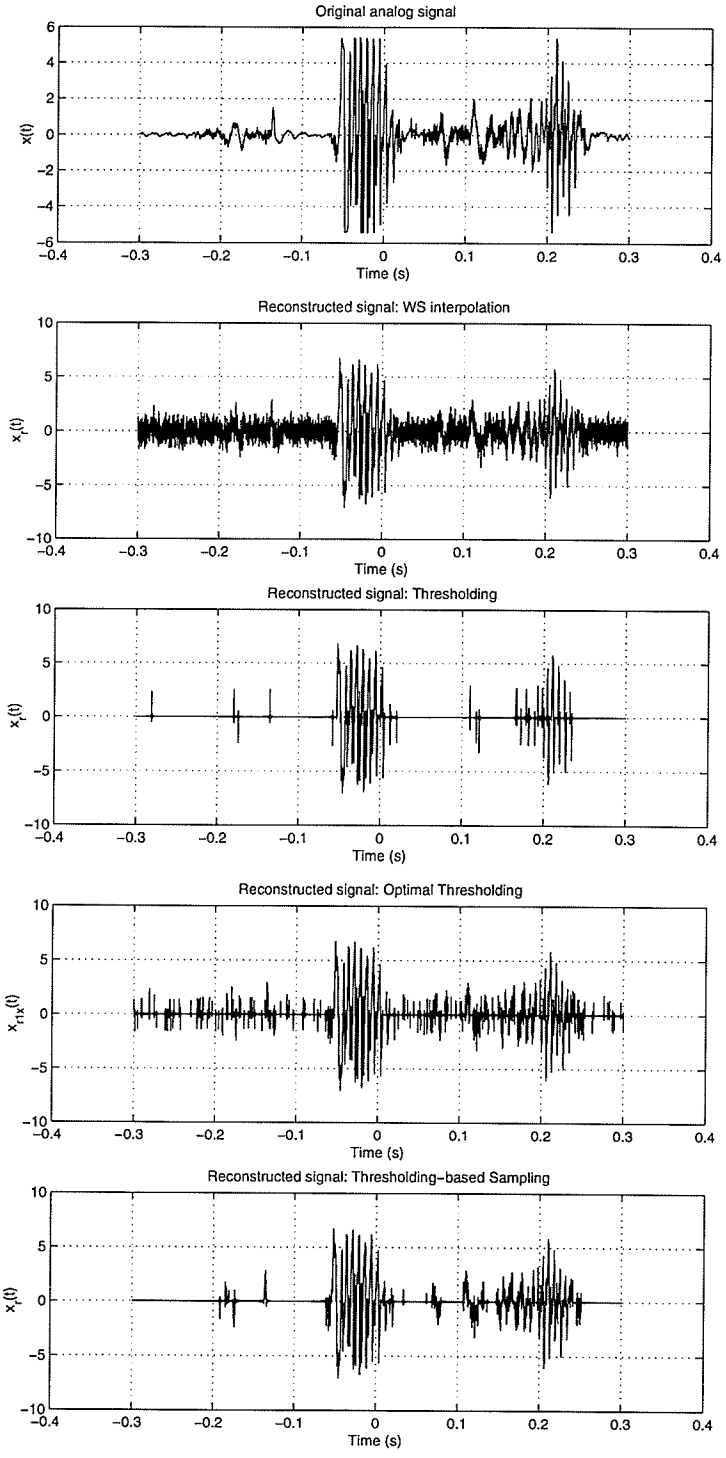

Figure F.12: Reconstructed signals in Chapter 3 and Chapter 5 (Speech signal, $E_0/\sigma^2 = 5$ dB)

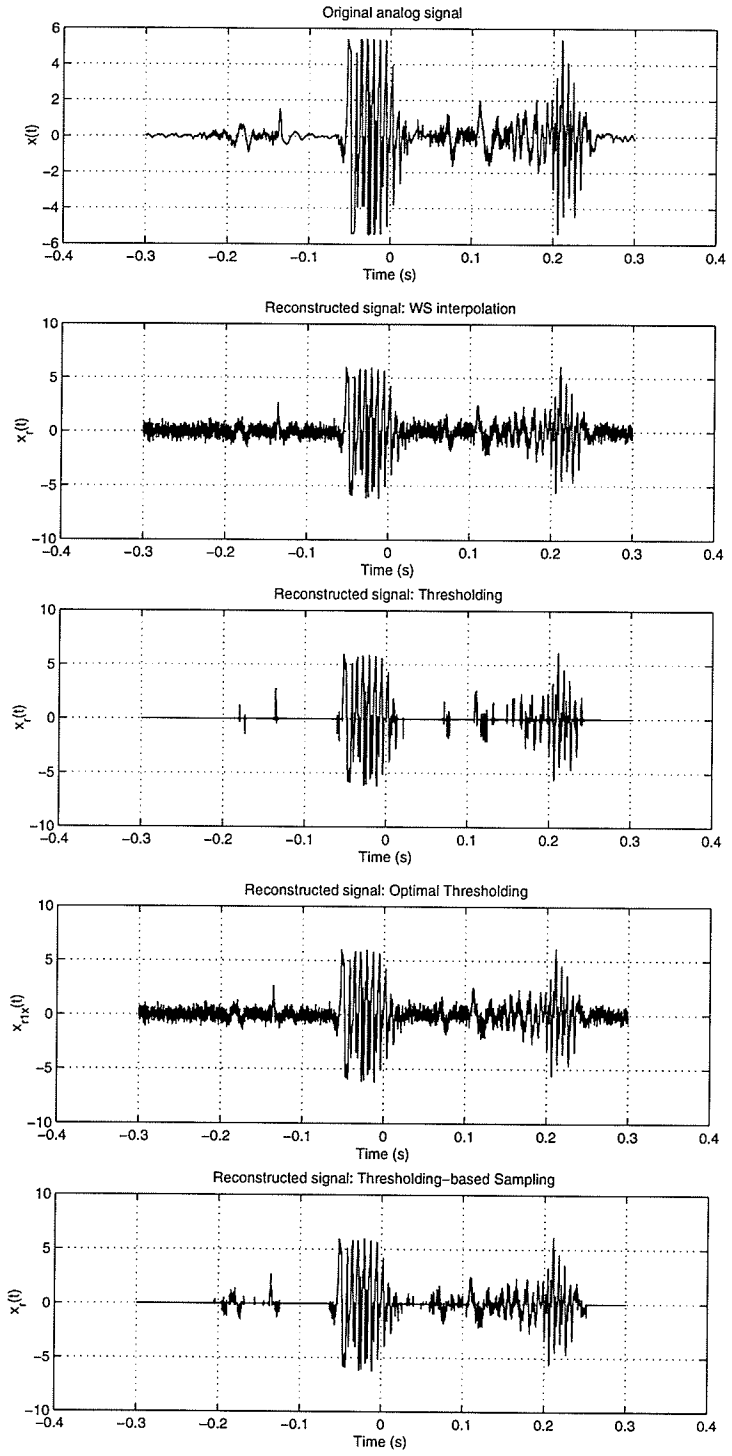

Figure F.13: Reconstructed signals in Chapter 3 and Chapter 5 (Speech signal, $E_0/\sigma^2 = 10$ dB)

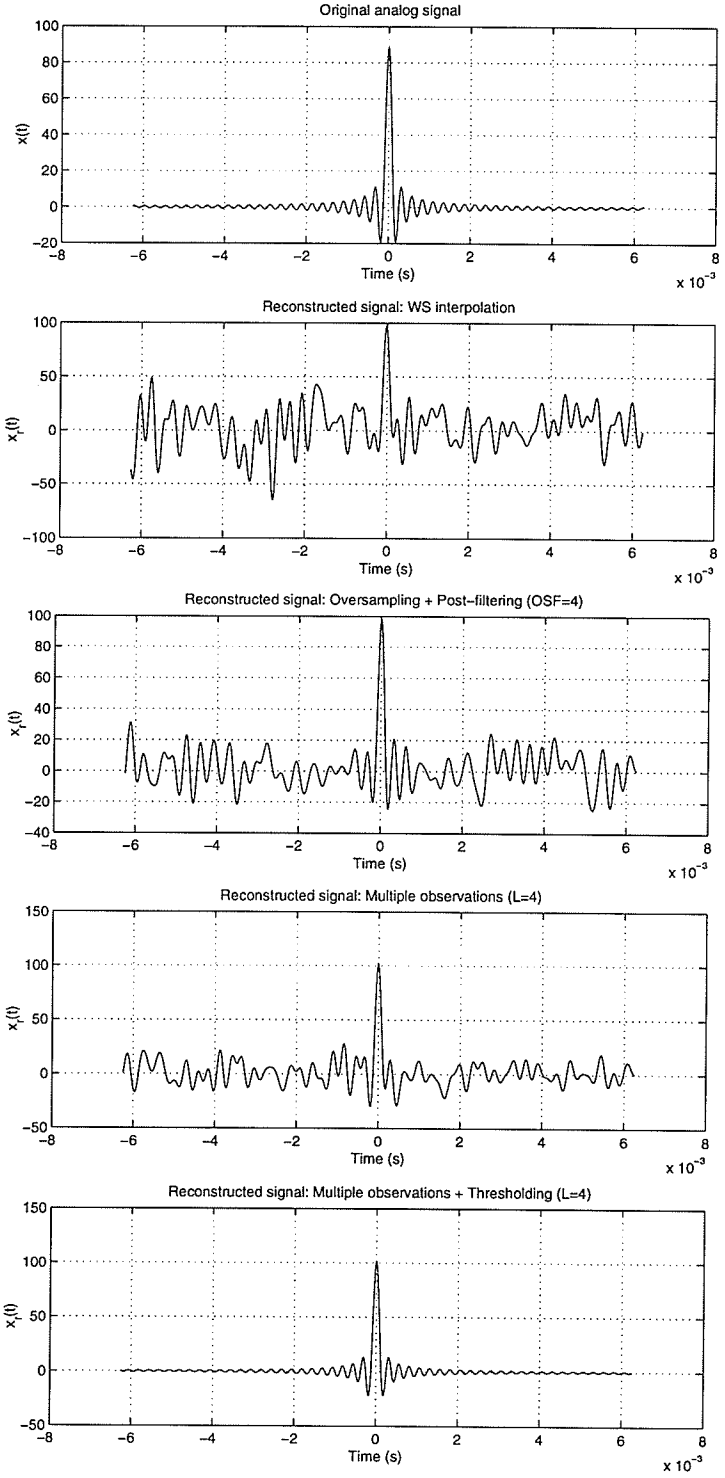

Figure F.14: Reconstructed signals in Chapter 6 (Test signal $x_1(t)$, $E_0/\sigma^2 = -25$ dB)

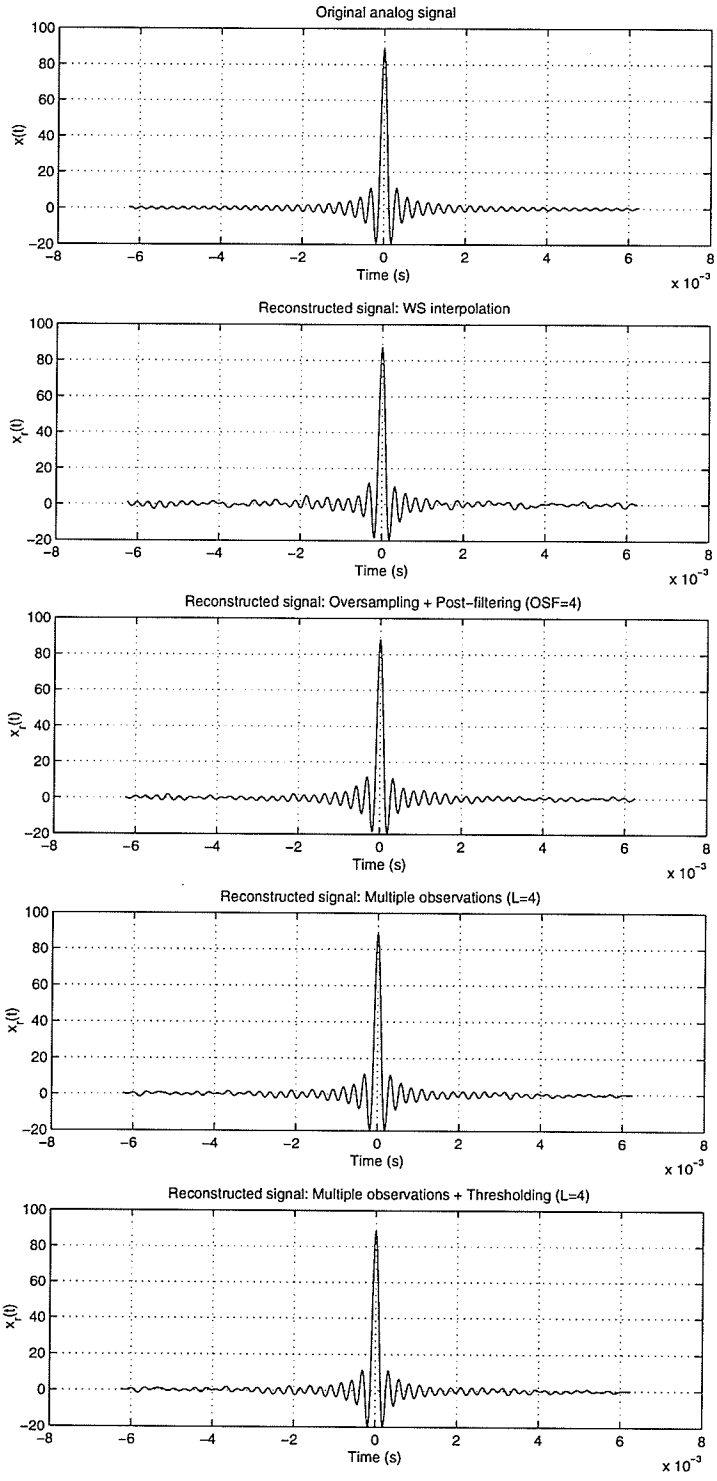

Figure F.15: Reconstructed signals in Chapter 6 (Test signal $x_1(t)$, $E_0/\sigma^2 = 0$ dB)

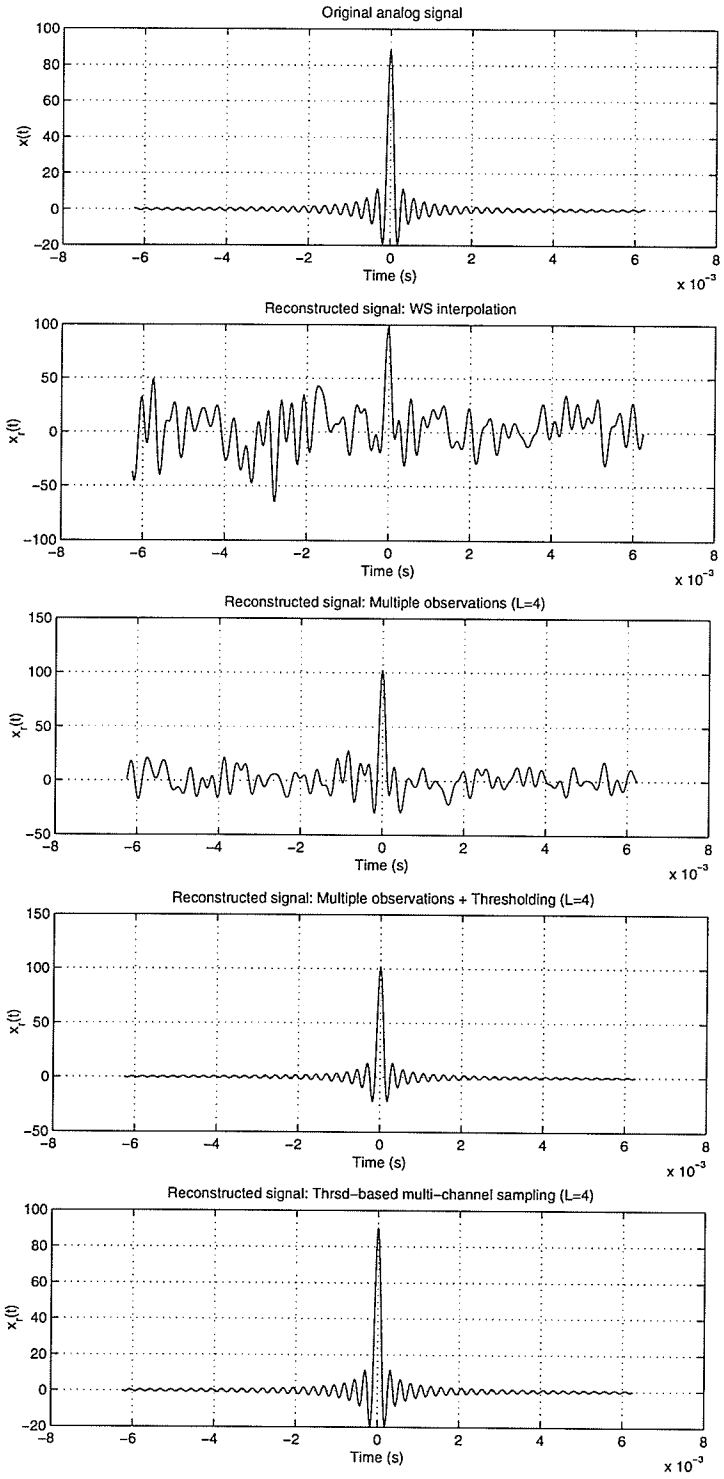

Figure F.16: Reconstructed signals in Chapter 7 (Test signal $x_1(t)$, $E_0/\sigma^2 = -25$ dB)

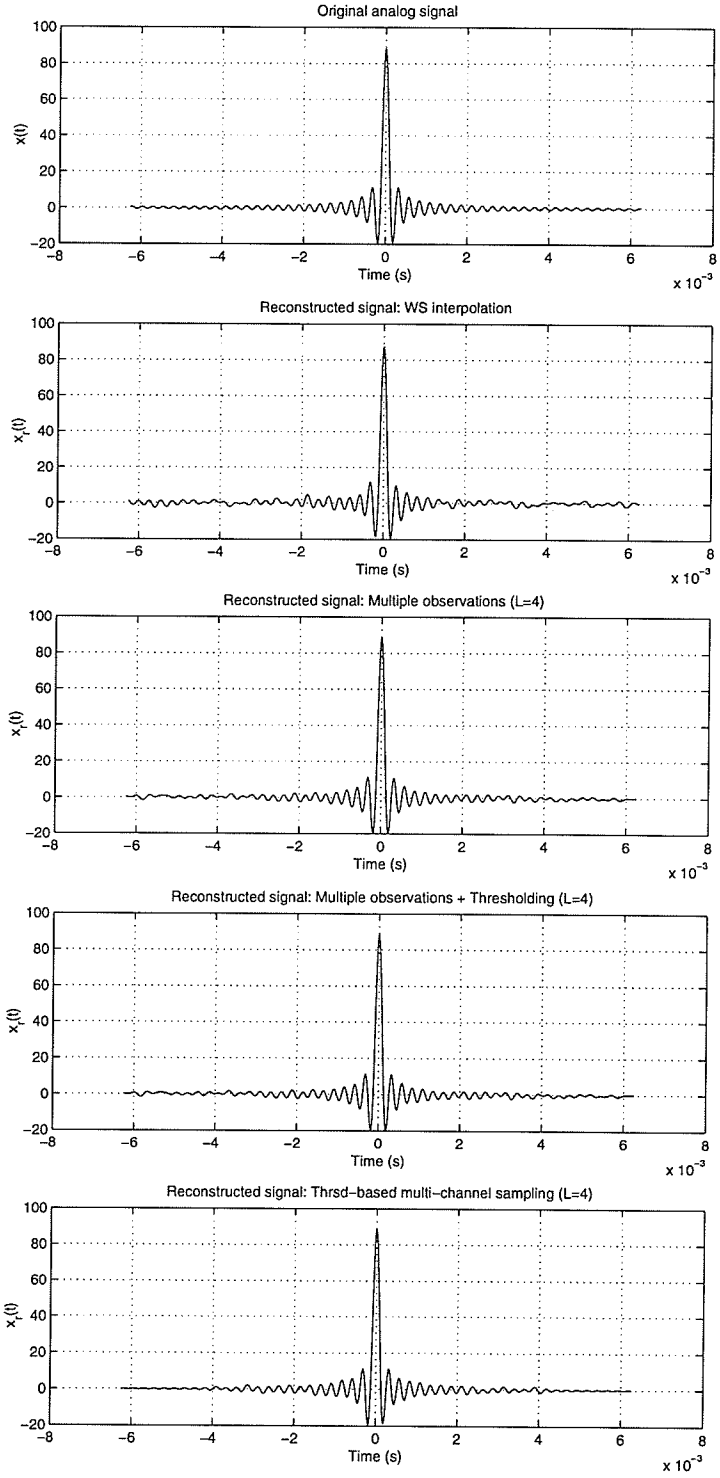

Figure F.17: Reconstructed signals in Chapter 7 (Test signal $x_1(t)$, $E_0/\sigma^2 = 0$ dB)

Bibliography

[1] E.T. Whittaker, "On the functions which are represented by the expansion of the interpolation theory," *Proc. Roy. Soc. Edinburgh*, vol. 35, pp. 181–194, 1915.

[2] C.E. Shannon, "Communications in the presense of noise," *Proceedings of the IRE*, vol. 37, pp. 10–21, Jan. 1949.

[3] M. Pawlak and E. Rafajlowicz, "On restoring band-limited signals," *IEEE Transactions on Information Theory*, vol. 40, pp. 1490–1503, Sep. 1994.

[4] A. Krzyzak, E. Rafajlowicz, and M. Pawlak, "Moving average restoration of bandlimited signals from noisy observations," *IEEE Transactions on Signal Processing*, vol. 45, pp. 2967–2976, Dec. 1997.

[5] R.J. Marks II, *Introduction to Shannon Sampling and Interpolation Theory*, Springer-Verlag, New York, NY, 1991.

[6] M. Pawlak and U. Stadmuller, "Statistical aspects of sampling for noisy and grouped data," *In J. Benedetto and P. Ferreira, editors, Advances in Shannon Sampling Theory: Mathematics and Applications*, Boston, TX, pp. 317-342, 2001.

[7] M. Pawlak, E. Rafajlowicz, and A. Krzyzak, "Exponential weighting algorithms for reconstruction of bandlimited signals," *IEEE Transactions on Signal Processing*, vol. 44, pp. 538–545, Mar. 1996.

[8] M. Pawlak and U. Stadmuller, "Recovering band-limited signals under noise," *IEEE Transactions on Information Theory*, vol. 42, pp. 1425–1438, Sept. 1996.

[9] N.S. Jayant and P. Noll, *Digital Coding of Waveforms: Principles and Applications to Speech and Video*, Prentice-Hall, Englewood Cliffs, NJ, 1984.

[10] G.G. Walter, "A sampling theorem for wavelet subspaces," *IEEE Transactions on Information Theory*, vol. 38, no. 2, pp. 881–884, Mar. 1992.

[11] M. Unser, "Sampling-50 years after Shannon," *Proceedings of the IEEE*, vol. 88, no. 4, pp. 569–587, Apr. 2000.

[12] P.P. Vaidyanathan, "Generalizations of the sampling theorem: Seven decades after Nyquist," *IEEE Transactions on Circuits and Systems I: Fundamental Theory and Applications*, vol. 48, no. 9, pp. 1094 –1109, Sept. 2001.

[13] A. Aldroubi and K. Grochenig, "Nonuniform sampling and reconstruction in shift-invariant spaces," *SIAM review*, vol. 43, no. 4, pp. 585–620, 2001.

[14] Y.C. Eldar, *Quantum Signal Processing*, Ph.D. thesis, Massachusetts Institute of Technology, December 2001.

[15] J.R. Higgins, *Sampling Theory in Fourier and Signal Analysis*, Clarendon Press, Oxford, 1996.

[16] A.J. Jerri, "The Shannon sampling theorem - its various extensions and applications: A tutorial review," *Proceedings of the IEEE*, vol. 65, pp. 1565–1596, Nov. 1977.

[17] P.L. Butzer and R.L. Steins, "Sampling theory for not necessary band-limited functions: A historical overview," *SIAM Review*, vol. 34, no. 1, pp. 40–53, Mar. 1992.

[18] F. Marvasti, *Nonuniform sampling: Theory and practice*, Kluwer Academic, New York, NY, 2001.

[19] J. L. Yen, "On the nonuniform sampling of bandwidth limited signals," *IRE Transactions on Circuit Theory*, vol. 3, pp. 251–257, December 1956.

[20] F. J. Beutler, "Error-free recovery of signals from irregularly spaced samples," *SIAM Review*, vol. 8, no. 3, pp. 328–335, July 1966.

[21] R.E.A. Paley and N. Wiener, *Fourier transform in complex domain*, vol. 19, American Mathematics Society, New York, NY, 1934.

[22] M. I. Kadec, "The exact value of the paley-wiener constant," *Soviet Math. Dokl.*, vol. 5, pp. 559–561, 1964.

[23] A. Papoulis, "Generalized sampling expansion," *IEEE Transaction on Circuits and Systems*, pp. 652–654, 1977.

[24] D. A. Linden, "A discussion of sampling theorems," *Proceedings of the IRE*, pp. 1219–1226, 1959.

[25] A. Aldroubi and M. Unser, "Sampling procedures in function spaces and asymptotic equivalence with Shannon's sampling theory," *Numerical Functional Analysis and Optimization*, vol. 16, pp. 1–21, Feb. 1994.

[26] M. Unser and A. Aldroubi, "A general sampling theory for nonideal acquisition devices," *IEEE Transactions on Signal Processing*, vol. 42, no. 11, pp. 2915–2925, Nov. 1994.

[27] A. Papoulis, "Error analysis in sampling theory," *Proceedings of The IEEE*, vol. 54, pp. 947–955, Jul. 1966.

[28] P.L. Butzer, W. Engels, and U. Scheben, "Magnitude of the truncation error in sampling expansions of bandlimited signals," *IEEE Transactions on Acoustics, Speech and Signal Processing*, vol. 30, pp. 906–912, Dec. 1982.

[29] S. Cambanis and E. Marsy, "Truncation error bounds for the cardinal sampling expansions of band-limited signals," *IEEE Transactions on Information Theory*, vol. 28, no. 4, pp. 605–612, Jul. 1982.

[30] J. L. Brown, "On mean square aliasing error in the cardinal series expansion of random processes," *IEEE Transactions on Information Theory*, vol. 24, pp. 254–256, 1978.

[31] H. S. Shapiro and R. A. Silverman, "Alias free sampling of random noise," *SIAM Journal*, vol. 8, pp. 225–236, June 1960.

[32] F. J. Beutler, "Alias-free randomly timed sampling of stochastic processes," *IEEE Transactions on Information Theory*, vol. 16, pp. 147–152, 1970.

[33] K. Yao and J. B. Thomas, "On some stability and interpolatory properties of nonuniform sampling expansions," *IEEE transactions on circuit theory*, vol. 14, no. 4, pp. 404–408, Dec. 1967.

[34] H.J. Landau, "Sampling, data transmission, and the Nyquist rate," *Proceedings of The IEEE*, vol. 55, no. 10, pp. 1701–1706, Oct. 1967.

[35] K. F. Cheung and R. J. Marks II, "Ill-posed sampling theorems," *IEEE transactions on circuits and systems*, vol. 32, no. 5, pp. 481–484, May 1985.

[36] R. J. Marks II, "Noise sensitivity of band-limited signal derivative interpolation," *IEEE transactions on acoustics, speech, and signal processing*, vol. 31, no. 4, pp. 1028–1032, Aug. 1983.

[37] J. L. Brown and S. D. Cabrera, "On well-posedness of the papoulis generalized sampling theorem," *IEEE Transactions on Circuits and Systems*, vol. 38, no. 5, pp. 554–556, May 1991.

[38] D. Seidner and M. Feder, "Noise amplification of periodic nonuniform sampling," *IEEE Transactions on Signal Processing*, vol. 48, no. 1, pp. 275–277, Jan. 2000.

[39] D. Seidner and M. Feder, "Vector sampling expansion," *IEEE Transactions on Signal Processing*, vol. 48, no. 5, pp. 1401–1416, May 2000.

[40] P.C. Ching and S.Q. Wu, "On approximated sampling theorem and wavelet denoising for arbitrary waveform restoration," *IEEE Transaction on Circuits and Systems-II: Analog and Digital Signal Processing*, vol. 45, no. 8, pp. 1102–1106, Aug. 1998.

[41] J. J. Knab and M. I. Schwartz, "A system error bound for self-truncating reconstruction filter class," *IEEE Transactions on Information Theory*, pp. 341–342, May 1975.

[42] J. A. Stuller, "Reconstruction of finite duration signals," *IEEE Transactions on Information Theory*, pp. 667–669, Sept. 1972.

[43] R. E. Totty and G. C. Clark, "Reconstruction error in waveform transmission," *IEEE Transactions on Information Theory*, pp. 336–338, April 1967.

[44] I. Mavaric and M. Vetterli, "Exact sampling results for some classes of parametric nonbandlimited 2-D signals," *IEEE Transactions on Signal Processing*, vol. 52, no. 1, pp. 175–189, Jan. 2004.

[45] Y. Yamashita, "Optimum sampling vectors for wiener filter noise reduction," *IEEE Transactions on Signal Processing*, vol. 50, no. 1, pp. 58–68, Jan. 2002.

[46] M. Pawlak, E. Rafajlowicz, and A. Krzyzak, "Postfiltering versus prefiltering for signal recovering from noisy samples," *IEEE Transactions on Information Theory*, vol. 49, no. 12, pp. 3195–3212, Dec. 2003.

[47] D. L. Donoho and I. Johnstone, "Ideal spatial adaptation via wavelet shrinkage," *Biometrika*, vol. 81, pp. 425– 455, Dec. 1994.

[48] D. L. Donoho, "De-noising by soft-thresholding," *IEEE Transactions on Information Theory*, vol. 41, no. 3, pp. 613–627, May 1995.

[49] M. Jansen, *Noise Reduction by Wavelet Thresholding*, Lecture Notes in Statistics. Springer, New York, NY, 2001.

[50] I.S. Gradshteyn and I.M. Ryzhik, *Table of Integrals, Series, and Products*, Academic Press, New York, 4th edition, 1980.

[51] A. Papoulis, *Signal Analysis*, McGraw-Hill, New York, NY, 1977.

[52] A.V. Oppenheim and R.W. Schafer, *Discrete-Time Signal Processing*, Prentice-Hall, Englewood Cliffs, NJ, 1989.

[53] J. G. Proakis, *Digital Communications*, McGraw-Hill, New York, NY, 3rd edition, 1995.

[54] A. Papoulis, *Probability, Random Variables, and Stochastic Processes*, McGraw-Hill, New York, NY, 1965.

[55] Yih-Chyun Jenq, "Digital specta of nonuniformly sampled signals: Fundamentals and high-speed waveform digitizers," *IEEE Transactions on Instrumentation and Measurement*, vol. 37, no. 2, pp. 245–251, June 1988.

[56] J. Elbornsson and J.-E. Eklund, "Blind estimation of timing errors in interleaved ad converters," *Proc. International Conference on Acoustics, Speech and Signal Processing*, pp. 3913–3916, 2001.

[57] V. Tarokh, N. Seshadri, and A. R. Calderbank, "Space-time codes for high data rate wireless communication: Performance criterion and code construction," *IEEE Transactions on Information Theory*, vol. 4, no. 2, pp. 744–765, March 1998.

[58] F. Zhao and L. Guibas, *Information Processing in Sensor Networks*, vol. XII of *Lecture Notes in Computer Science*, Springer-Verlag, 2003.

[59] P. Hall, G. Kerkyachanrian, and D. Picard, "Block threshold rules for curve estimation using kernel and wavelet methods," *The Annals of Statistics*, vol. 26, no. 3, pp. 922–942, 1998.